FORCE CONTROL OF A NEW SEMI-ACTIVE PIEOZOELECTRIC-BASED FRICTION DAMPER

By

MEMET UNSAL

A THESIS PRESENTED TO THE GRADUATE SCHOOL
OF THE UNIVERSITY OF FLORIDA IN PARTIAL FULFILLMENT
OF THE REQUIREMENTS FOR THE DEGREE OF
MASTER OF SCIENCE

UNIVERSITY OF FLORIDA

2002

I would like to dedicate this work to my family whose love and support always found a way to reach me from thousands of miles away.

ACKNOWLEDGMENTS

I would like to express my gratitude to my advisor, Dr. Niezrecki, for his guidance, enthusiasm, and continual support throughout this work. I would also like to thank Dr. Crane and Dr. Schueller for serving on my supervisory committee. I also thank Howard Purdy at the Machine Shop and my fellow students in the Smart Structures and Acoustics Laboratory.

TABLE OF CONTENTS

page

ACKNOWLEDGMENTS iv

LIST OF TABLES vii

LIST OF FIGURES viii

ABSTRACT xiii

CHAPTER

1 INTRODUCTION 1

1.1 Need for New Devices in Vibration Isolation 1
1.2 Review of Vibration Control 1
1.3 Semi-Active Dampers 4
1.3.1 Dampers Utilizing Smart Fluids 4
1.3.2 Hydraulic Damper 7
1.3.3 Mechatro Damper 7
1.3.4 Tuned Liquid Damper (TLD) 8
1.3.5 Friction Damper 9
1.4 Semi-Active Friction Control Strategies 14
1.5 Approach 15

2 THEORETICAL DEVELOPMENT 17

2.1 Friction Modeling 17
2.2 Stick-Slip Behavior 22
2.3 System Model 25

3 EXPERIMENTAL SETUP 26

3.1 Experimental Friction Damper Setup 26
3.1.1 Piezoelectric Actuator 28
3.1.2 Shaker 29
3.1.3 Transducers 30
3.1.4 Air Bearing 31
3.1.5 Other Parts 31
3.2 Experimental Vibration Isolator Setup 32
3.3 Simulink® Model of the System 34

3.4 Experiments 35
3.4.1 Calibration of the Transducers 35
3.4.2 System Identification 36
3.4.3 Determining the Displacement Capability of the Piezoelectric Actuator 36
3.4.4 Varying the Damping Characteristics of the System 37
3.4.5 Friction Force Experiments 37

4 RESULTS 38

4.1 System Identification 38
4.1.1 Modal Hammer Test 38
4.1.2 Initial Displacement Test 40
4.1.3 Determining the Displacement Capability of the Piezoelectric Actuator 42
4.2 Varying the Damping Characteristics of the System through the Actuator 44
4.3 Friction Force Capability of the Base Damper 46
4.3.1 Determining the Experimental Uncertainty of the Measurements 46
4.3.2 Calculation of the Friction Force for Varying Normal Force, Excitation Amplitude and Frequency Values 47
4.3.3 Controlling the Normal Force 52
4.3 Summary of Results 54

5 SUMMARY AND CONCLUSIONS 56

5.1 System Identification 56
5.2 Tests Investigating the Friction Force Capability of the Piezoelectric-Based Damper 57
5.3 Future Work 57

APPENDIX TESTS EVALUATING THE FRICTION FORCE CAPABILITY OF THE PIEZOELECTRIC ACTUATOR 59

LIST OF REFERENCES 84

BIOGRAPHICAL SKETCH 88

LIST OF TABLES

Table page

4-1 Summary of system parameters.....54

4-2 Friction force amplitudes at various shaker voltages and excitation frequencies 55

LIST OF FIGURES

Figure page

1-1 RD-1005 MR damper from Lord Corporation 6

1-2 Force characteristics of RD-1005 MR damper at 0.2 in/sec.....6

1-3 Construction of semi-active fluid damper 7

1-4 Structure of mechatro damper 8

1-5 Tuned liquid column dampers 9

1-6 Semi-active friction-based damper.....10

1-7 Cantilevered piezoelectric and THUNDER™ actuators 12

1-8 Setup utilizing THUNDER™ actuator.....13

2-1 Coulomb + static friction model.....18

2-2 Coulomb + viscous + static friction model.....19

2-3 Negative viscous + coulomb + viscous friction model (Stribeck friction).....19

2-4 LuGre model of the friction interface.....21

2-6 Representation of stick-slip as used in Blau's model 23

2-7 Schematic drawing and free body diagram 25

3-1 Friction damper (front and side view) 27

3-2 Friction damper (3D view) 27

3-3 FPA-1700-LV piezoelectric actuator 28

3-4 Block force test of FPA 1700-LV piezoelectric actuator 29

3-5 Sine performance curves for the Vibration Exciter Type 4808 30

3-6 Transducers.....31

3-7 Friction damper with shaker and transducers (side view) 32

3-8 Friction damper with shaker and transducers (3D view).....32

3-9 Experimental setup 33

3-10 Schematic drawing of the experimental setup.....34

3-11 Schematic diagram of the calculation of the friction force 35

4-1 Modal hammer test 39

4-2 Autospectrum of modal hammer test.....39

4-3 Response of the system to one inch initial displacement 40

4-4 Autospectrum of the one inch initial displacement test.....41

4-5 Comparison of the theoretical and experimental models 42

4-6 Swept sine test of the actuator's displacement capability 43

4-7 Displacement capability of one side of the actuator at 3 Hz 43

4-8 Magnitude of acceleration over excitation force from swept sine test 44

4-9 Phase angle of acceleration over excitation force from swept sine test 45

4-10 Coherence data of the swept sine test 45

4-11 Input force, inertial force and the resulting friction force at 5 V shaker input voltage and 20 Hz excitation frequency with no contact of the friction pads 46

4-12 Input force, inertial force and the resulting friction force at 0 V actuator input voltage, 9 V shaker input voltage and 20 Hz excitation frequency 48

4-13 Input force, inertial force and the resulting friction force at 30 V actuator input voltage, 9 V shaker input voltage and 20 Hz excitation frequency 48

4-14 Input force, inertial force and the resulting friction force at 60 V actuator input voltage, 9 V shaker input voltage and 20 Hz excitation frequency 49

4-15 Input force, inertial force and the resulting friction force at 90 V actuator input voltage, 9 V shaker input voltage and 20 Hz excitation frequency 49

4-16 Input force, inertial force and the resulting friction force at 120 V actuator input voltage, 9 V shaker input voltage and 20 Hz excitation frequency 50

4-17 Friction force amplitudes at varying excitation amplitudes 51

4-18 Comparison of the friction force 52

4-19 Friction force capability of the actuator when the actuator input voltage is varied in steps.....53

4-20 Friction force capability of the actuator when the actuator input voltage is varied linearly 54

5-1 Special 6-6 platform 58

A-1 Results at 0 V actuator voltage, 5 V shaker voltage and 20 Hz frequency.....59

A-2 Results at 0 V actuator voltage, 5 V shaker voltage and 25 Hz frequency.....60

A-3 Results at 0 V actuator voltage, 5 V shaker voltage and 30 Hz frequency.....60

A-4 Results at 30 V actuator voltage, 5 V shaker voltage and 20 Hz frequency.....61

A-5 Results at 30 V actuator voltage, 5 V shaker voltage and 25 Hz frequency.....61

A-6 Results at 30 V actuator voltage, 5 V shaker voltage and 30 Hz frequency.....62

A-7 Results at 60 V actuator voltage, 5 V shaker voltage and 20 Hz frequency.....62

A-8 Results at 0 V actuator voltage, 5 V shaker voltage and 25 Hz frequency.....63

A-9 Results at 60 V actuator voltage, 5 V shaker voltage and 30 Hz frequency.....63

A-10 Results at 90 V actuator voltage, 5 V shaker voltage and 20 Hz frequency.....64

A-11 Results at 90 V actuator voltage, 5 V shaker voltage and 25 Hz frequency.....64

A-12 Results at 90 V actuator voltage, 5 V shaker voltage and 30 Hz frequency.....65

A-13 Results at 120 V actuator voltage, 5 V shaker voltage and 20 Hz frequency.....65

A-14 Results at 120 V actuator voltage, 5 V shaker voltage and 25 Hz frequency.....66

A-15 Results at 120 V actuator voltage, 5 V shaker voltage and 30 Hz frequency.....66

A-16 Results at 0 V actuator voltage, 7 V shaker voltage and 20 Hz frequency.....67

A-17 Results at 0 V actuator voltage, 7 V shaker voltage and 25 Hz frequency.....67

A-18 Results at 0 V actuator voltage, 7 V shaker voltage and 30 Hz frequency.....68

A-19 Results at 30 V actuator voltage, 7 V shaker voltage and 20 Hz frequency.....68

A-20 Results at 30 V actuator voltage, 7 V shaker voltage and 25 Hz frequency.....69

A-21 Results at 30 V actuator voltage, 7 V shaker voltage and 30 Hz frequency.....69

A-22 Results at 60 V actuator voltage, 7 V shaker voltage and 20 Hz frequency.....70

A-23 Results at 60 V actuator voltage, 7 V shaker voltage and 25 Hz frequency.....70

A-24 Results at 60 V actuator voltage, 7 V shaker voltage and 30 Hz frequency.....71

A-25 Results at 90 V actuator voltage, 7 V shaker voltage and 20 Hz frequency.....71

A-26 Results at 90 V actuator voltage, 7 V shaker voltage and 25 Hz frequency.....72

A-27 Results at 90 V actuator voltage, 7 V shaker voltage and 30 Hz frequency.....72

A-28 Results at 120 V actuator voltage, 7 V shaker voltage and 20 Hz frequency.....73

A-29 Results at 120 V actuator voltage, 7 V shaker voltage and 25 Hz frequency.....73

A-30 Results at 120 V actuator voltage, 7 V shaker voltage and 30 Hz frequency.....74

A-31 Results at 0 V actuator voltage, 9 V shaker voltage and 20 Hz frequency.....74

A-32 Results at 0 V actuator voltage, 9 V shaker voltage and 25 Hz frequency.....75

A-33 Results at 0 V actuator voltage, 9 V shaker voltage and 30 Hz frequency.....75

A-34 Results at 30 V actuator voltage, 9 V shaker voltage and 20 Hz frequency.....76

A-35 Results at 30 V actuator voltage, 9 V shaker voltage and 25 Hz frequency.....76

A-36 Results at 30 V actuator voltage, 9 V shaker voltage and 30 Hz frequency.....77

A-37 Results at 60 V actuator voltage, 9 V shaker voltage and 20 Hz frequency.....77

A-38 Results at 60 V actuator voltage, 9 V shaker voltage and 25 Hz frequency.....78

A-39 Results at 60 V actuator voltage, 9 V shaker voltage and 30 Hz frequency.....78

A-40 Results at 90 V actuator voltage, 9 V shaker voltage and 20 Hz frequency.....79

A-41 Results at 90 V actuator voltage, 9 V shaker voltage and 25 Hz frequency.....79

A-42 Results at 90 V actuator voltage, 9 V shaker voltage and 30 Hz frequency.....80

A-43 Results at 120 V actuator voltage, 9 V shaker voltage and 20 Hz frequency.....80

A-44 Results at 120 V actuator voltage, 9 V shaker voltage and 25 Hz frequency.....81

A-45 Results at 120 V actuator voltage, 9 V shaker voltage and 30 Hz frequency.....81

A-46 Results at 150 V actuator voltage, 9 V shaker voltage and 20 Hz frequency.....82

A-47 Results at 150 V actuator voltage, 9 V shaker voltage and 25 Hz frequency.....82

A-48 Results at 150 V actuator voltage, 9 V shaker voltage and 30 Hz frequency.....83

Abstract of Thesis Presented to the Graduate School
of the University of Florida in Partial Fulfillment of the
Requirements for the Degree of Master of Science

FORCE CONTROL OF A NEW SEMI-ACTIVE PIEZOELECTRIC-BASED FRICTION DAMPER

By

Memet Unsal

August 2002

Chair: Dr. Christopher Niezrecki
Department: Mechanical Engineering

We developed a new way to perform vibration control on a single-degree-of-freedom system using a piezoelectric friction damper. The damper consists of an actuator, which is based on a piezoelectric stack with a mechanical amplifying mechanism that provides symmetric forces within the isolator. The advantages of such an actuator are its high bandwidth, actuating response and its ability to operate in vacuum environments such as in space. The damper is constrained to move using an air bearing that produces a virtually ideal single-degree-of-freedom spring-mass system. Within this work, the actuating ability of the friction-based actuator is characterized. The relationship between the force generated by the actuator and the applied voltage was found to be linear. The maximum force generated by the actuator in this study is 85 N for the specific friction pads used.

CHAPTER 1
INTRODUCTION

Reasons for developing a new semi-active piezoelectric-based friction damper are described in this chapter. The advantages of semi-active vibration control over passive and active vibration control are discussed. A brief review of the dampers commonly used in semi-active vibration control is given and a general view of piezoelectric actuators and other actuators considered is presented. Lastly, friction damping is reviewed.

1.1 Need for New Devices in Vibration Isolation

As technology continues to advance, the need for vibration isolation becomes increasingly necessary. More reliable devices with a higher bandwidth, smaller size, and lower power requirement are needed. Semi-active control of vibration isolation is an area of much interest because of its potential to provide these characteristics. Piezoelectric actuators have only recently been proposed to be used in vibration isolation. However, there is still a lot of room for research and development.

1.2 Review of Vibration Control

Structures and mechanical systems should be designed to enable better performance under different types of loading, particularly dynamic and transient loads. There are three fundamental control strategies to regulate or control the response of a system: passive control, active control, and semi-active control.

Traditionally, vibration isolation has focused on passive control. For passive control, mechanical devices such as energy-dissipation devices or isolators are added to a mechanical system to increase energy-dissipation and improve the performance of the

system (Taniwangsa and Kelly, 1997). Several applications of this method have been reported and implemented (Tarics et al., 1984; The Salt Lake City Corp., 1988). For example, rubber isolators have been used in structures to decrease ground motion from earthquakes. An external power source for operation is not required for passive control systems. Instead the relative motion of the structure is used to develop the control forces to induce strain within the damping material (Symans and Constantinou, 1997). The primary advantage of passive damping systems is that they have robust stability under any degree of model uncertainty (Lane and Ferri, 1995). However, the performance of such a system is limited because system parameters, especially damping cannot be varied. This causes a passive system to behave differently under changing conditions and therefore they cannot always meet the design requirements. It has been shown that if the parameters of an isolation system can be adjusted in response to varying external conditions, the performance of the system can be significantly improved (Guntur and Sankar, 1983).

Unlike passive systems, active systems can constantly supply and vary the flow of energy into the system. Based on the change in the instantaneous operating conditions as measured by sensors, the properties of the system can be adjusted (Hac and Youn, 1992). The heart of the control system is the actuator, which behaves as an artificial muscle and can potentially affect the system in an intelligent manner. This enables the active system to command arbitrary control forces (Lee and Clark, 1999). The actuators that are typically used in active control are either hydraulic, electromagnetic or intelligent material actuators. The practical disadvantages to these types of control approaches are the large power requirements needed for these actuators to do work on relatively stiff and

massive structures and the limitations of the actuators. Hydraulic actuators offer a significant amount of force and displacement; however, they lack the frequency response to mitigate the forces induced by a shock. They cannot respond quickly enough to actively control shock or vibration (except at very low frequencies). Typically, intelligent material actuators are capable of generating sufficient force and have the required bandwidth. Unfortunately, they lack the required displacement capabilities for large stroke applications. Traditional piezoelectric stacks can only generate a few micrometers of displacement when they are not being loaded. When they are loaded, the displacement is severely impaired. The current designs implementing intelligent material actuators can only control microvibrations (Bamford et al., 1995; Fudita et al., 1993; Vaillon et al., 1999). It is possible that in the near future, these actuators will have better authority, as new materials are developed. One such material is the new relaxor ferroelectric single crystals (PZN-PT and PMN-PT), that can develop strains in excess of 1% and has ~5 times the strain energy density of conventional piezoceramics (Park and Shrout, 1997). Electromechanical actuators have the necessary force and displacement capabilities for many applications. However, their implementation is often not practical because of their large weight, electrical demands, and limited bandwidth. An electromechanical actuator required to induce the necessary force and displacement would be extremely heavy and demand a significant electrical current. This makes electromagnetic actuators poorly suited to directly control vibrations of large amplitude and high bandwidth. Besides requiring a significant external power supply for actuators, active control has the inherent danger of becoming unstable through the injection of mechanical energy into the system.

Semi-active control has recently been developed as a compromise between passive and active control. Karnopp and co-workers first proposed varying the properties of a passive element by using active control, which was termed semi-active control. They suggested controlling the orifice area of a viscous damper to vary the force it provided. A semi-active control system is incapable of injecting energy into a system comprising the structure and actuator, but can achieve favorable results through selective energy dissipation (Scruggs and Lindner, 1999). Instead of directly opposing a primary disturbance, semi-active vibration control is used to apply a secondary force, which counteracts the effects of the disturbance by altering the properties of the system, such as stiffness and damping (Brennan et al, 1998). The adjustment of mechanical properties, which is based on feedback from the excitation and/or from the measured response, is what differentiates semi-active control from passive control. A controller monitors the feedback measurements and an appropriate command signal is generated for the semi-active devices. Unlike an active system, the control forces developed are related to the motion of the structure. Furthermore, the stability of the semi-active system is guaranteed as the control forces typically oppose the motion of the structure (Symans and Constantinou, 1997). In principle, a semi-active damper can emulate an active system as long as the required control force input of the active system is used to dissipate energy and the supply of energy into the system is not required.

1.3 Semi-Active Dampers

1.3.1 Dampers Using Smart Fluids

Performance limitations of purely passive vibration control devices and the costs associated with upgrading this performance using active systems explain why there is so much interest in the development of hybrid solutions. The use of so-called smart fluids is

a particularly attractive solution. By applying a low-power control signal, smart fluids can be used to continuously vary the force developed in a suitable damping device (Sims et al., 1999). These smart fluids exploit the rheological effect, which causes the solid particles in the fluid to align when the appropriate energy field is applied. This alignment creates a reduction in the ability of the fluid to flow, or shear. Each of the two main types of rheological fluids that have been researched is based on different applied energy fields. Electro-rheological (ER) fluids are responsive to a voltage field and magneto-rheological (MR) fluids are responsive to a magnetic field. ER fluids have been extensively investigated. Some of the disadvantages of these fluids are that they require thousands of volts for operation, and yield low shear stresses. The fact that these fluids are sensitive to contaminants and the high voltage needed for operation clearly make safety and packaging significant design problems. On the other hand, MR fluids operate with minimal voltage and generate high fluid shear stress (Pinkos et al., 1993). Commercially produced ER fluids are now available, but despite the design, construction, and testing of numerous prototype devices, the mass-production of an ER device is still awaited. However, the more recent MR devices are commercially available. This is because of the performance characteristics of MR fluids. They generate much higher dynamic yield stress, they have a wider temperature range, and they are insensitive to temperature variations and contaminants. The low power requirement is also a clear advantage. A certain linear MR damper (RD-1005, Lord Corporation), which is shown in Figure 1-1, was tested as a possible candidate for the vibration isolator developed in this work. Tensile and compression tests were conducted using an Instron universal tester. The force

that the damper can generate is shown in Figure 1-2. The test was conducted at 0.2 in/s and is representative of the quasi-static force capability of the isolator.

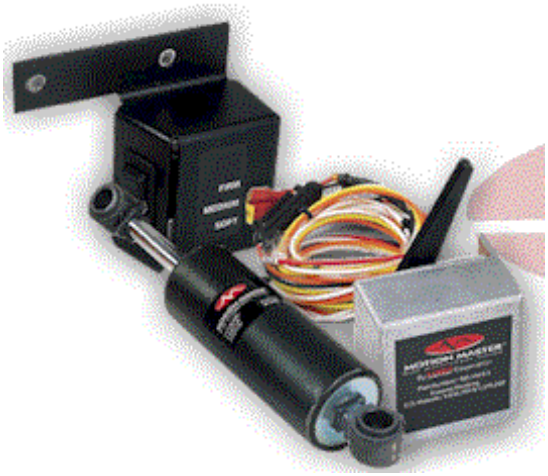

Figure 1-1 RD-1005 MR damper from Lord Corporation

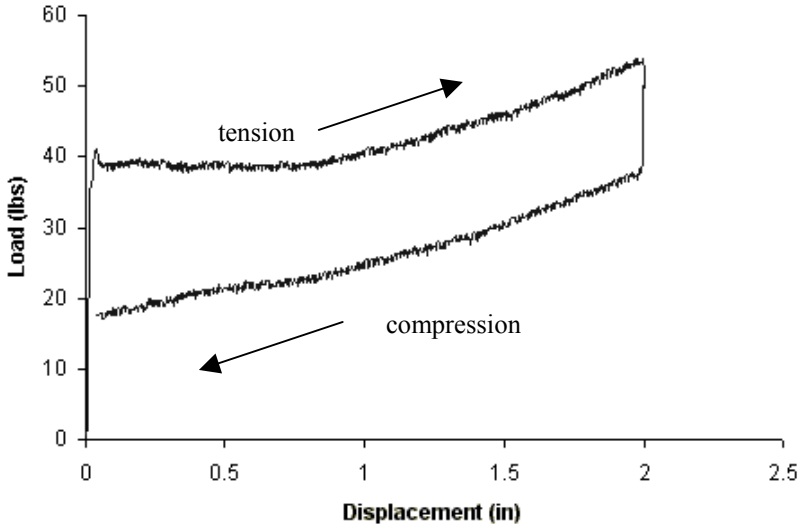

Figure 1-2 Force characteristics of RD-1005 MR damper at 0.2 in/sec

Fluid dampers typically do not have a wide frequency bandwidth. They cannot respond quickly to vibrations at high frequencies. In spite of its high force capability, this damper was determined to be not suitable for high-speed applications.

1.3.2 Hydraulic Damper

Semi-active fluid dampers, which are commonly studied, generally consist of a fluid damper combined with an external bypass loop containing a servo valve. The amount of fluid passing through the bypass loop is varied to control the behavior of the device, which essentially behaves as a variable force device with hysteretic type of damping. The control valve is a normally closed direct-drive servo valve, which offers fail-safe operation. In case of a power loss, the valve is fully closed and therefore, the semi-active damper behaves as a passive device with high damping characteristics (Symans and Constantinou, 1997). The construction of the semi-active fluid damper tested is shown in Figure 1-3.

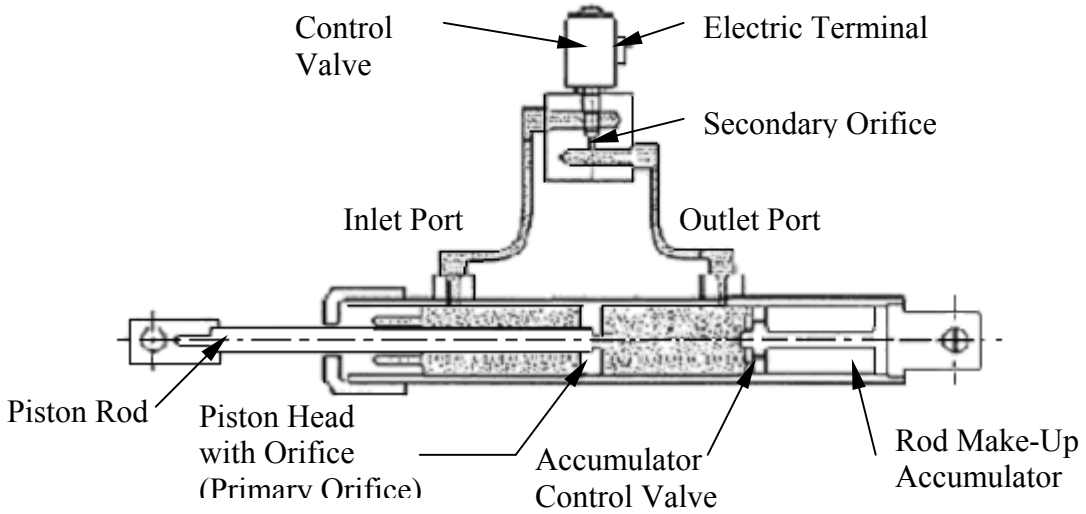

Figure 1-3 Construction of semi-active fluid damper

1.3.3 Mechatro Damper

The mechatro damper uses a ball-screw mechanism to transform vibrational motion between a vibrating structure and a base into rotational motion. The structure of the mechatro damper is shown in Figure 1-4.

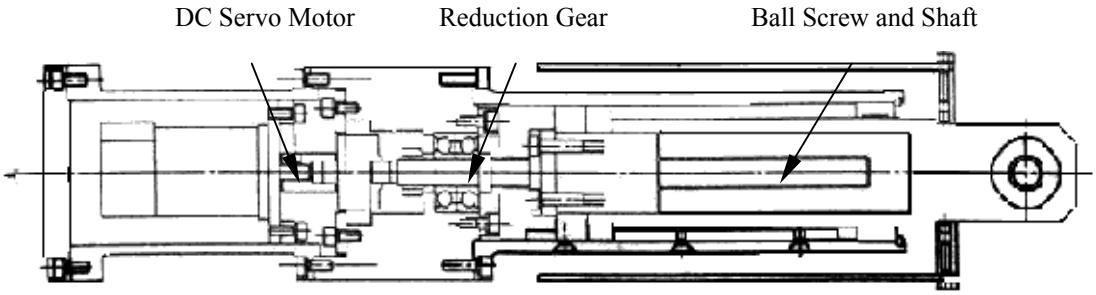

Figure 1-4 Structure of mechatro damper

A servomotor is driven by this rotational motion through a speed-increasing gear, which in turn generates an inverse induced electromotive force. This electromotive force is used to create the damping force of the mechatro damper. The resistance between the terminals of the servomotor may be varied to adjust the level of the electromotor force and therefore, the damping force (Iiyama et al., 1998).

1.3.4 Tuned Liquid Damper (TLD)

Tuned Liquid Dampers use water in a U-shaped tank as a mass for a dynamic damper. An air space is provided on each side of the U-tube above the water. The volume and the pressure of the air space are changed to adjust the natural frequency of the damper. These dampers are generally used for the reduction of noise and vibrations in structures. They may be used in multistory buildings to counteract the effects of disturbances such as wind, earthquake, and traffic, in marine structures like ships and floating platforms, where propulsion and the engine generate vibrations. Accurate measurement of the natural frequency of the structure in question is critical to tuning the frequency of the dynamic damper (Kagawa et al., 1994). Tuned Liquid Column Dampers (TLCD) are a special type of Tuned Liquid Dampers (TLD) where the motion of the liquid column in a U-tube is used to counteract the action of external forces acting on the structure. The oscillating liquid column is passed through an orifice, which can be

controlled to vary the damping force (Yalla et al., 2000). Two Tuned Liquid Column Dampers are shown in Figure 1-5.

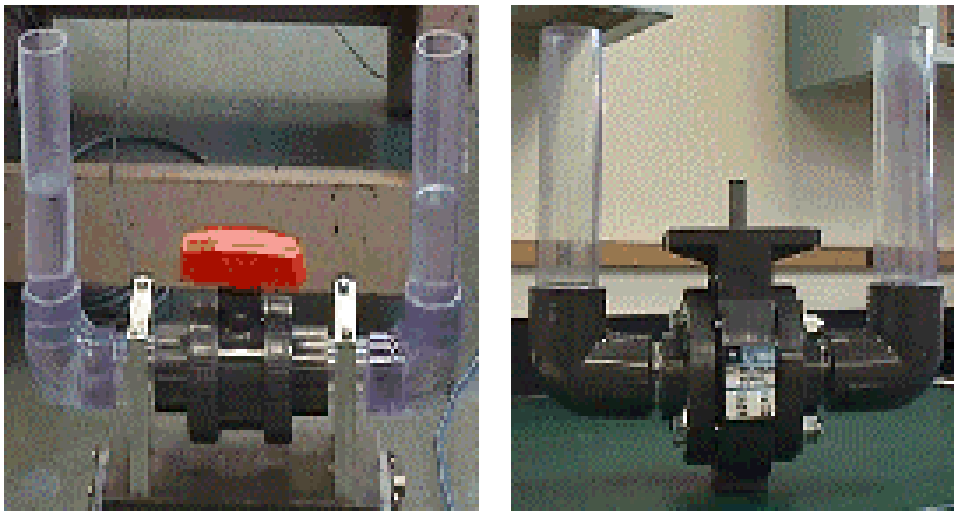

Figure 1-5 Tuned liquid column dampers

1.3.5 Friction Damper

Friction damping has long been used as an effective and simple method to add passive damping to mechanical systems. It requires only the direct contact of two parts moving relative to each other and it can be incorporated into harsh environments and vacuum environments where the use of elastomeric damping treatments and fluid filled dampers is limited (Lane et al., 1992). Ferri and Heck (Ferri and Heck, 1992) first came up with the idea of varying the normal force in a frictional joint to enhance energy dissipation from a vibrating structure. A semi-active friction damper feeds back an actuation force to the mechanical system whose dynamics can be altered in this way. The properties of the system, such as stiffness and damping can be actively changed through the control of this actuation force. A cross-sectional drawing where the friction damper

actively alters the normal force between the base structure and the outer housing of the isolator is seen in Figure 1-6.

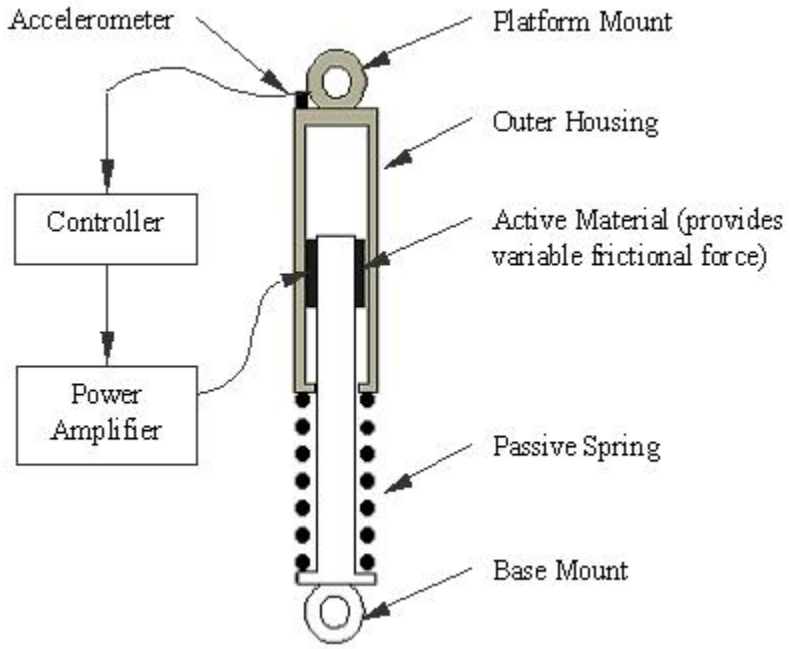

Figure 1-6 Semi-active friction-based damper

In contrast to viscous dampers, dry friction dampers can provide an excellent mechanism for shock isolation since the friction force transmitted through a friction damper is limited. This is the reason why it has been incorporated in motorcycle shock absorbers and other types of road and rail vehicle shocks. In theory, the performance of friction dampers can rival that of semi-active viscous dampers in every respect. Through the use of a simple low bandwidth feedback control system, it may be possible to provide good vibration suppression while retaining the excellent shock isolation characteristics. A friction damper can supply considerable force even for small velocities, something which is not possible for viscous dampers as they require a relatively large velocity to transmit the same amount of force (Ferri and Heck, 1992).

The development of friction dampers to the extent of other semi-active dampers has been impeded due to three primary reasons. First of all, because of the discontinuity of friction at zero velocity, the differential equation of motion of the dynamic system is dependent on the direction of velocity (Lane et al, 1992). Secondly, when the static coefficient of friction is noticeably greater than the kinetic coefficient, the "stick-slip" phenomenon occurs. This phenomenon is caused by the fact that the friction force does not remain constant as a function of some other variable, such as temperature, displacement, time, or velocity. For the two reasons stated, friction dampers are non-linear and will require a non-linear controller. The third and most important reason friction dampers have not been fully developed is due to the actuator. In past research, the normal force was altered through the use of hydraulics (Kannan et al., 1995). The main disadvantage of hydraulics is the time delay that is required for the actuator to reach the required pressure. Rapid modulation of the actuation force is not possible and it could cause a backlash effect when used. In a variable friction damper system, the speed with which the actuation force can be adjusted is of utmost importance (Garrett et al, 2001). Modern electromagnetic actuators are well suited to provide rotational motion (electric motors); however, their use as linear actuators is limited. Although they are capable of generating sufficient force and displacement, the large size, weight, electrical demands and cost of these actuators make them impractical. Recently, piezoelectric actuators have been proposed as a method of applying the varying normal force (Chen and Chen, 2000). Piezoelectricity is the ability of certain crystalline materials to develop an electric charge proportional to a mechanical stress and vice versa. Piezoelectric materials can generate a significant amount of stress/strain in a constrained condition

when exposed to an electric field. This property has been extensively used to suppress excessive vibration of mechanical and aerospace systems and is still an active area of research and development (Garrett et al., 2001). Due to their high force and bandwidth capability, piezoelectric actuators appear to be a natural candidate for use in friction dampers. However until only recently, the maximum (freely loaded) mechanical strain of these devices did not exceed 0.1%. This means that an actuator 1 inch long could only deflect 0.001 inch (significantly less under load). As a result, the development of a practical frictional damper has been hampered. Recently a new line of piezoelectric-based actuators called THUNDER™ actuators have taken a major step forward in overcoming a useable displacement hurdle (see Figure 1-7).

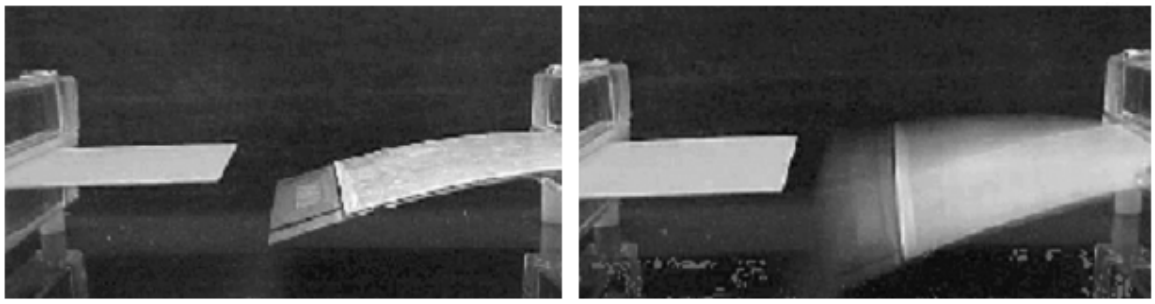

a) b)

Figure 1-7 Cantilevered piezoelectric and THUNDER™ actuators a) at rest; b) energized

When appropriate electrical fields are applied, the relative strains induced on the surfaces cause large changes in curvature of the structure and large lateral displacements. THUNDER™ actuators have among the highest displacement response of any intelligent material actuator to date.

The recently developed relaxor ferroelectric single crystals (PZN-PT and PMN-PT), can develop strains in excess of 1% (~10 times larger than traditional piezoelectric actuators) and have ~5 times the strain energy density of conventional piezoceramics

(Park and Shrout,1997). Piezoelectric stacks using the new single crystals are currently commercially available (TRS Ceramics). These new actuators have the ability to generate the required force and displacement to control the friction between the sliding elements. It is possible to use a flextensional mechanical amplifier to increase the displacement of the actuator. The THUNDER™ actuators have been tested using a custom made setup as shown in Figure 1-8, but their low force capability proved them to be poorly suited for energy dissipation. The single crystal actuators have not been used because of their high voltage requirements.

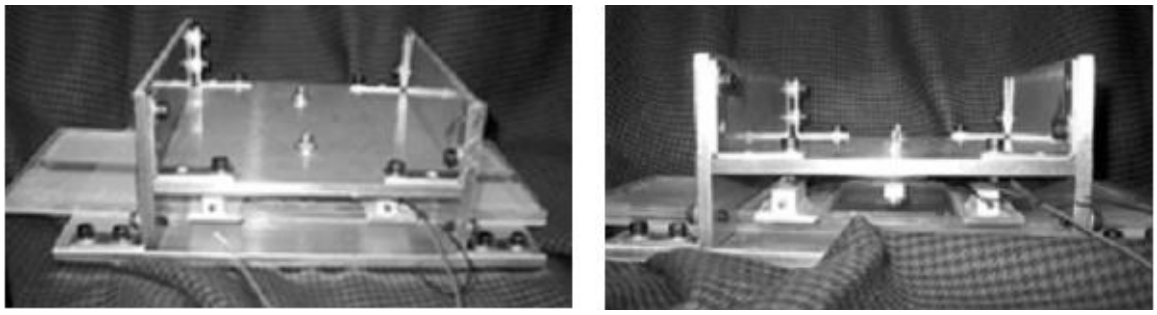

Figure 1-8 Setup utilizing THUNDER™ actuator

A flextensional piezoelectric amplifier (using an ordinary piezoelectric material) has recently been developed (FPA-1700, Dynamic Structures and Materials, LLC) that can generate a 1.5 mm displacement having a load of 10 lbs. This specific actuator was chosen to be implemented in the developed vibration isolator due to its displacement capability and also due to the inherent characteristics of piezoelectric actuators, which make them favorable when compared with other actuators. They have the potential to be effective over a wide frequency range with high-speed actuation, low power consumption, reliability and compactness (Chen and Chen, 2000). This actuator has potential application to space environments in which other viscous dampers as well as electro-rheological and magneto-rheological dampers are not suitable. It may also have

application to civil engineering structures, parallel platform mechanisms, large space structures, and vehicle suspensions.

1.4 Semi-Active Friction Control Strategies

Several approaches have been taken in past research to vary the friction damping of mechanical systems through semi-active control. One control algorithm increases the friction force as slippage increases. The normal force applied by the damper at the contact area is given as a function of slip and slip rate which are multiplied by gain coefficients. The controller essentially combines the effects of a viscous damper and a non-linear Reid damper, creating a nearly rectangular hysteretic loop. Therefore, the energy dissipation from the system is maximized (Chen and Chen, 2001). Other researchers proposed varying the contact force with respect to the deformation (Dowdell and Cherry, 1990; Inaudi, 1997). Also, a multistage controller has been developed, which alters the normal force applied by the damper if the structure undergoes a deformation that exceeds the specified threshold (Yang and Lu, 1994). Another controller varies the friction force in predetermined increments at fixed intervals based on the presence of slippage. If slippage does not occur in the previous sampled time step, the friction force is lowered and it is raised if slippage occurs (Akbay and Aktan, 1991). Ferri and Heck (Ferri and Heck, 1992) used a relatively simple controller for a two degree of freedom automobile suspension system. Displacement and velocity were both fed back and a saturation was applied to the normal force, which was proportional to the relative velocity. The simulation results showed that the overall controller could provide excellent shock isolation while having a very low bandwidth, which was achieved by filtering the normal force (Ferri and Heck, 1992). Lane et al. (Lane et al., 1992) used a two beam system with a frictional joint to compare a linear quadratic regulator (LQR)

and a design, which uses a velocity proportional controller. The design was termed viscous joint design because its frictional moment was equivalent to that generated by a rotary viscous damper. Numerical results showed that the energy dissipation with the LQR control was significantly more than the viscous damper design (Lane et al., 1992). Dupont et al. applied bang-bang control to adjust the normal force to improve the energy dissipation of the friction damper. A boundary layer was used to prevent quasi-sticking of the damper (Dupont et al., 1996; Dupont and Stokes, 1995). They also investigated the dependence of the friction on forcing amplitude and frequency. It was seen that the energy dissipated increases with increasing amplitude of oscillation. However, there is a certain amount of stored energy that is returned to the system and this returned energy also reaches a maximum as the amplitude of the oscillation is increased. Therefore, the controller that was developed removes the normal force during the energy return phases of the forcing cycle to maximize energy dissipation. Experimental results also indicated that the friction force was largely independent of the frequency of the oscillation (Dupont et al., 1997).

1.5 Approach

The objective of this work is to investigate the performance of a flextensional piezoelectric actuator as a means of providing normal force to a semi-active friction damper. In the following chapters, the instrumentation and the experimental setup are presented. How the friction force is influenced with varying excitation frequency and amplitude and how the transfer function of acceleration with respect to the input force changes with varying excitation frequency is observed. The actuating ability of the flextensional piezoelectric actuator as its input voltage is varied linearly and in steps is

also investigated. Finally, the frictional force capabilities of the actuator are characterized experimentally.

CHAPTER 2
THEORETICAL DEVELOPMENT

In this chapter, friction models are reviewed. The more simple and common models as well as recent dynamic models are discussed. Additionally, the stick-slip behavior is reviewed. Finally, the system model is presented.

2.1 Friction Modeling

One of the challenges in analyzing structural systems that rely on dry frictional damping stems from the nonlinear, discontinuous mathematical expressions that are used to characterize friction. The simplest and most common friction model is known as Coulomb friction and is governed by,

$$F_f = \mu_k N \operatorname{sgn}(\dot{x}(t)) \tag{2-1}$$

where F_f is the frictional force, μ_k is the kinetic friction coefficient, N is the normal load between the two contacting surfaces, $\dot{x}$ is the relative slip velocity and *sgn(.)* is the signum function that represents the sign of the argument. Coulomb friction is independent of velocity and even though this friction model is dependable at high levels of slip velocity, it is not well-suited to low slip velocities. This is due to a higher coefficient of friction near zero slip velocity, where a hysterisis is known to be present (Lane et al., 1992). The *sgn(.)* function only works for the case of sliding. Sticking must be studied as a separate case. The relative slip velocity is zero for nonzero lengths of time during sticking and the static coefficient of friction is applicable to the calculation of

the friction force (Ferri, 1995). This phenomenon, which is called stiction can be modeled as

$$F_f = \begin{cases} F_{external} & if\ \dot{x} = 0\ and\ |F_{external}| < F_s \\ F_s \cdot \mathrm{sgn}(F_{external}) & if\ \dot{x} \neq 0\ and\ |F_{external}| > F_s \end{cases} \tag{2-2}$$

where the force $F_{external}$ is the tangential force applied to a block over a flat surface and F_s is the static friction force. The Coulomb friction model including stiction is illustrated in Figure 2-1.

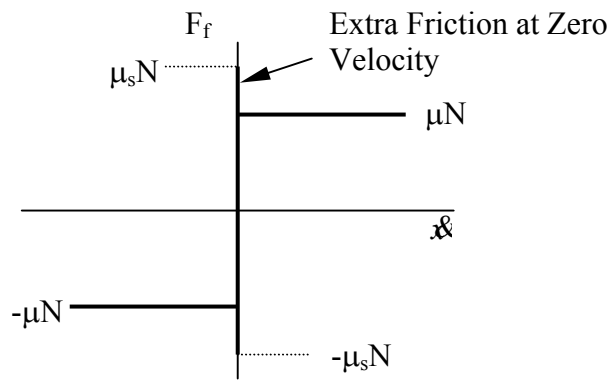

Figure 2-1 Coulomb + static friction model

Viscous friction is a friction component that is present in fluid lubricated surface contacts. It is proportional to velocity as shown in Figure 2-2. The model with Coulomb and viscous friction has been used very successfully for friction compensation in velocity drives (Canudas de Wit et al., 1987).

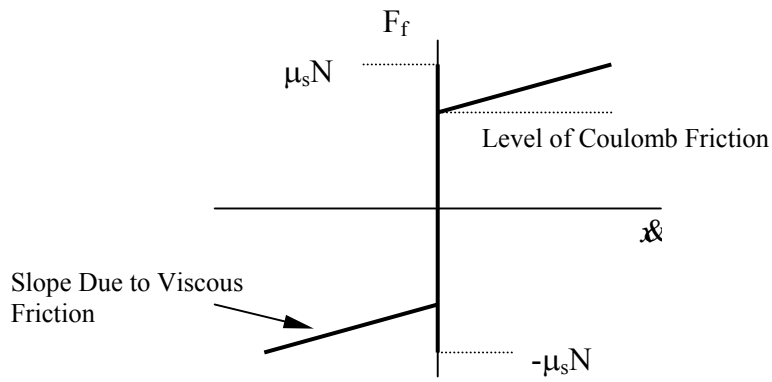

Figure 2-2 Coulomb + viscous + static friction model

There is experimental evidence that the friction force does not drop suddenly when the break-away force is reached and the static friction is overcome. Stribeck observed that the friction had the shape shown in Figure 2-3.

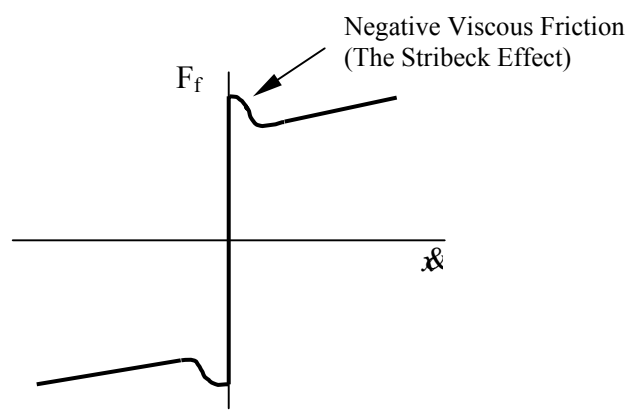

Figure 2-3 Negative viscous + coulomb + viscous friction model (Stribeck friction)

Stribeck's model can be described by

$$F_f = \begin{cases} F(\dot{x}) & \text{if } \dot{x} \neq 0 \\ F_{external} & \text{if } \dot{x} = 0 \text{ and } |F_{external}| < F_s \\ F_s \cdot \operatorname{sgn}(F_{external}) & \text{if } \dot{x} = 0 \text{ and } |F_{external}| = F_s \end{cases} \tag{2-3}$$

The function $F(\dot{x})$ can be determined by measuring the steady-state friction force required to maintain a constant velocity. One form of $F(\dot{x})$ that has been proposed is

$$F(\dot{x}) = F_c + (F_s - F_c)e^{(-\dot{x}/\dot{x}_s)^2} \tag{2-4}$$

where F_c is the Coulombic friction level and $\dot{x}_s$ is the Stribeck velocity which corresponds to the minimum value of the friction force in the region of negative viscous friction. This region, where the friction force drops with increasing velocity, is shown in Figure 2-3 (Armstrong-Helouvry, 1991).

It has been previously shown that frictional forces generated by sliding surfaces also contain dynamics associated with slip velocity. There are several dynamic friction models. The first one to be introduced was the Dahl model (Dahl, 1968). Dahl modeled the stress-strain curve by a differential equation which has the form

$$\frac{dF}{dx} = \sigma\left(1 - \frac{F}{F_c}\operatorname{sgn}(\dot{x})\right)^{\alpha} \tag{2-5}$$

where σ is the stiffness coefficient and α is a parameter that determines the shape of the stress-strain curve. The time domain model when α=1 is

$$\frac{dF}{dt} = \frac{dF}{dx} \cdot \frac{dx}{dt} = \sigma\dot{x} - \sigma\frac{F}{F_c}|\dot{x}| . \tag{2-6}$$

This model is only position dependent; therefore, it does not take into account the Stribeck effect and stiction. Bliman and Sorine have come up with a model to include the Stribeck effect in Dahl's model. In their model, the Stribeck effect is only present in the transient system dynamics (Bliman and Sorine, 1995).

A new dynamic friction model, named LuGre model, where the friction interface is thought of as a contact between bristles, was proposed by Canudas de Wit et al. as a generalization of Dahl's model (Canudas de Wit et al., 1995). In this model, the surfaces, which are irregular at the microscopic scale, make contact at a number of asperities. This

is seen as two bodies coming into contact through elastic bristles. In the case of a normal force being applied, these bristles will deflect as shown in Figure 2-4 and this will create the friction force. For simplicity, only the bristles on the upper part are shown as being elastic.

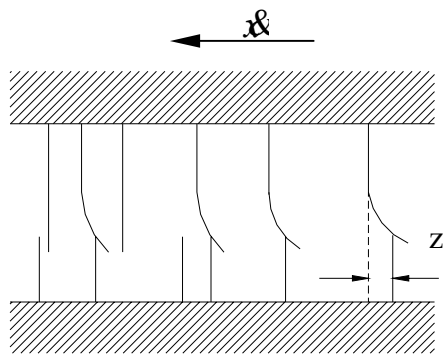

Figure 2-4 LuGre model of the friction interface

The average behavior of the bristles is the basis to the model that is proposed. Introducing $F_f = \sigma \cdot z$, where F_f is the friction force generated from the bending of the bristles and z is the average asperity junction deflection, Dahl's model in (2-6) can be written as

$$\frac{dz}{dt} = \dot{x} - \sigma \frac{F}{F_c} |\dot{x}| . \tag{2-7}$$

Adding a term for damping, where σ_1 is a damping coefficient and taking into account viscous friction, which is proportional to the relative velocity, the expression for friction force becomes

$$F_f = \sigma_o z + \sigma_1 \dot{z} + \alpha_2 \dot{x} . \tag{2-8}$$

2.2 Stick-Slip Behavior

Stick-slip is a phenomenon which happens when sliding one body over another under a steady pulling force and the sliding velocity fluctuates widely. These fluctuations consist of sticking where the motion stops and slipping where the bodies suddenly accelerate again. In most practical sliding systems, these fluctuations of the sliding velocity are considered a serious nuisance. Eliminating or reducing the amplitude of the fluctuations is usually necessary.

When two bodies in contact move relative to each other in the tangential direction, the motion can be categorized as either stable or unstable. In the stable case, the coefficient of friction remains basically constant and the movement is steady. In the unstable case, the relative motion of the two bodies alternates between stick periods and slip events, usually with different values of the coefficient of friction in stick and slip phases. The stick-slip system is generally thought of as a spring-loaded contact with a damper to account for viscoelastic response as shown in Figure 2-5.

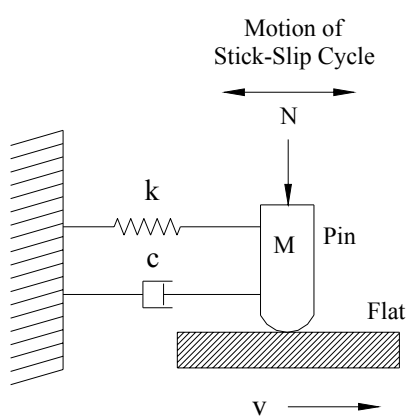

Figure 2-5 Spring and damper representation of stick-slip

The stick-slip phenomenon can be considered on a molecular level; however, in a classical mechanics approach, the behavior is thought to be caused by making and breaking bonds in unlubricated solid sliding (Blau, 1996).

Stick-slip can be modeled in several ways. Bowden and Tabors consider a free surface of inertial mass being driven at a uniform speed v in the positive x direction against a spring with stiffness k as shown in Figure 2-6 (Blau, 1996).

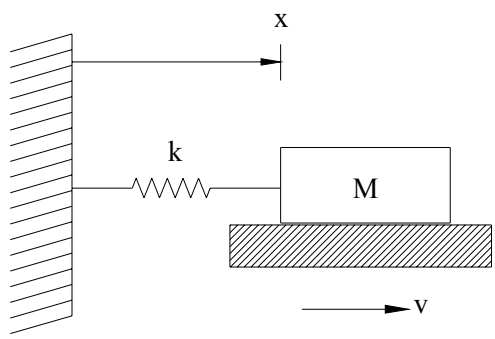

Figure 2-6 Representation of stick-slip as used in Blau's model

In this case, with no damping of the resulting oscillation, the instantaneous resisting force equals

$$ma = -kx \tag{2-9}$$

where a is the acceleration and the frequency of the oscillation is

$$\omega_n = \sqrt{\frac{k}{M}} \ . \tag{2-10}$$

The friction force with load *P* (mass M acting downward with gravity g) is

$$F_s = \mu_s \cdot P \tag{2-11}$$

and the deflection at the point of slip is

$$x = \frac{F_s}{k} \ . \tag{2-12}$$

If the friction coefficient μ is assumed to be constant during slip, then,

$$ma - \mu P = kx \ . \tag{2-13}$$

If we let time to be equal to zero at the point of slip and the forward velocity, v be less than the velocity of the slip, $\dot{x}$, then,

$$x = \left(\frac{P}{k}\right) \cdot \left[(\mu_s - \mu)\cos\omega_n t + \mu\right] \ . \tag{2-14}$$

The magnitude of the stick-slip oscillations, δ is

$$\delta = \left[P(2\mu_s - 2\mu)/k\right] \ . \tag{2-15}$$

From this equation, we can conclude that the greater the kinetic coefficient of friction relative to the static coefficient of friction, the less the effects of stick-slip will be observed. When both are equal, stick-slip will not occur and the sliding will become steady (Blau, 1996).

Stick-slip occurs at low velocity levels. Increasing velocity leads to a decrease in stick-slip. One explanation of this is based on dwell time. Increased velocity reduces the dwell time, which lowers the static friction. At some critical velocity, the dwell time is not enough to build up destabilizing static friction and stick-slip is extinguished (Armstrong-Helouvry et al., 1994). Stick-slip can also be avoided by stiffening a mechanism. Rabinowicz conducted experiments using springs with different stiffness and it was observed that the stiffest spring did not exhibit stick-slip at any velocity (Rabinowicz, 1965).

2.3 System Model

The system tested in this work can be modeled as shown in Figure 2-7

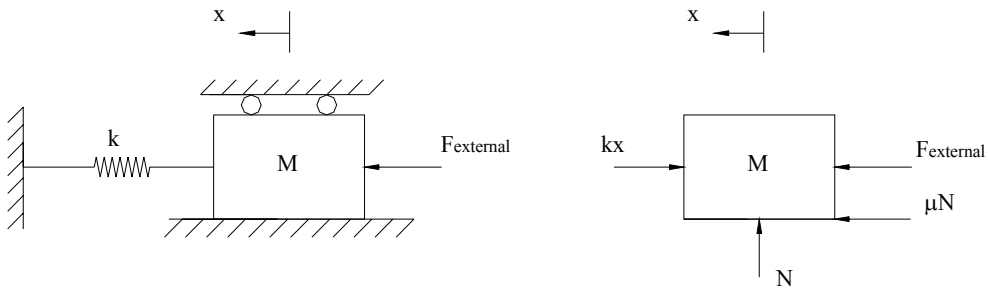

Figure 2-7 Schematic drawing and free body diagram

The forces acting on the moving mass are the spring force, the friction force and the external force applied by the shaker. The sum of these forces provides the inertial force. Therefore,

$$\sum F = m\ddot{x} = -F_{spring} - F_{friction} + F_{external} \ . \tag{2-16}$$

The acceleration and the applied external force are measured using an accelerometer and a force transducer, respectively. While for the system identification experiments, the spring is included in the damper, it is removed from the system for the friction force experiments. Therefore, by rearranging Equation 2-16 and taking out the spring force, it is possible to measure the friction force generated by the actuator. Therefore, the friction is given by,

$$F_{friction} = F_{external} - m\ddot{x} \ . \tag{2-17}$$

As is described in chapter three, Equation 2-17 is used to quantify the performance of the new semi-active friction damper. The acceleration and the external force are measured in order to compute the frictional force capabilities of the damper.

CHAPTER 3
EXPERIMENTAL SETUP

The objective of this experiment is to characterize the actuating ability of the piezoelectric actuator, which is implemented into a vibration isolator design. The isolator is excited at varying forcing amplitudes and frequencies while the normal force that the actuator applies is adjusted in order to control the damping of the system. This chapter will discuss how the experiments are set up and run.

3.1 Experimental Friction Damper Setup

The friction damper consists of several moving and stationary components as shown in Figure 3-1 and 3-2. A 0.75" diameter shaft is fixed to the base of the damper. Mounted to the shaft is the flextensional mechanical amplifier of the piezoelectric actuator. The moving components consist of the outer housing and the air bearing. The outer housing also comes in contact with the friction pads as it vibrates. The friction pads are fixed to both sides of the actuator so that the normal force that the actuator applies is symmetrical. The normal force provided between the friction pads and the outer housing induces a frictional load which retards the motion of the outer housing. Within this damper, there is also a spring which connects the moving housing to the stationary base. With the frictional pads not engaged, the air bearing provides a relatively frictionless contact surface. As a result, the damper is essentially an ideal SDOF system.

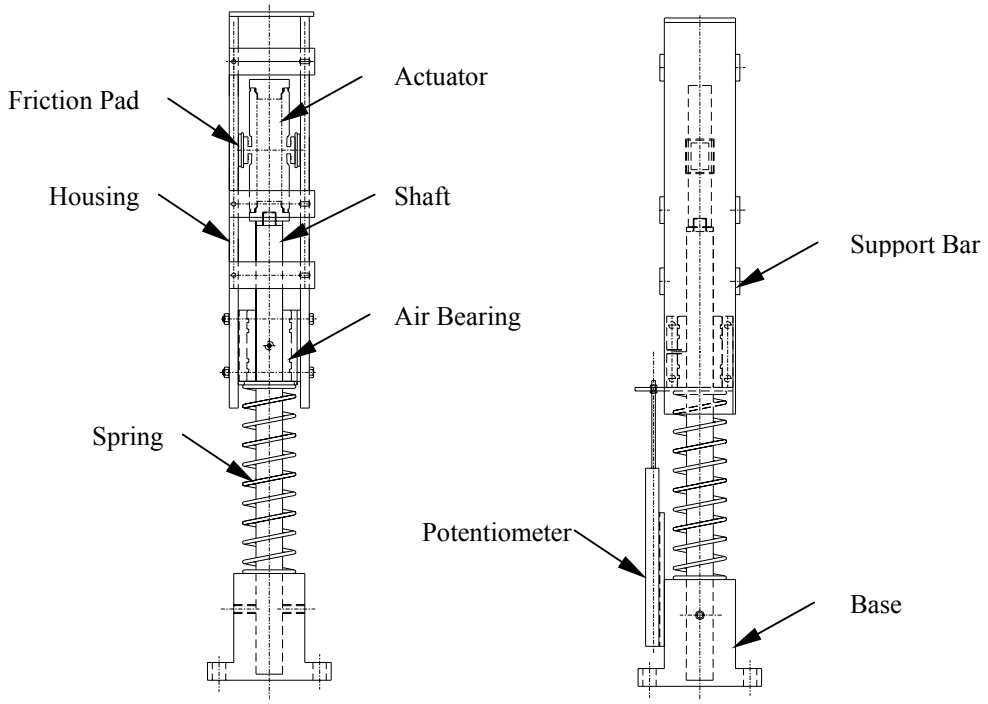

Figure 3-1 Friction damper (front and side view)

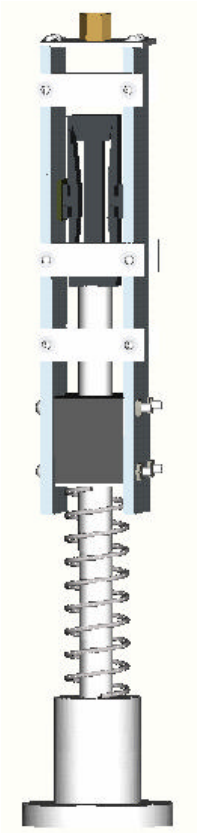

Figure 3-2 Friction damper (3D view)

3.1.1 Piezoelectric Actuator

The actuator that is used within this work is the FPA-1700 Low Voltage Piezoelectric Actuator by Dynamic Structures & Materials, LLC and it is shown in Figure 3-3. The actuator incorporates a shape memory alloy preload wire for bi-directional motion and a titanium flexure-based amplification mechanism. The mechanical amplifier allows for high displacement. The peak output stroke of the actuator when it is not loaded is about 1.6 mm. The displacement of the mechanism is transmitted through two parallel output plates. Wires are insulated with Teflon® for vacuum compatibility.

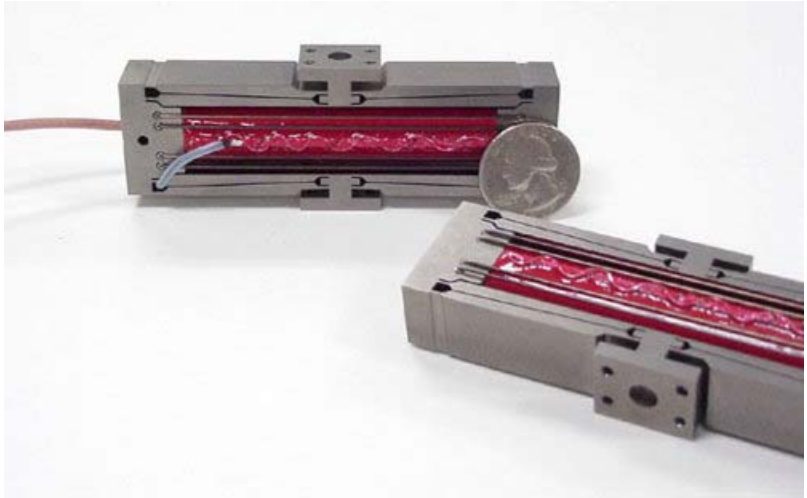

Figure 3-3 FPA-1700-LV piezoelectric actuator (Courtesy of Dynamic Structures & Materials, LLC)

The actuator has a mass of 175 g and its dimensions are 101 x 37 x 16.5 mm. The capacitance of the actuator is 30 μF and its resonance frequency is 105 Hz. It can exert a compressive blocked force of 145 N as shown in Figure 3-4 (Dynamic Structures & Materials, LLC).

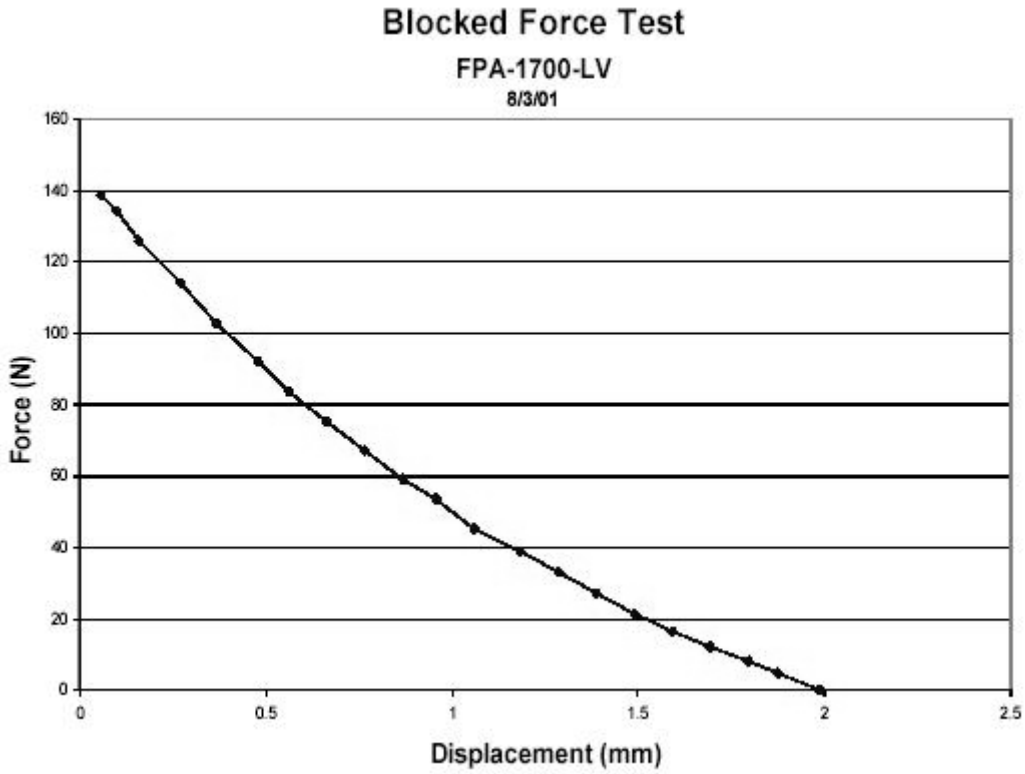

Figure 3-4 Block force test of FPA 1700-LV piezoelectric actuator (Courtesy of Dynamic Structures & Materials, LLC)

The maximum voltage that can be applied to the actuator is 150 V. The amplifier that is used to drive this actuator is the LV-1200 Low Voltage Transducer Driver by Dynamic Structures & Materials, LLC. It can provide a maximum peak current of 1.2 A. For this amplifier and the 30 μF load, the maximum frequency that the actuator can achieve without overloading the amplifier is 39 Hz.

3.1.2 Shaker

The shaker that is used to excite the vibration isolator is the PM Vibration Exciter Type 4808 from B&K. It has a force rating of 112 N and a frequency range of 5 Hz to 10 kHz. Its maximum displacement is 12.7 mm. The amplifier that is used to drive this

shaker is the Power Amplifier Type 2712 from B&K. The sine performance curves for the shaker are shown in Figure 3-5.

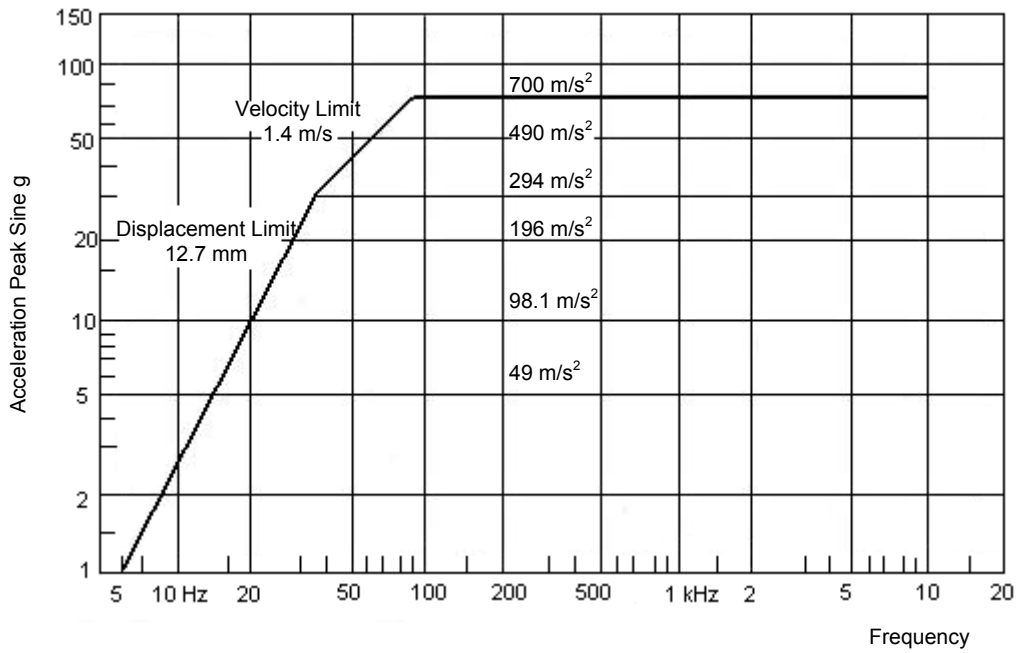

Figure 3-5 Sine performance curves for the Vibration Exciter Type 4808 (Courtesy of B&K)

A custom made aluminum stinger is used to transfer the force from the fixing hole at the center of the vibration table on the shaker. The stinger is threaded on one side to this fixing hole and to the force transducer on the other side.

3.1.3 Transducers

A force transducer, ICP® Force Sensor 208C02 from PCB Piezoelectronics as shown in Figure 3-6 a), is used to measure the force that is applied to the vibration isolator by the shaker. The force transducer is threaded onto the outer housing on one side and the stinger on the other side. It has a measurement range of 444.8 N for compression and tension and its sensitivity is 11.241 mV/N.

Two accelerometers, models 333B42 and 353B15 from PCB Piezoelectronics, were used to measure acceleration. The model 333B42, displayed in Figure 3-6 b), has a

sensitivity of 526 mV/g and it was used in calculating the friction force. Its signal was compared with the signal of the other accelerometer, which has a sensitivity of 9.85 mV/g, in order to verify its accuracy.

a) b)

Figure 3-6 Transducers a) PCB Accelerometer 333B4; b) PCB Force Sensor 208C02

A 20 kΩ linear potentiometer by Maurey Instrumentation Corp. was used to measure the displacement of the housing. 10 V DC was supplied to the potentiometer with HP's 3617A DC Power Supply.

3.1.4 Air Bearing

A cylindrical air bearing, model S301901, from New Way Machine Components was used with a 0.7500" diameter (+. 0000 / -. 0003) shaft. Air was supplied from a compressor at 80 psi pressure. Two sets of air filters (Eliminizer Combo from RTI) used, one after the compressor, the other one right before the bearing, to filter out any humidity in the air that was supplied to the bearing.

3.1.5 Other Parts

A stainless steel spring (S-467) from Century Springs was used. Its stiffness was calculated to be 1852 N/m. The friction pads are kevlar bike disc brake pads (CODA® QPDPAD/BLU) and the housing is stainless steel. The mass of the moving outer housing is 1.69 kg.

3.2 Experimental Vibration Isolator Setup

The vibration isolator has been designed so that the friction damper is fixed horizontally as shown in Figure 3-7 and 3-8. The base of the friction damper is screwed onto a vertical steel plate and the moving outer housing is connected to the shaker through the force transducer and the stinger. The shaker is bolted onto two steel plates. It is positioned so that the friction damper's line of symmetry is in line with the central fixing hole of the shaker. The potentiometer is fixed to the base of the friction damper on one side and the housing on the other. The accelerometers are fixed to the outer housing using wax.

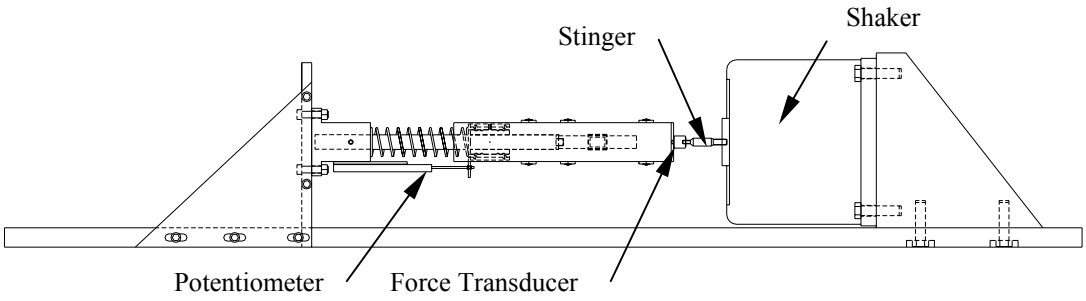

Figure 3-7 Friction damper with shaker and transducers (side view)

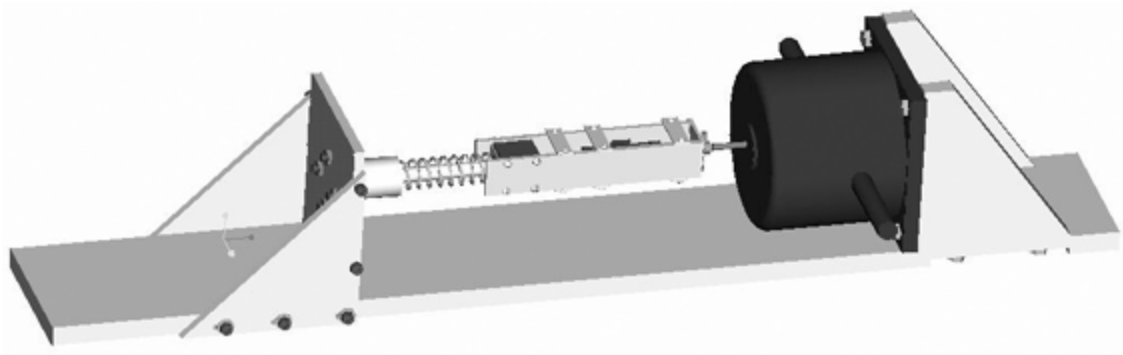

Figure 3-8 Friction damper with shaker and transducers (3D view)

The signals from all the transducers are fed to the DSPT SigLab (20-42) analyzer through the signal conditioner, model 482A16 from PCB Piezoelectronics, as displayed in Figure 3-9. The shaker input signal is generated with the SigLab analyzer. The air required by the air bearing is filtered through an air filter.

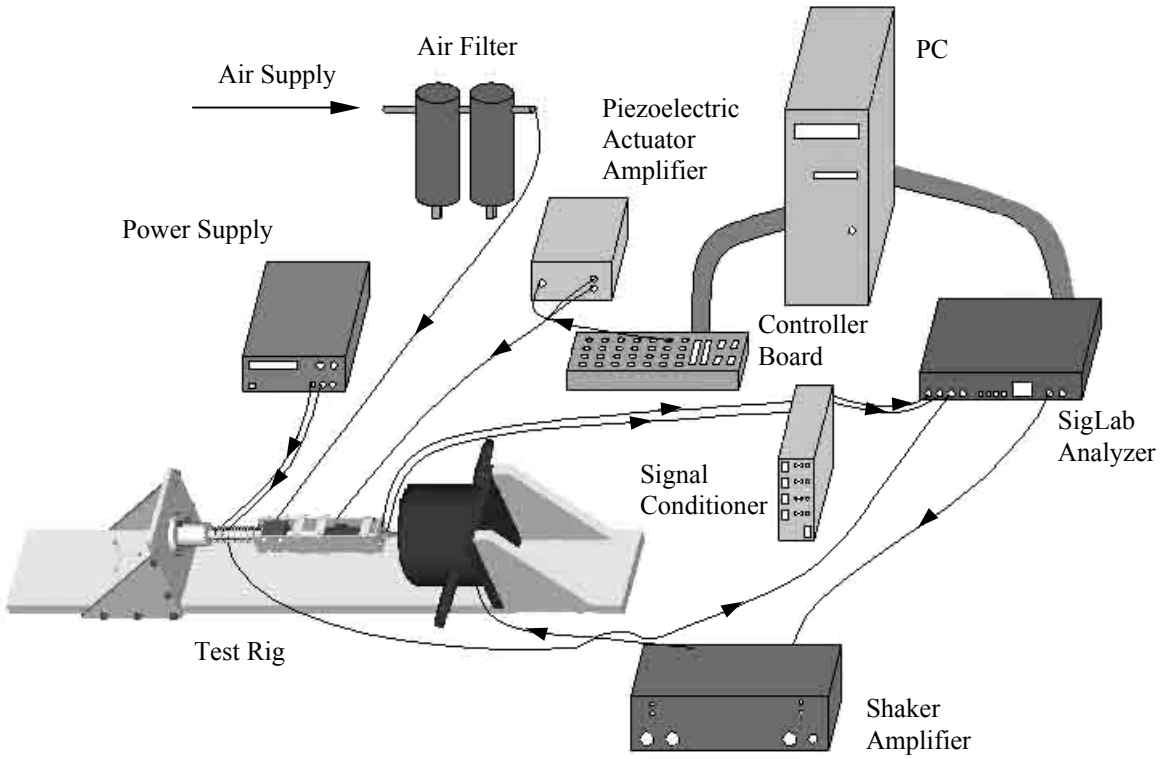

Figure 3-9 Experimental setup

The normal force controller is designed in Simulink®, a MATLAB® plug-in, and implemented in real-time through dSPACE. The actuator input signal is generated in dSPACE and output through the digital-to-analog converter (DAC) as shown in Figure 3-10. The actuator input signal can also be generated with the SigLab analyzer.

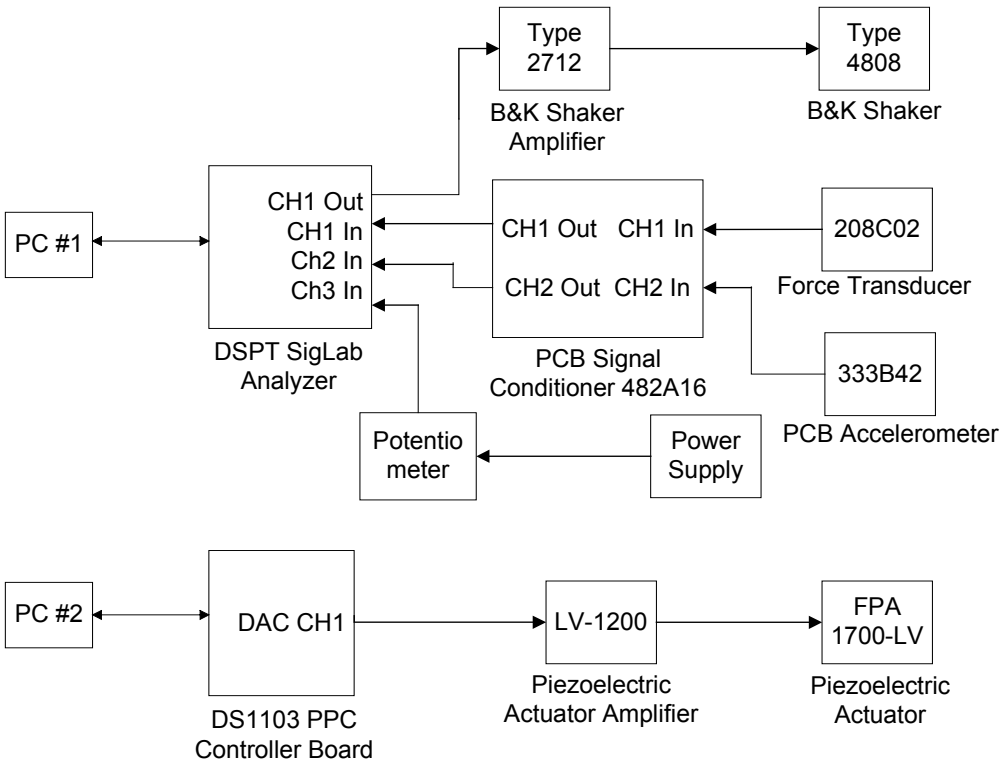

Figure 3-10 Schematic drawing of the experimental setup

3.3 Simulink® Model of the System

The tests results are presented in Chapter 4 were performed using the SigLab spectrum analyzer. However, the experiment setup can also be modeled in Simulink® as displayed in Figure 3-11 and implemented in real-time through dSPACE in order to verify the accuracy of the results.

The shaker input signal is generated in dSPACE and output through the digital-to-analog converter (DAC) channel five. When the damper is excited, the signals from the transducers are fed back to the analog-to-digital converter (ADC) channels of the DS1103 PPC controller board. A gain of 10 is added to all of these signals because dSPACE multiplies input signals by 0.1. The force transducer signal is input to channel four where it is multiplied by one over the sensitivity of the transducer in order the obtain the force

applied by the shaker to the friction damper. The potentiometer signal is input to channel eight where it is multiplied by the potentiometer gain to convert the displacement from volts to mm and then multiplied by the stiffness constant of the spring in order to obtain the spring force. The accelerometer signal is input to channel 12 where it is multiplied by one over the sensitivity of the transducer and the gravity to get the acceleration of the moving elements of the damper. The acceleration is then multiplied by the mass of the moving elements to obtain the inertial force. These values are then added based on Eq. 2-16 to obtain the friction force.

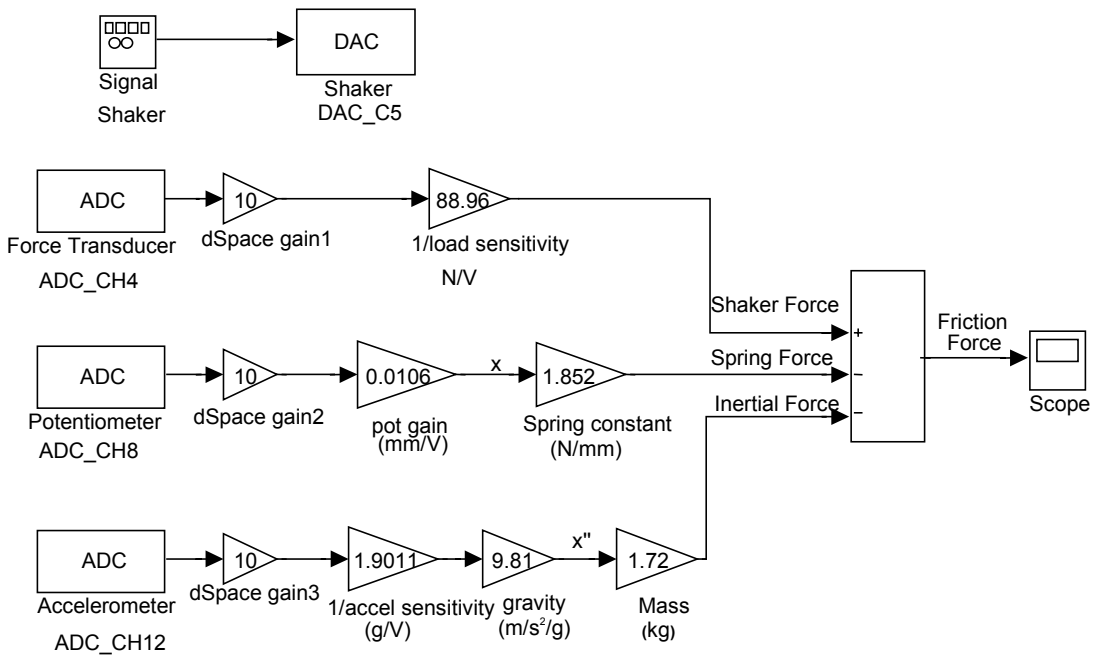

Figure 3-11 Schematic diagram of the calculation of the friction force

3.4 Experiments

3.4.1 Calibration of the Transducers

First of all, the accelerometers were calibrated using B&K's Calibration Exciter Type 4294. Then in order to make sure that the force transducer signal was correct, it

was compared with the acceleration signal. For this experiment, the friction pads have been removed so that there is negligible friction in the system. In this case, the force input to the system should be equal to the inertial force theoretically. The force transducer was calibrated based on the acceleration signal.

3.4.2 System Identification

In order to obtain the natural frequency of the system, the outer housing was excited first using a modal hammer (PCB model 086C03). There was no contact between the friction pads and the moving parts of the damper. Following, the outer housing was excited by giving an initial displacement of one inch and varying the normal force. After the natural frequency was determined, the mass of the moving elements of the friction damper was measured. For this purpose, a digital scale (Navigator™, model NOB110) was used. Then the stiffness of the system was calculated using the mass and the natural frequency values. The model that was acquired experimentally was compared with the theoretical model which was based on these values.

3.4.3 Determining the Displacement Capability of the Piezoelectric Actuator

In order to investigate the displacement capability of the actuator, an LVDT (D5/200HK from RDP Group) was used. The LVDT was connected to one side of the actuator and the displacement signal was input to the SigLab analyzer at varying frequencies of actuation. The maximum displacement of the actuator was determined by applying the maximum voltage of 150 V. To show that the displacement capability of the actuator was not strongly dependent on frequency, virtual swept sine (vss) tests were carried out at varying frequencies.

3.4.4 Varying the Damping Characteristics of the System

Finally, in order to observe how the normal force applied by the actuator alters the damping of the system, swept sine tests were performed at various frequencies (1-25 Hz) and actuator input voltages (0, 15, 30, 45 V) and when the friction pads were barely touching the outer housing. Transfer functions of acceleration over input force and phase angle vs. frequency plots were acquired.

3.4.5 Friction Force Experiments

Several experiments were carried out in order to characterize the friction induced by the actuator. First of all, with the only contact of the moving elements being the air bearing which has negligible friction, the force input and the inertial force were compared at various excitation amplitudes and frequencies. After this, applying an input voltage to the actuator, a normal force was exerted onto the outer housing through the friction pads. Tests were carried out by varying the actuator voltage (0, 30, 60, 90, 120, and 150 V), the shaker voltage (5, 7, and 9 V), and the shaker frequency (20, 25, and 30 Hz). The results of these experiments are presented in the appendix. The applied voltage to the actuator is sinusoidal and the frictional force is determined using Equation 2-17, by measuring the acceleration and the input force. From the results of these experiments, friction force amplitudes were compared. Finally, the actuator input voltage was controlled by dSPACE to vary the normal force linearly and in steps.

CHAPTER 4
RESULTS

This chapter presents the results obtained from analyzing the piezoelectric-based semi-active friction damper. First of all, the friction damper is analyzed to find out its natural frequency and stiffness. How the normal force applied by the piezoelectric actuator alters the damping characteristics of the system is investigated. Finally, the displacement and friction force capabilities of the actuator are characterized.

4.1 System Identification

To obtain the natural frequency of the damper, two methods are employed. In these tests, the friction damper is standing vertically.

4.1.1 Modal Hammer Test

For the first test, the damper is excited using a modal hammer. During this test, there is no contact between the friction pads and the outer housing. The air bearing provides a relatively frictionless contact. Therefore, when the damper is excited, it takes about one minute for the oscillations to decay as shown in Figure 4-1. As displayed in the autospectrum plot of the same experiment in Figure 4-2, the resonance peak occurs at 5.23 Hz. Therefore, the natural frequency of the damper is determined to be approximately 5.23 Hz.

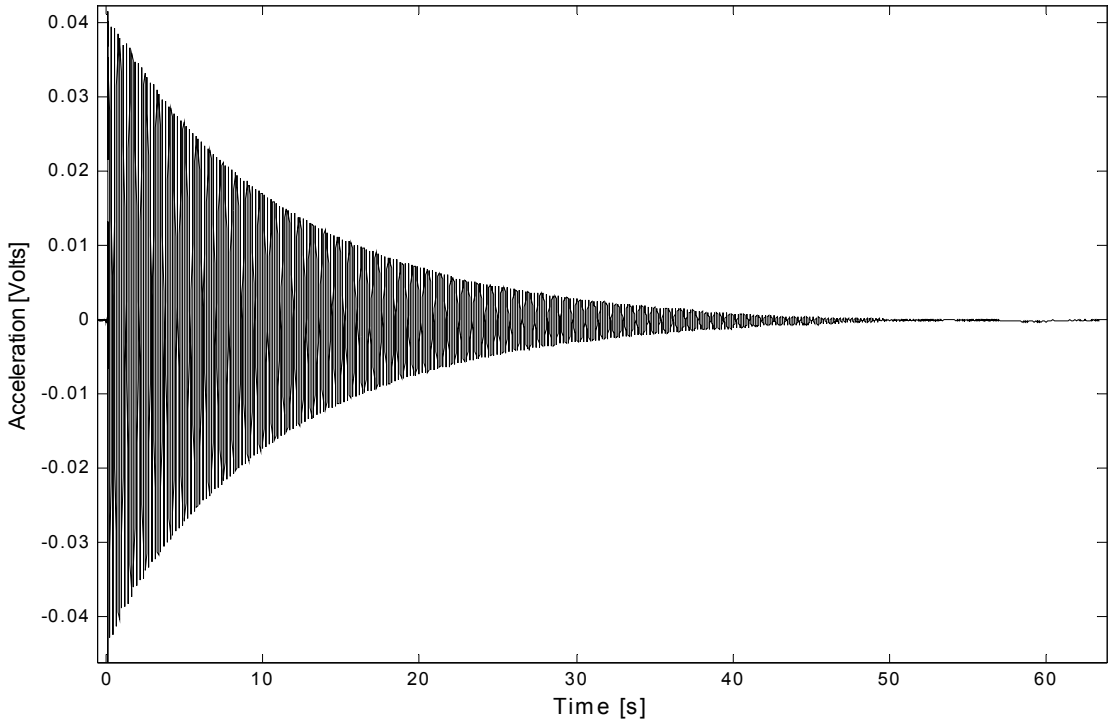

Figure 4-1 Modal hammer test

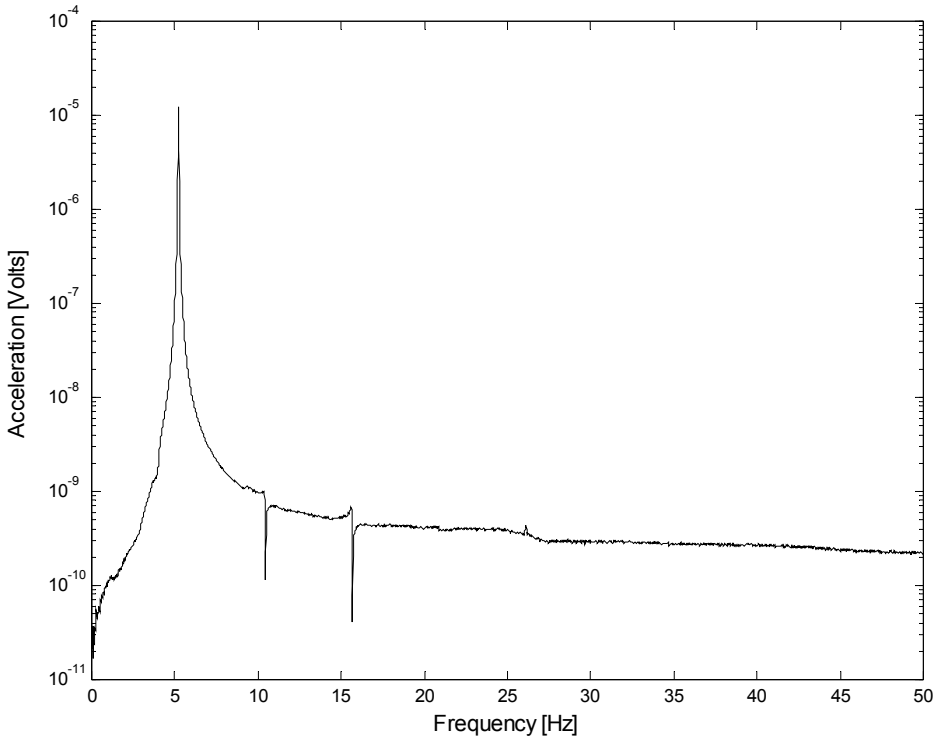

Figure 4-2 Autospectrum of modal hammer test

4.1.2 Initial Displacement Test

Another set of experiments is carried out by displacing the damper one inch. The difference between this experiment and the previous one is that the friction pads are introduced into the system and they are in contact with the outer housing. The degree of contact is determined by the voltage to the actuator. The damping of the system is altered when the normal force is varied by adjusting the actuator input voltage. The acceleration of the damper is displayed in Figure 4-3 when the outer housing is let go with an initial displacement of one inch at the actuator input voltages of 0, 25, and 50 V. The oscillations are highly damped for actuator voltages higher than 25 V as displayed in Figure 4-3 b) and c).

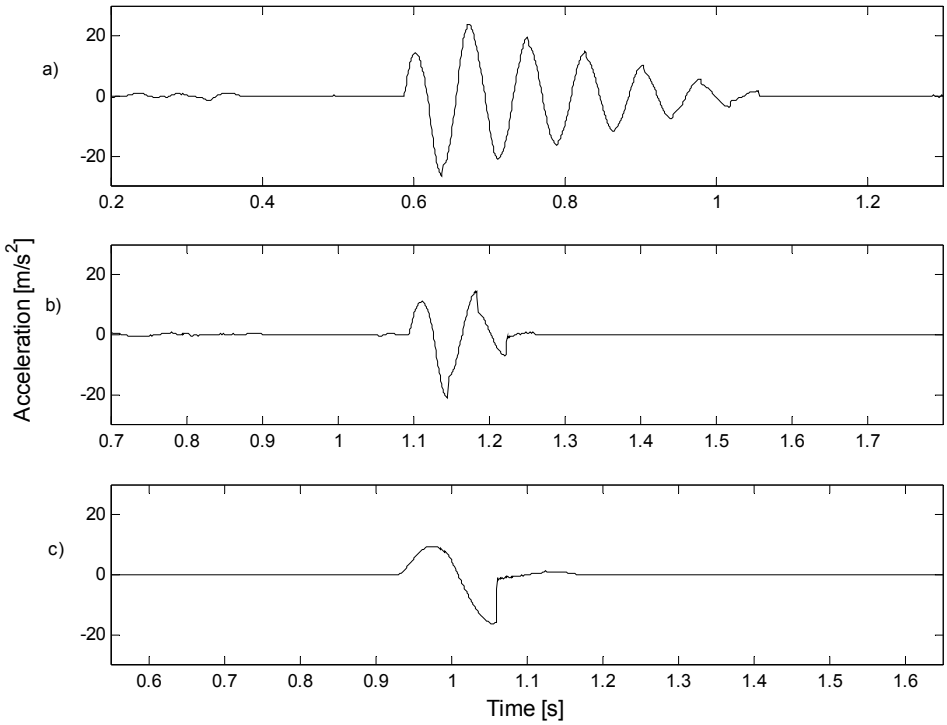

Figure 4-3 Response of the system to one inch initial displacement at actuator voltages of a) 0 V b) 25 V c) 50 V

The autospectrum plots of the same experiment are shown in Figure 4-4.

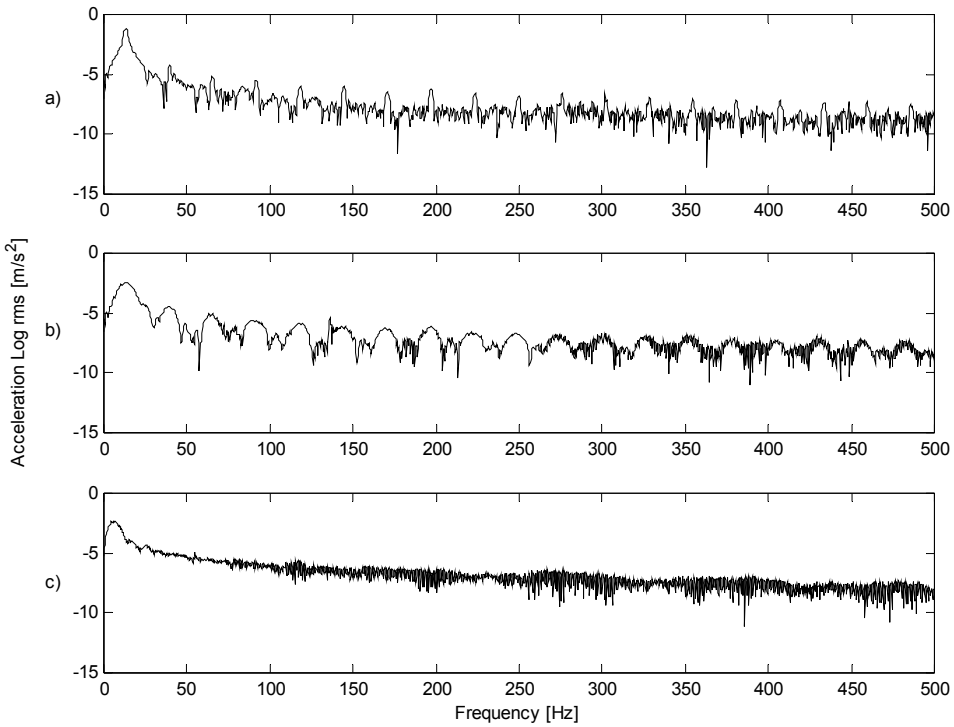

Figure 4-4 Autospectrum of the one inch initial displacement test at actuator voltages of a) 0 V b) 25 V c) 50 V

The natural frequency of the system was found to be 5.23 Hz previously. The total mass of the moving parts of the damper is 1.690 kg. To this, 1/3 of the mass of the spring (0.032 kg) is added to find the effective mass. Using the equation of natural frequency,

$$\omega_n = \sqrt{\frac{k}{M}} \tag{4-1}$$

the stiffness of the spring is found to be $k = \omega_n^{\ 2} \cdot M = (5.23 \cdot 2\pi)^2 \cdot 1.722 = 1859.5$ N/m.

Using this value of stiffness, the theoretical model is obtained and it is compared in Figure 4-5 to the experimental model displayed previously in Figure 4-2.

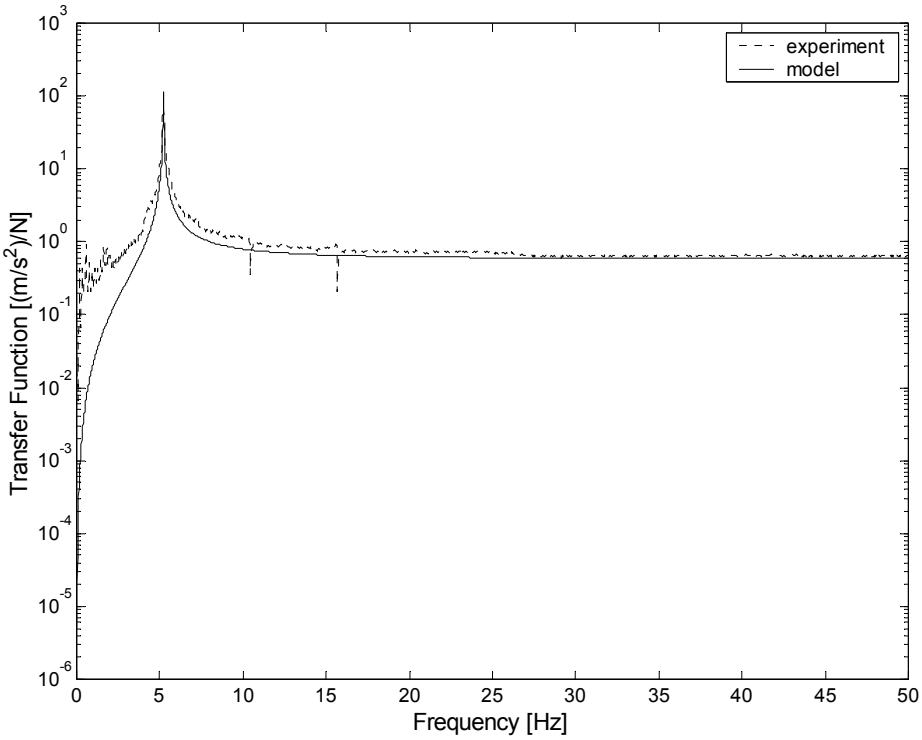

Figure 4-5 Comparison of the theoretical and experimental models

4.1.3 Determining the Displacement Capability of the Piezoelectric Actuator

In order to find out the displacement capability of the FPA 1700-LV actuator, an LVDT is attached one side of the actuator. The actuator is operated at 150 V and various frequencies while the displacement signal is input to the SigLab analyzer. It is observed that the displacement of the actuator remains fairly constant with varying frequency. The swept sine test results for 1-6 Hz are displayed in Figure 4-6. The displacement of the actuator with the maximum allowable voltage (150 V) applied is approximately 0.8 mm as shown in Figure 4-7. Note that this is the displacement on one side of the actuator, but the actuator has two parallel output plates, one on each side. Therefore, the total displacement of the actuator is twice that which is 1.6 mm. This agrees with the specifications provided by Dynamic Structures & Materials, LLC which gives the maximum displacement stroke of the actuator to be 1.7 mm ± 10%.

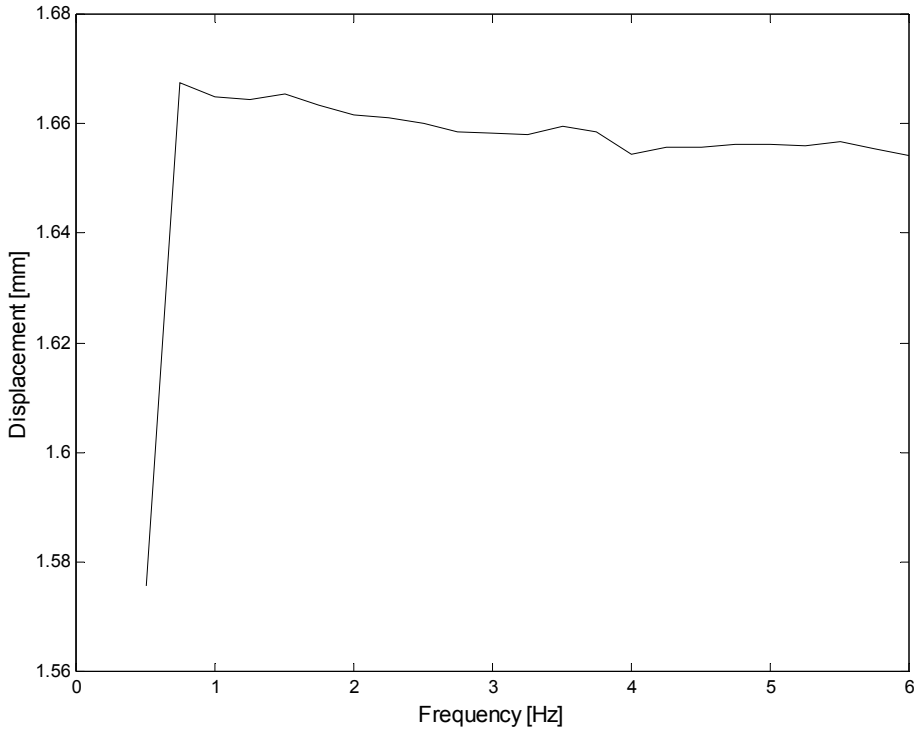

Figure 4-6 Swept sine test of the actuator's displacement capability

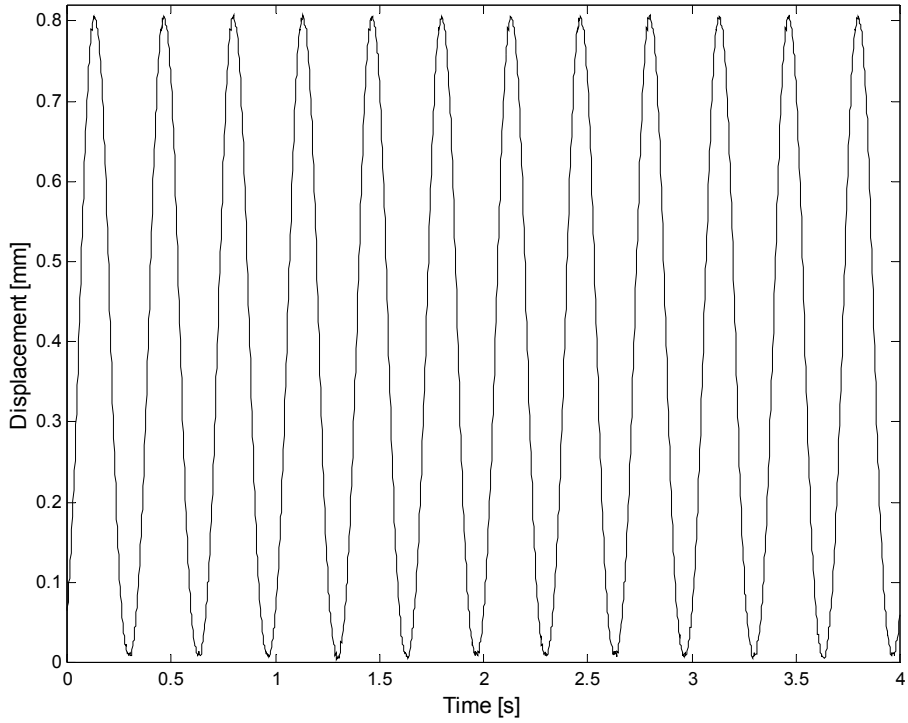

Figure 4-7 Displacement capability of one side of the actuator at 3 Hz

4.2 Varying the Damping Characteristics of the System through the Actuator

In order to observe how the normal force applied by the actuator alters the damping of the system, swept sine tests are performed from 0 to 25 Hz when the friction pads are barely touching the outer housing and also at several actuator input voltages (0, 15, 30, and 45 V). Note that the friction force is higher for the actuator input voltage of 0 V than when the friction pads are barely touching the outer housing. The transfer function of acceleration with respect to force is displayed in Figure 4-8 for the swept sine test. The graph indicates how the normal force applied to the actuator effectively alters the damping characteristics of the system. The phase angle obtained from the same experiment and the coherence data are shown in Figure 4-9 and 4-10, respectively. At frequencies below 1 Hz, the force applied by the shaker is unable to move the friction damper when the friction pads are engaged. This causes the loss of coherence at lower frequencies.

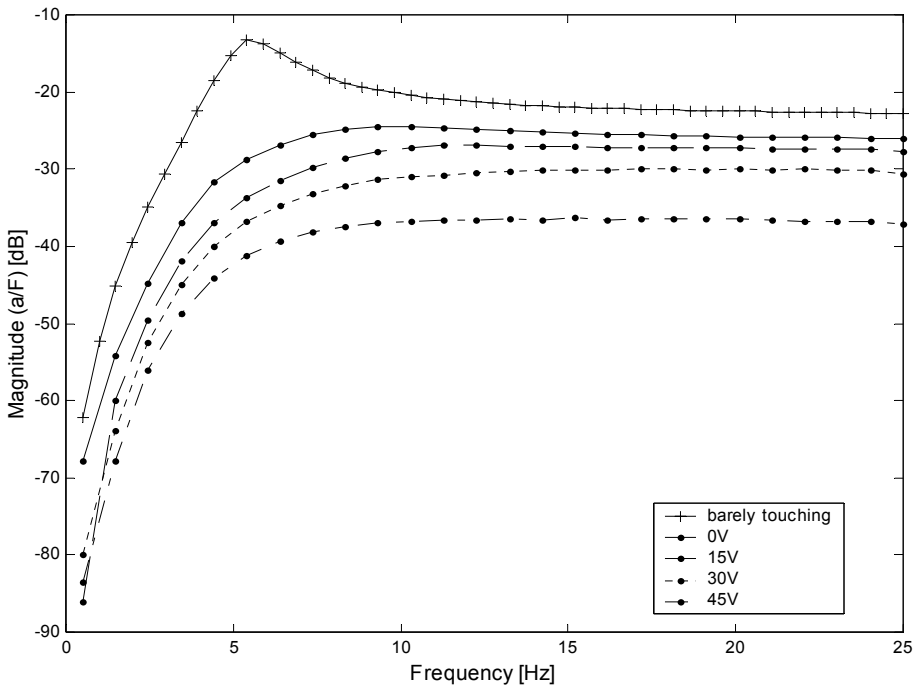

Figure 4-8 Magnitude of acceleration over excitation force from swept sine test

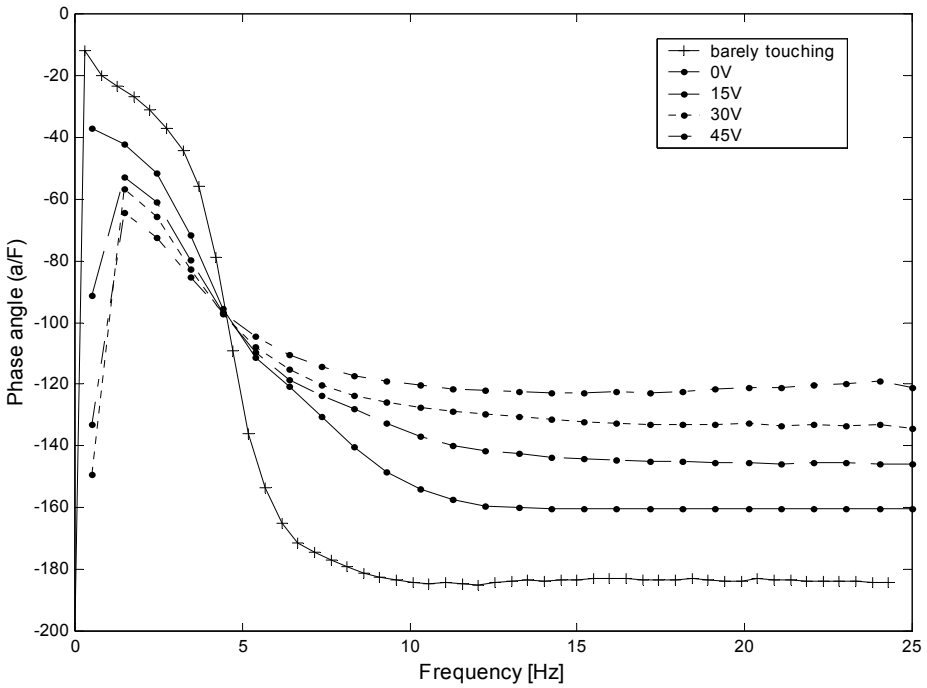

Figure 4-9 Phase angle of acceleration over excitation force from swept sine test

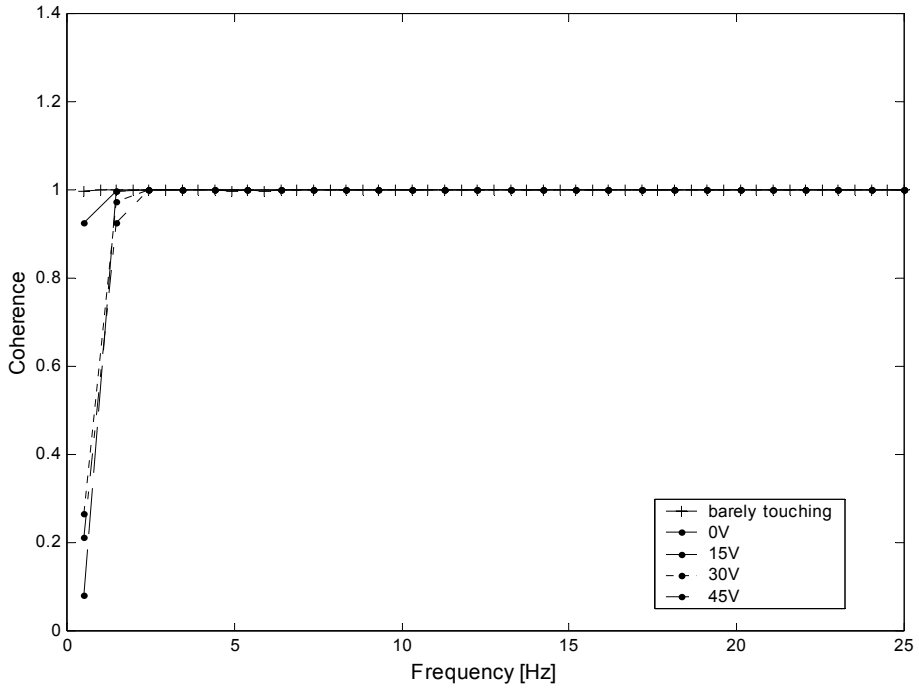

Figure 4-10 Coherence data of the swept sine test

4.3 Friction Force Capability of the Base Damper

Several experiments are carried out in order to characterize the friction force capability of the novel piezoelectric-based isolator.

4.3.1 Determining the Experimental Uncertainty of the Measurements

Experiments are performed with the spring and the friction pads removed from the system. In this case, the only source of friction is the air bearing which is negligible. Therefore, from Equation 2-17, the force input to the system by the shaker has to be equal to the inertial force when there is no friction. In other words, the resulting friction force in Figure 4-11, which is the difference between the input force and the inertial force, ideally has to be equal to zero.

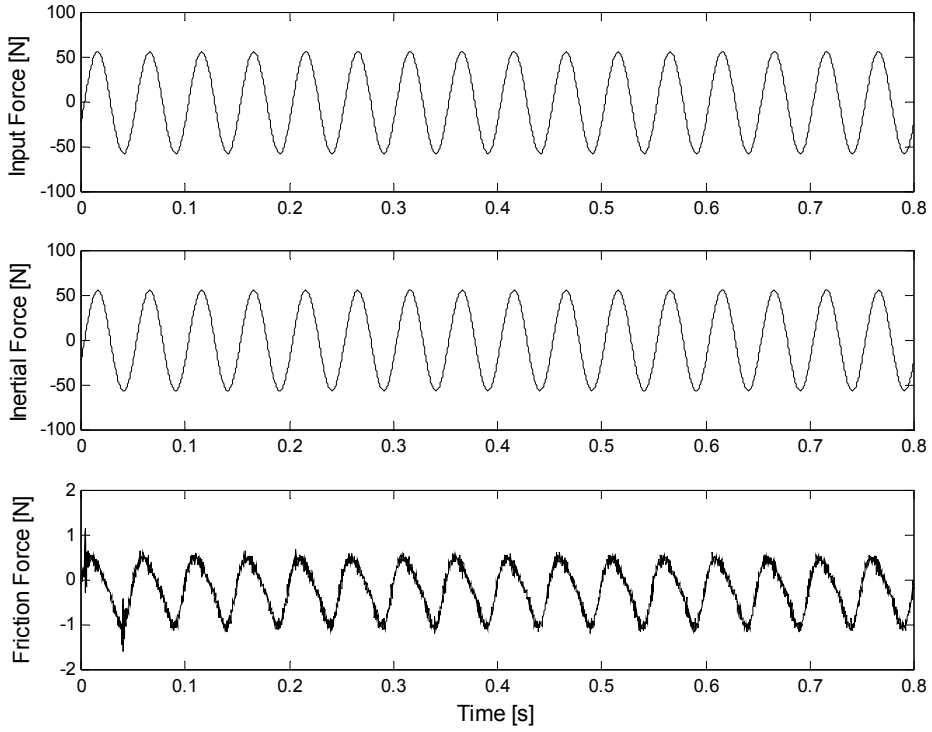

Figure 4-11 Input force, inertial force and the resulting friction force at 5 V shaker input voltage and 20 Hz excitation frequency with no contact of the friction pads

However, it is seen that the friction force in Figure 4-11 has a value of less than ± 1 N and this is caused by the inaccuracy of the transducer signals plus the friction in the air bearing. This defines the uncertainty of the measurements and the results in this work are not more accurate than ± 1 N.

4.3.2 Calculation of the Friction Force for Varying Normal Force, Excitation Amplitude and Frequency Values

In the following tests, the friction pads are in contact with the outer housing and the spring is removed. Therefore, the difference between the input force and the inertial force yields the friction force induced by the actuator. The results of the experiments for a shaker input voltage of 9 V, excitation frequency of 20 Hz and several values of actuator input voltage (0, 30, 60, 90, 120 V) are displayed in Figures 4-12 to 4-16. In the inertial force plot, the oscillations caused by stick-slip are present after each peak. The peaks of acceleration correspond to moments of zero velocity when the velocity changes direction and the static friction force has to be overcome for the motion to start again. In other words, the motion comes to a stop and the start-up of sliding is impeded which causes a sharp drop in the acceleration. When the static friction force is exceeded, the stored potential energy is released in the system and a rapid acceleration occurs. As the motion slows down to match the externally imposed sliding velocity, the acceleration drops again. This process, which repeats until a certain sliding velocity is reached, is the cause of the oscillations seen in the inertial force and the corresponding friction force plots in Figures 4-12 to 4-16. The amplitude of the stick-slip oscillations increases with increasing friction force.

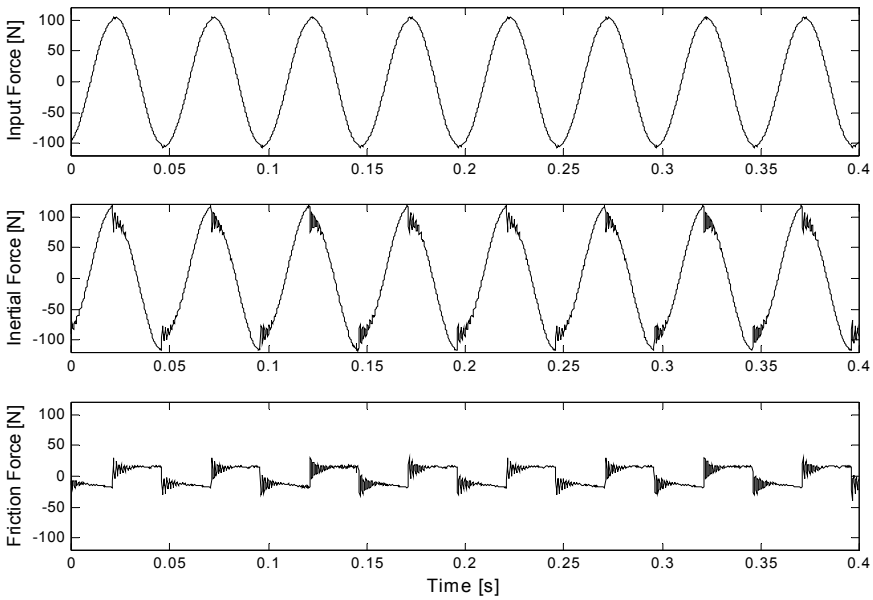

Figure 4-12 Input force, inertial force and the resulting friction force at 0 V actuator input voltage, 9 V shaker input voltage and 20 Hz excitation frequency

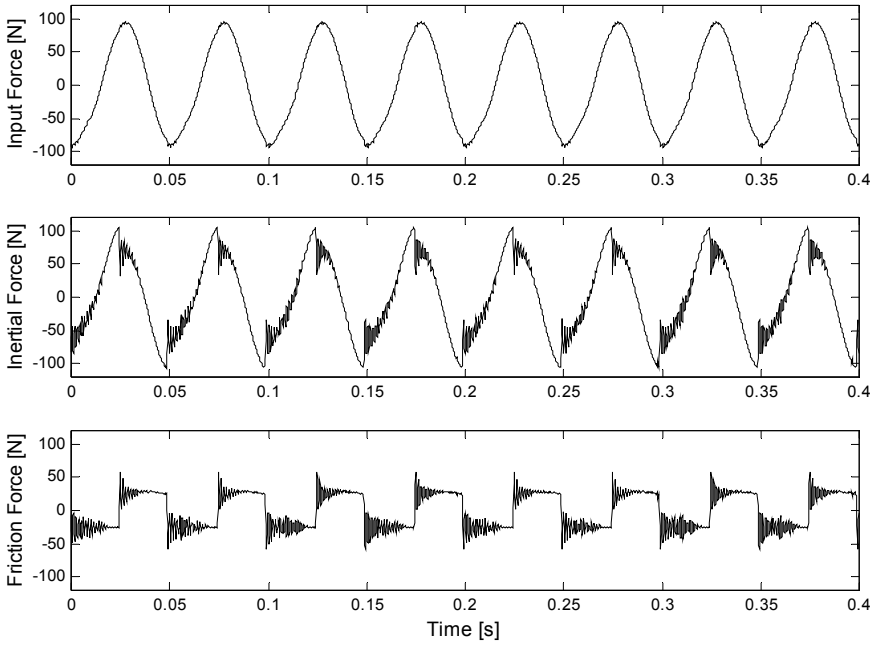

Figure 4-13 Input force, inertial force and the resulting friction force at 30 V actuator input voltage, 9 V shaker input voltage and 20 Hz excitation frequency

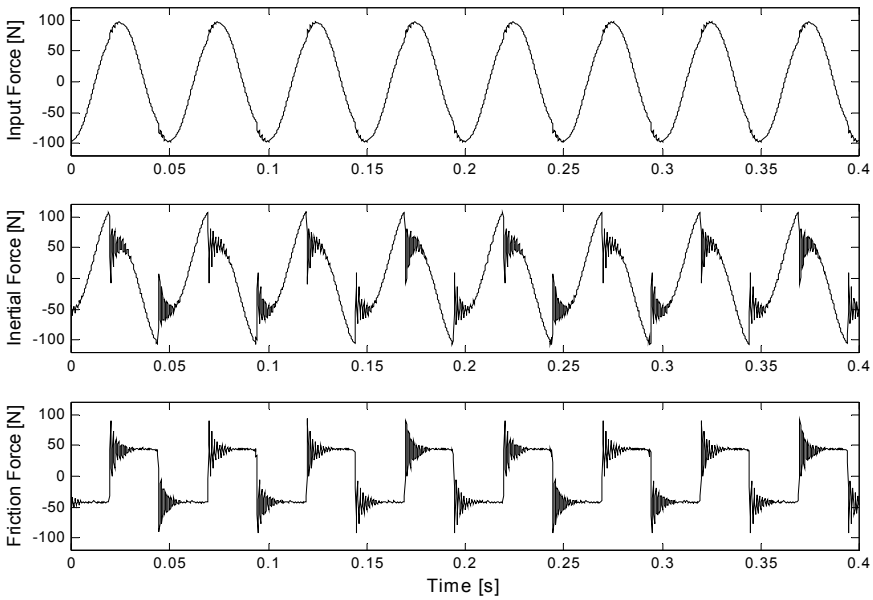

Figure 4-14 Input force, inertial force and the resulting friction force at 60 V actuator input voltage, 9 V shaker input voltage and 20 Hz excitation frequency

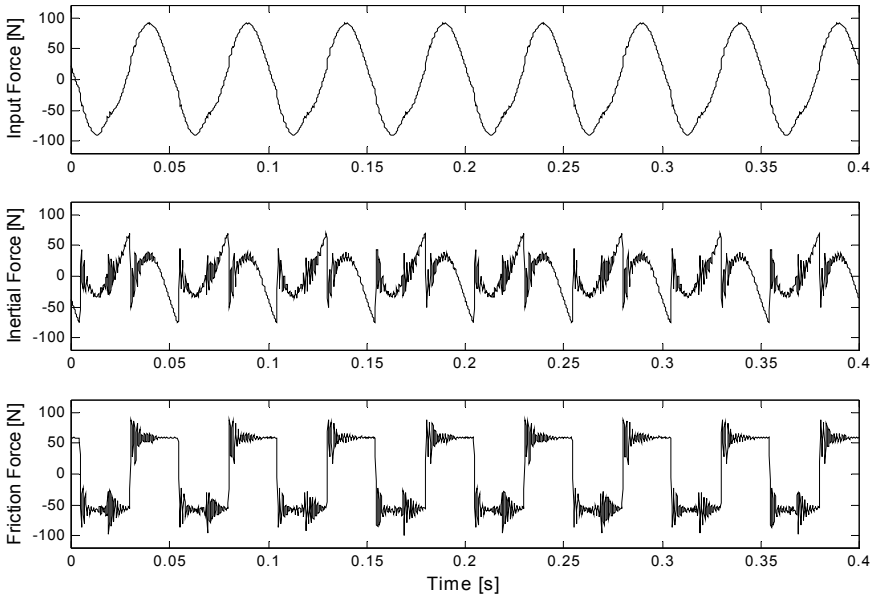

Figure 4-15 Input force, inertial force and the resulting friction force at 90 V actuator input voltage, 9 V shaker input voltage and 20 Hz excitation frequency

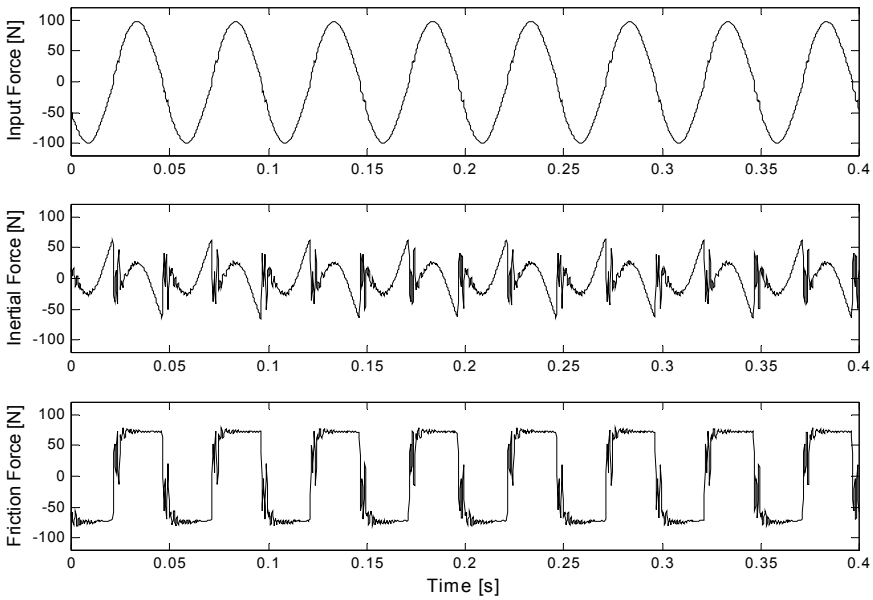

Figure 4-16 Input force, inertial force and the resulting friction force at 120 V actuator input voltage, 9 V shaker input voltage and 20 Hz excitation frequency

Similar tests to those shown in Figures 4-12 to 4-16 are repeated at shaker input voltages of 5, 7, and 9 V and at excitation frequencies of 20, 25, and 30 Hz. The results of these experiments are provided in the appendix. For all these experiments, the mean values of the amplitude of the friction force are calculated using MATLAB®. These values are plotted against the corresponding values of input actuator voltage separately according to the voltage applied to the shaker and the frequency of the excitation. The mean amplitudes of the friction force induced by the actuator with varying actuator input voltage are shown in Figure 4-17.

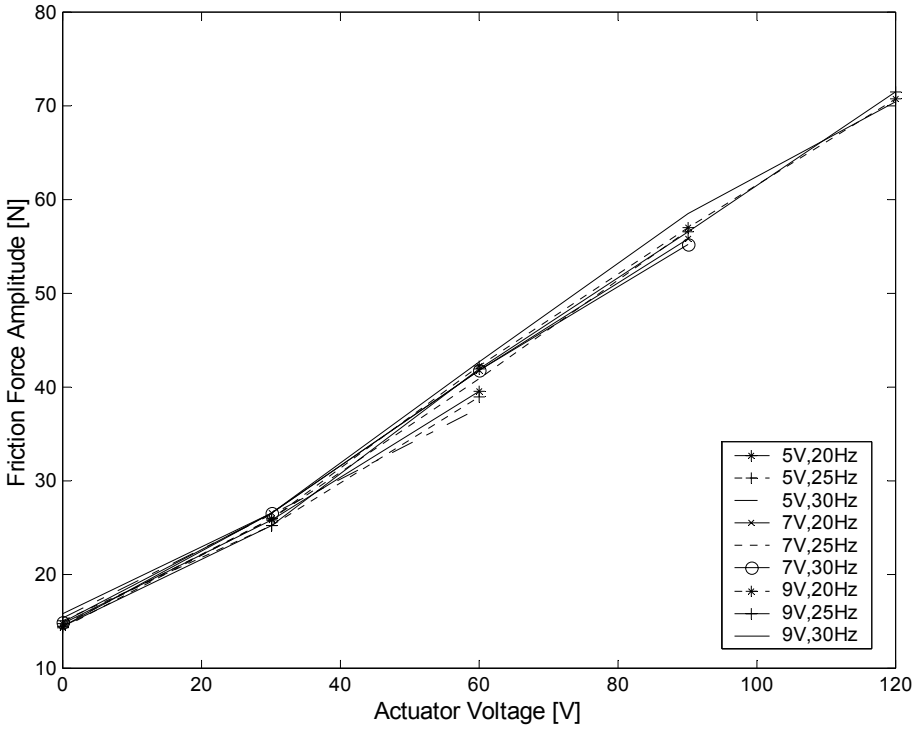

Figure 4-17 Friction force amplitudes at varying excitation amplitudes

For a shaker input voltage of 5 V, the damper ceases to move for actuator input voltages higher than 60 V. Therefore, only the values up to 60 V of actuator input voltage are included in this plot for a shaker input of 5 V. For 7 and 9 V shaker voltages, the damper ceases to move for actuator input voltages higher than 90 and 120 V, respectively. Therefore, even though the maximum voltage that can be applied to the actuator is 150 V, only the data that is relevant is included in this plot and the data which corresponds to the periods of sticking are excluded. It is seen that the friction force induced by the piezoelectric actuator has a fairly linear character and it does not vary much with the amplitude and the frequency of the excitation. If the data in Figure 4-17 is extrapolated , the maximum value of the friction force that can be induced by the friction damper is found to be approximately 85 N at 150 V of actuator input voltage. To show that the friction force is not dependent on frequency, friction force plots at varying

frequencies are compared. Figure 4-18 shows the friction force plots at shaker input voltage of 9 V, actuator input voltage of 60 V and varying frequencies.

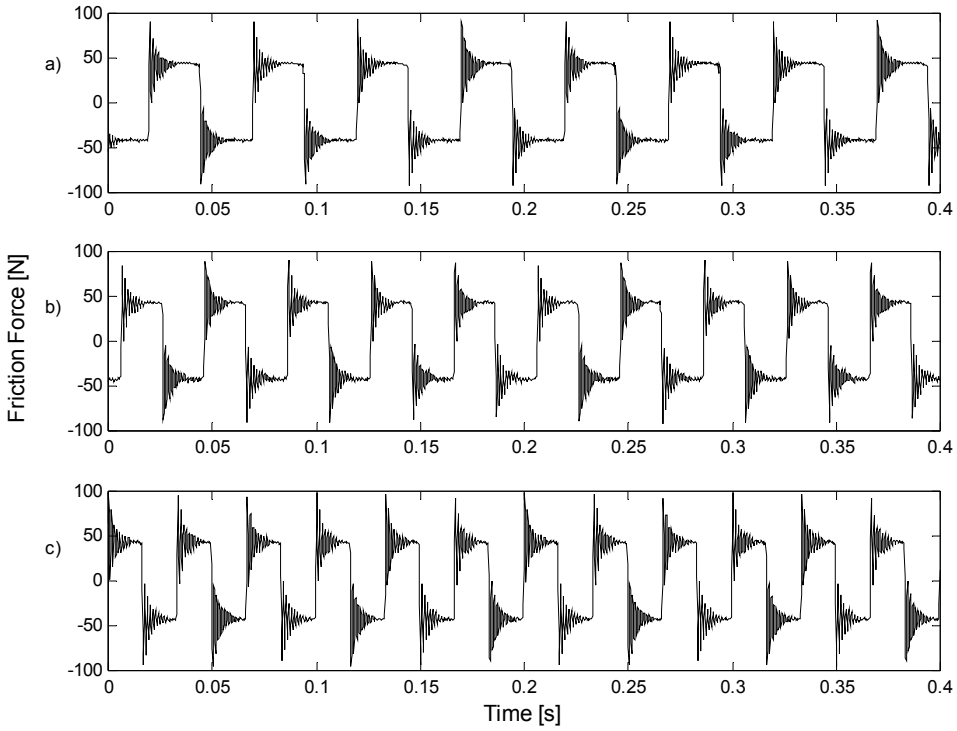

Figure 4-18 Comparison of the friction force at frequencies of 20 Hz b) 25 Hz c) 30 Hz

4.3.3 Controlling the Normal Force

In the final experiments that are conducted, the normal force is controlled using dSPACE. The actuator input voltage is increased in steps, starting from 0 V and ending at 150 V, and then returning to 0 V in increments of 15 V. The duration of each step is 1 second. The result is shown in Figure 4-19.

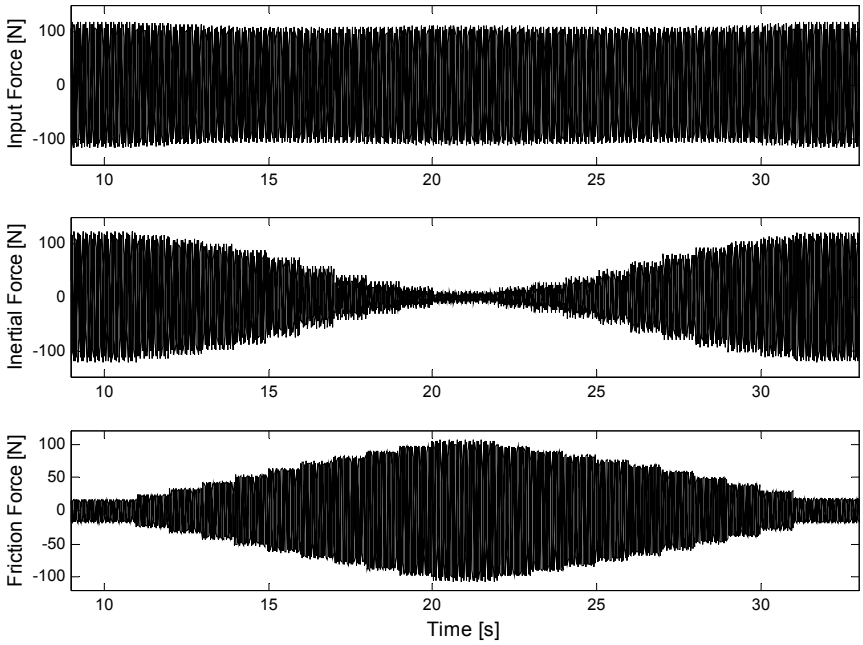

Figure 4-19 Friction force capability of the actuator when the actuator input voltage is varied in steps

The same experiment is repeated, but instead the actuator input voltage is increased linearly from 0 V to 150 in about 10 seconds and then decreased again linearly from 150 V to 0 V. As shown in Figure 4-20, the friction force increases linearly with the actuator input voltage.

The friction force values that are read in Figure 4-19 and 4-20 are slightly higher than the ones shown in Figure 4-17. This is due to the fact that the mean values are presented in Figure 4-17 where as Figure 4-19 and 4-20 show the peak values which are caused by the stick-slip phenomenon. When the direction of the motion is reversed, there is a sudden drop in acceleration due to sticking which lasts until the moving body overcomes the static friction force and starts to accelerate in the opposite direction. The drop in the acceleration causes an equivalent increase in the friction force which is seen as a peak. This is the reason why the friction force amplitudes in Figure 4-19 and 4-20

are approximately 10 N higher than the mean values of friction force displayed in Figure 4-17.

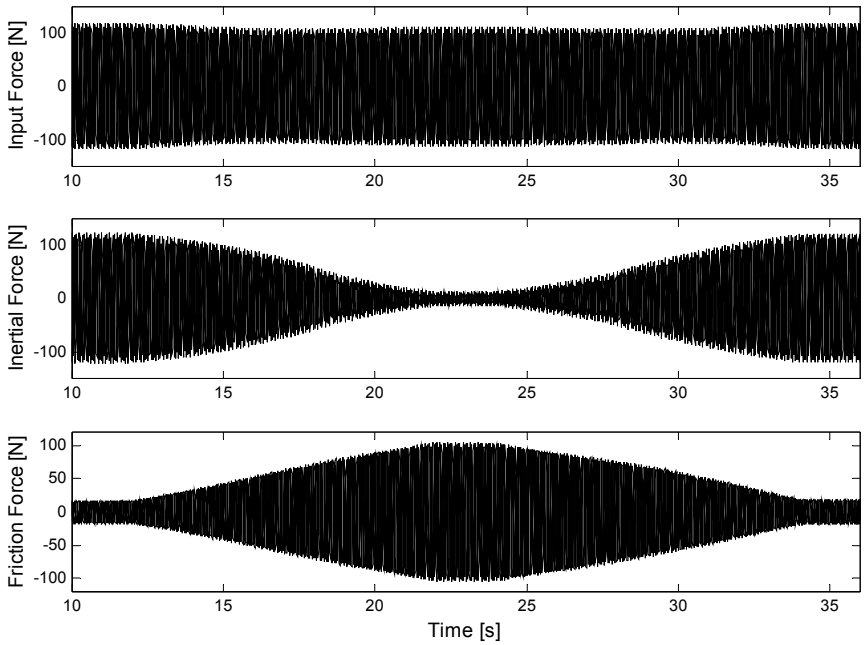

Figure 4-20 Friction force capability of the actuator when the actuator input voltage is varied linearly

4.3 Summary of Results

A summary of the results from the experiments carried out is shown in Table 4-1 and 4-2.

Table 4-1 Summary of system parameters

Natural Frequency of System	5.23 Hz
Stiffness of System	1859.5 N/m
Max. Displacement of Actuator	1.6 mm
Max. Stroke of Vibrations	12.0 mm
Max. Friction Force Induced by Isolator	85 N

Table 4-2 Friction force amplitudes at various shaker voltages and excitation frequencies

		FRICTION FORCE AMPLITUDES (N)								
Shaker Voltage		5 V			7 V			9 V		
Frequency		20 Hz	25 Hz	30 Hz	20 Hz	25 Hz	30 Hz	20 Hz	25 Hz	30 Hz
Actuator Voltage (V)	0	14.8	15.0	15.3	14.5	14.7	15.0	14.3	14.4	15.7
	30	25.8	25.3	26.4	26.6	26.0	26.6	26.6	25.2	26.5
	60	39.6	39.0	37.8	41.8	40.9	41.7	42.2	42.0	42.7
	90	36.4	36.3	36.6	55.8	56.8	55.2	57.1	56.6	58.6
	120	36.3	36.3	36.8	51.1	51.3	51.4	70.4	71.4	70.5
	150	36.3	36.2	36.5	50.8	50.8	51.2	60.4	60.6	61.0

CHAPTER 5
SUMMARY AND CONCLUSIONS

A new type of semi-active friction-based damper has been developed and has the potential to be used in several active vibration control applications. The heart of the damper is a piezoelectric stack with a mechanical amplifying mechanism. Within this work the frictional force capabilities of the actuator have been characterized experimentally.

5.1 System Identification

Before the friction damper could be analyzed, the transducers needed to be calibrated. First, the accelerometers were calibrated and the force transducer was calibrated based on the acceleration signal. The natural frequency and the stiffness of the system were found and based on these results, it was shown that the experimental hardware is well represented by a single degree of freedom model.

In order to find the displacement capability of the piezoelectric actuator, an LVDT was attached to the mounting plate on one side of the actuator and the displacement was measured for a variety of frequencies at the maximum actuator input voltage of 150 V. It was determined that the maximum displacement of the actuator is approximately 1.6 mm. This corresponds to a mechanical strain of about 5 %. Given the fact that the maximum mechanical strain of traditional piezoelectric actuators does not exceed 0.1 %, the displacement enabled by the use of a flextensional mechanical amplifier makes this piezoelectric actuator a natural candidate in practical applications

where high force and bandwidth capability as well as displacement capability are required.

Finally, by adjusting the normal force applied by the piezoelectric actuator, it was shown that the actuator effectively alters the damping characteristics of the system.

5.2 Tests Investigating the Friction Force Capability of the Piezoelectric-Based Damper

First of all, the friction pads and the spring were removed from the friction damper and in order to find the uncertainty of the system, the transducer signals were compared. Secondly, the friction pads were put back into the system and the friction damper was excited at various input voltages (5, 7, and 9 V) and frequencies (20, 25, and 30 Hz) while the normal force applied was adjusted by changing the actuator input voltage (0, 30, 60, 90, 120, and 150 V). The friction force was determined from these tests. When the results were compared, it was seen that the frictional force amplitude is not strongly dependent on frequency and is approximately linear with applied voltage. It was determined that the maximum force capability of the actuator is approximately 85 N for the specific friction pads used.

Finally, the normal force was controlled. The actuator input voltage was increased in steps and linearly and resulted in a similar response in the measured friction force.

5.3 Future Work

The friction damper can potentially be improved by changing the piezoelectric actuator used in this work to another that has better actuating capability. The new relaxor ferroelectric single crystals (PZN-PT and PMN-PT) may be a potential candidate compared to conventional piezoceramics. This material can develop strains in excess of 1% and has ~5 times the strain energy density of conventional piezoceramics. Taking

advantage of a flextensional amplifier similar to the one used in this work, the displacement capability of the actuator may greatly be enhanced.

Using velocity and displacement transducers, feedback control may be utilized to adjust the normal force applied by the actuator in order to increase energy dissipation. To start with, a simple control algorithm where the normal force is related to the slip and slip rate may be used. This algorithm increases the friction force as slippage increases.

The next step in this research is to incorporate this frictional damper in a practical application to control vibrations and enhance energy dissipation. One possible application is the special 6-6 platform shown in Figure 5-1. A friction damper could be implemented in each of the six legs of the platform.

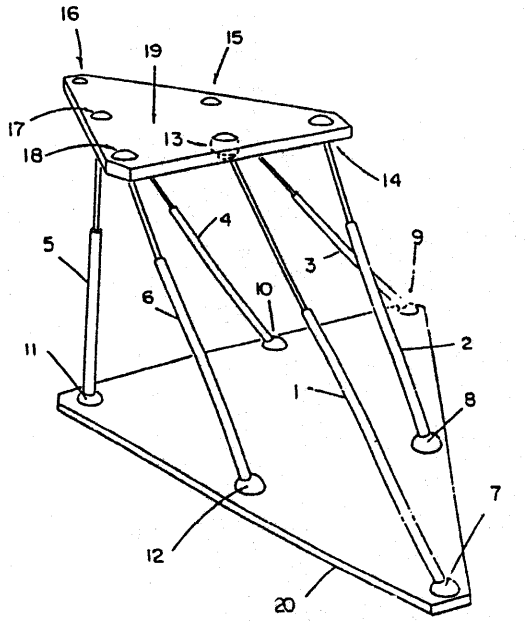

Figure 5-1 Special 6-6 platform

The developed friction damper can also be used to control the vibration of buildings, bridges, heavy machinery, and is especially well suited for operation in space (vacuum) environments and applications requiring large stroke and high bandwidth.

APPENDIX
TESTS EVALUATING THE FRICTION FORCE CAPABILITY OF THE PIEZOELECTRIC ACTUATOR

The appendix contains the results of the experiments performed to determine the friction force at varying excitation amplitudes and frequencies that were not included in the body of the text (see section 4.2).

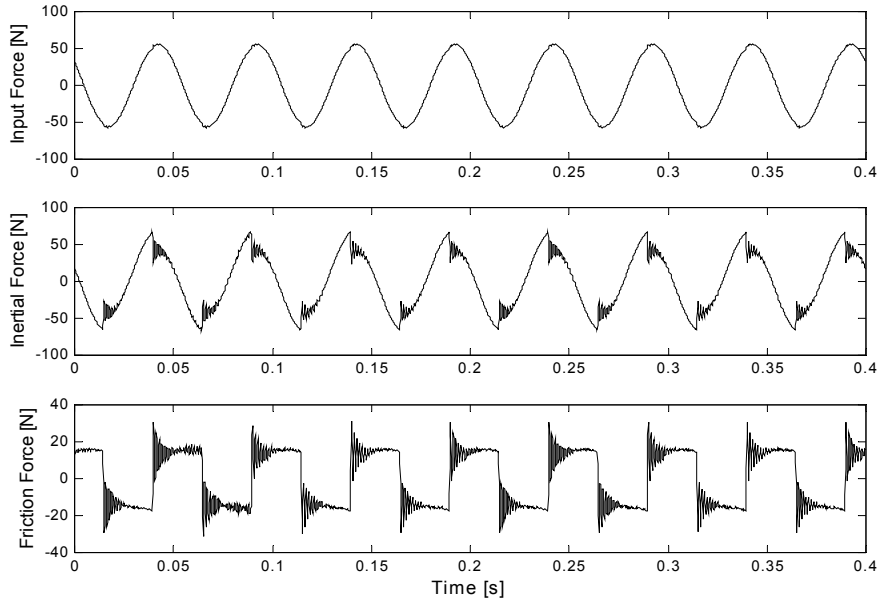

Figure A-1 Results at 0 V actuator voltage, 5 V shaker voltage and 20 Hz frequency

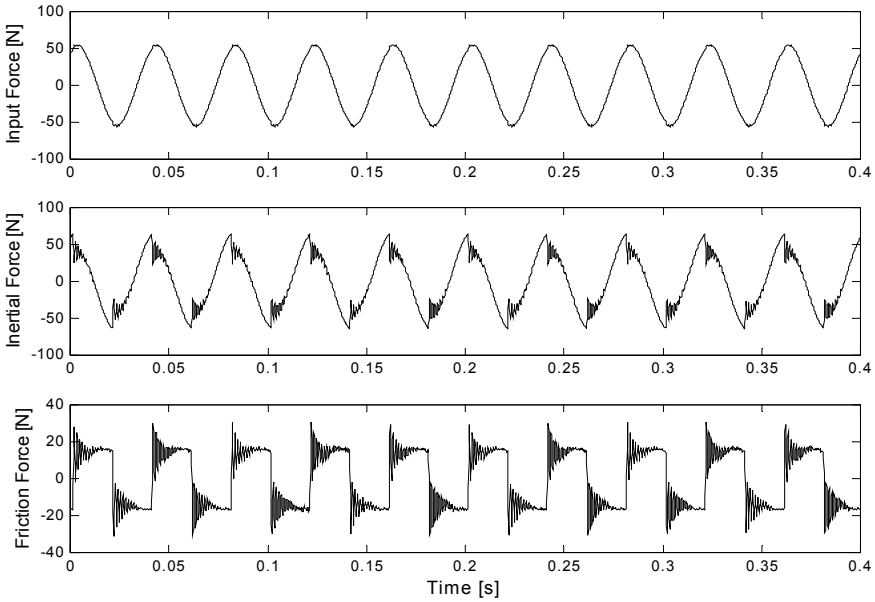

Figure A-2 Results at 0 V actuator voltage, 5 V shaker voltage and 25 Hz frequency

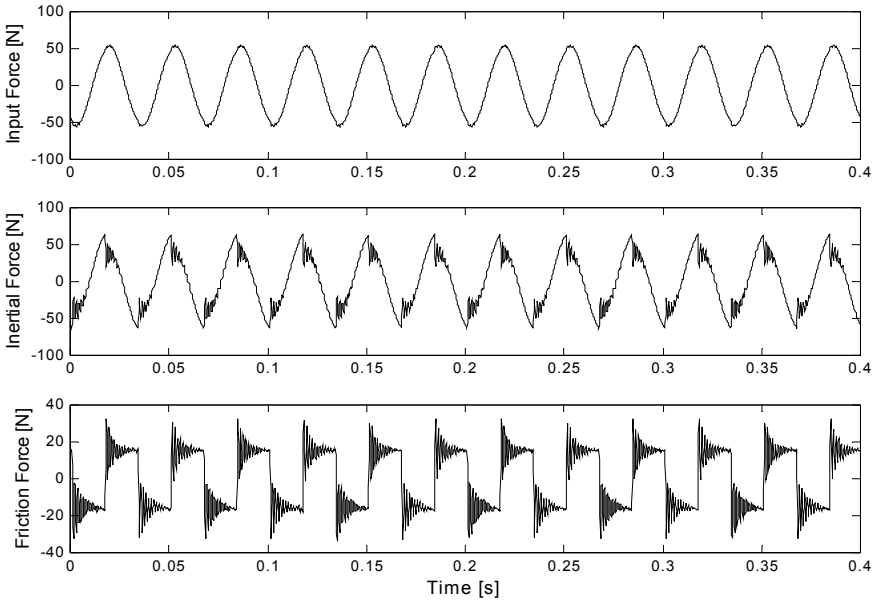

Figure A-3 Results at 0 V actuator voltage, 5 V shaker voltage and 30 Hz frequency

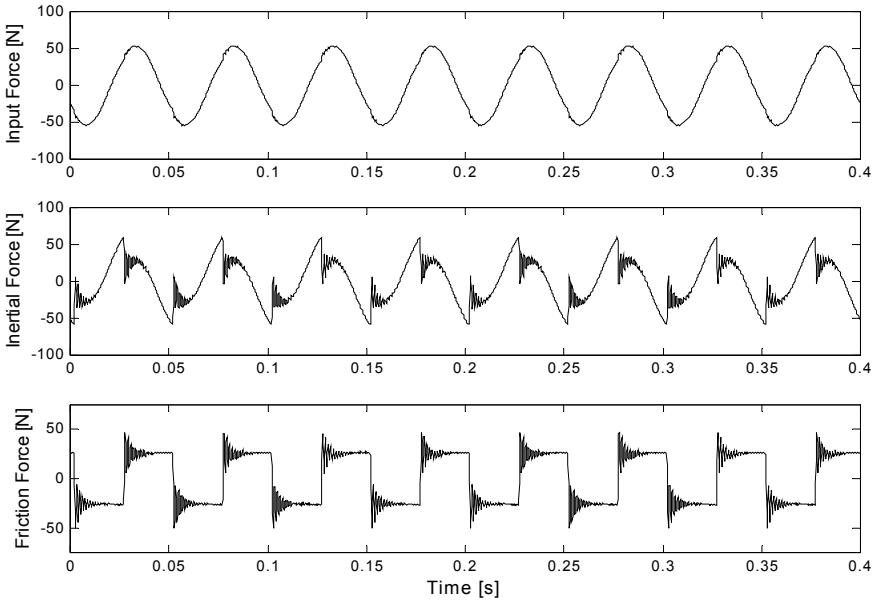

Figure A-4 Results at 30 V actuator voltage, 5 V shaker voltage and 20 Hz frequency

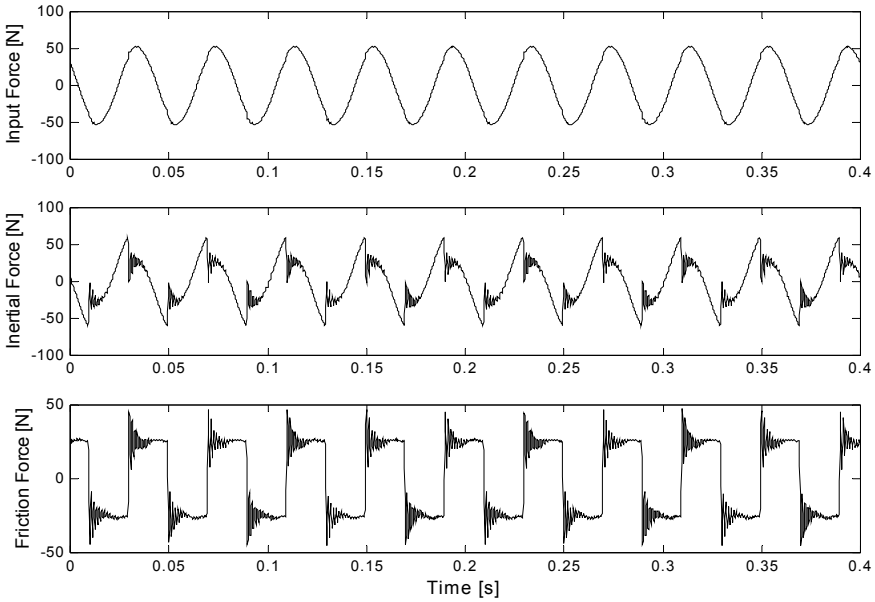

Figure A-5 Results at 30 V actuator voltage, 5 V shaker voltage and 25 Hz frequency

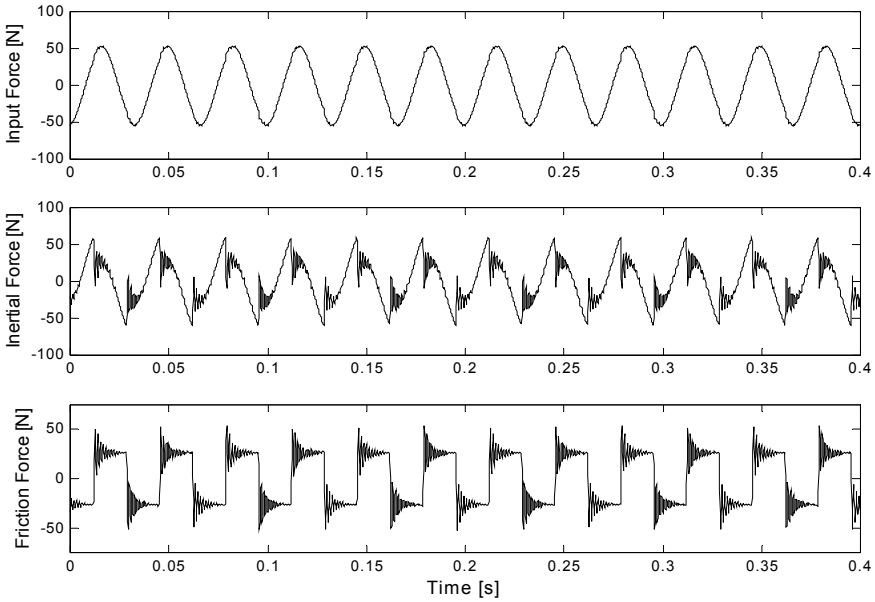

Figure A-6 Results at 30 V actuator voltage, 5 V shaker voltage and 30 Hz frequency

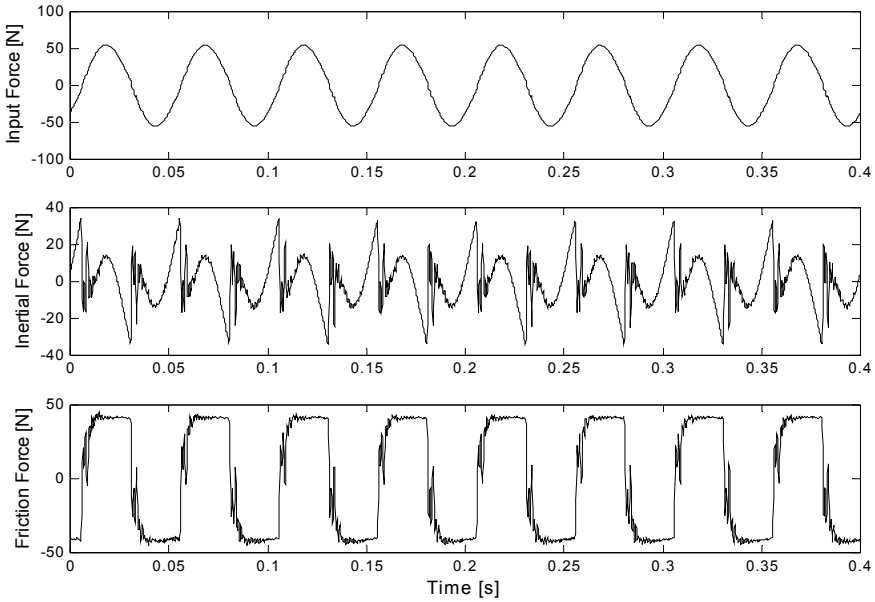

Figure A-7 Results at 60 V actuator voltage, 5 V shaker voltage and 20 Hz frequency

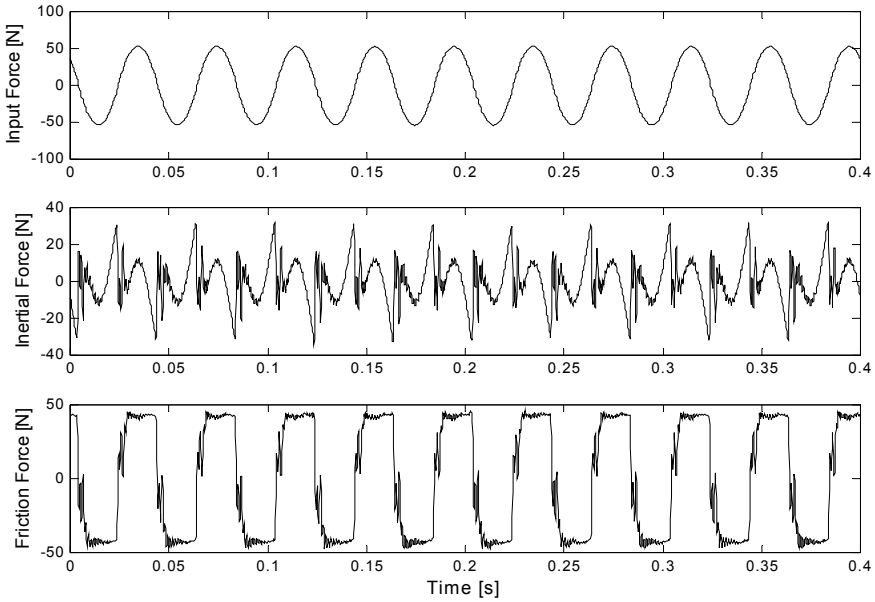

Figure A-8 Results at 0 V actuator voltage, 5 V shaker voltage and 25 Hz frequency

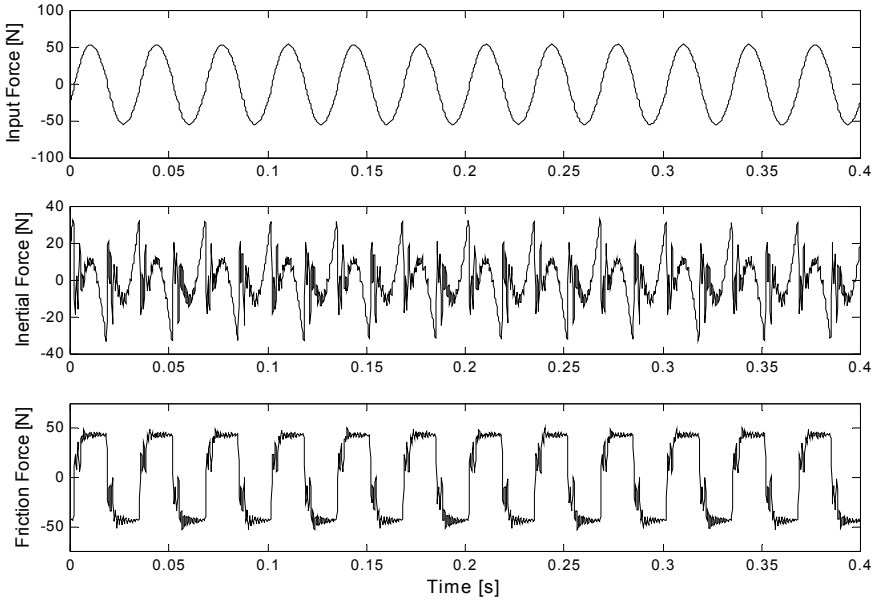

Figure A-9 Results at 60 V actuator voltage, 5 V shaker voltage and 30 Hz frequency

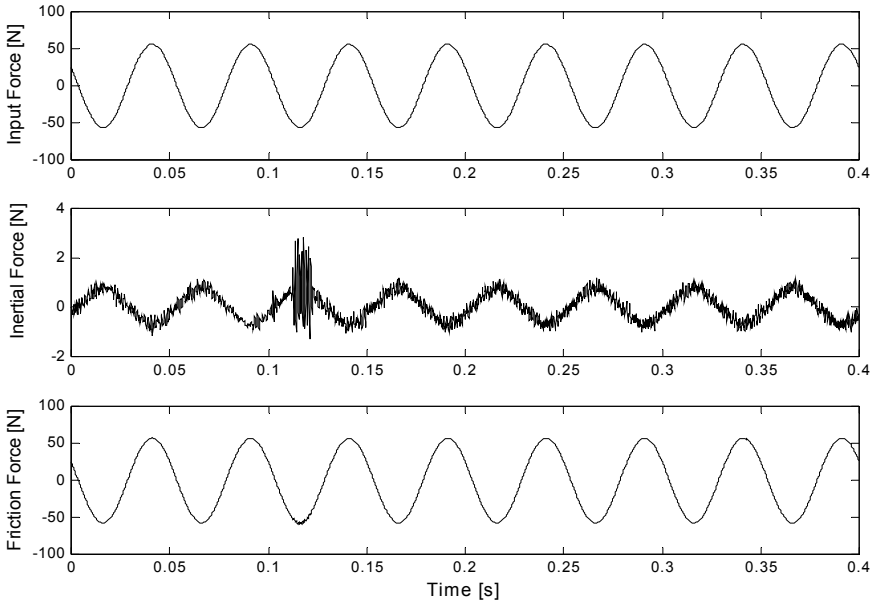

Figure A-10 Results at 90 V actuator voltage, 5 V shaker voltage and 20 Hz frequency

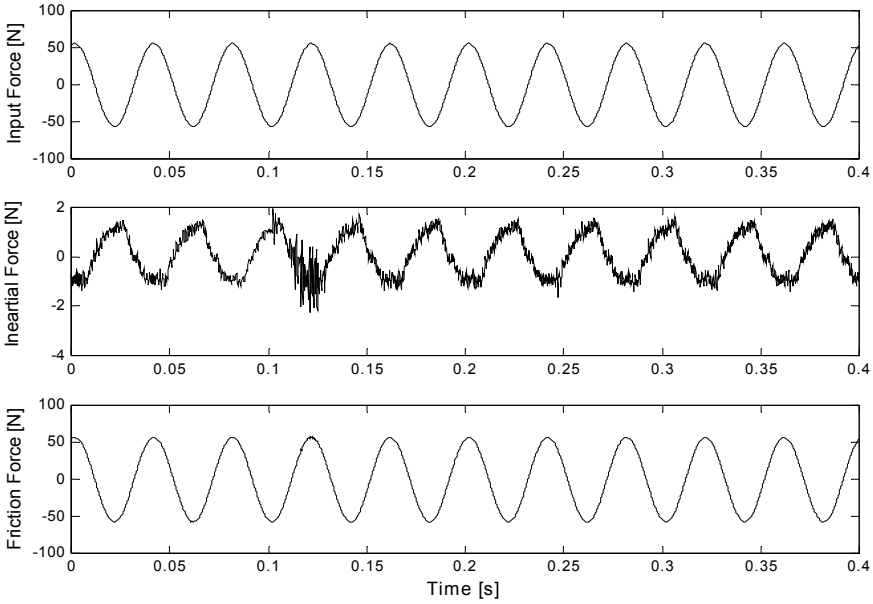

Figure A-11 Results at 90 V actuator voltage, 5 V shaker voltage and 25 Hz frequency

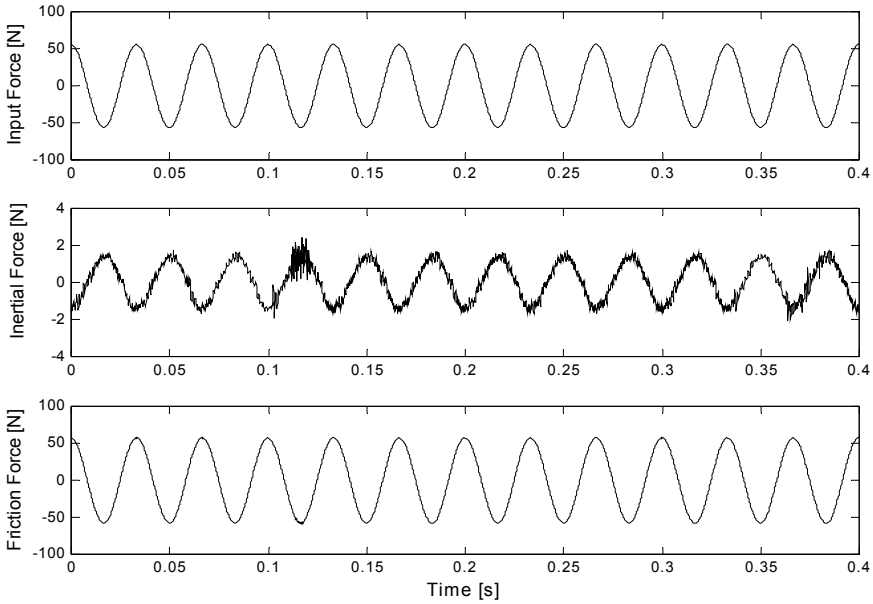

Figure A-12 Results at 90 V actuator voltage, 5 V shaker voltage and 30 Hz frequency

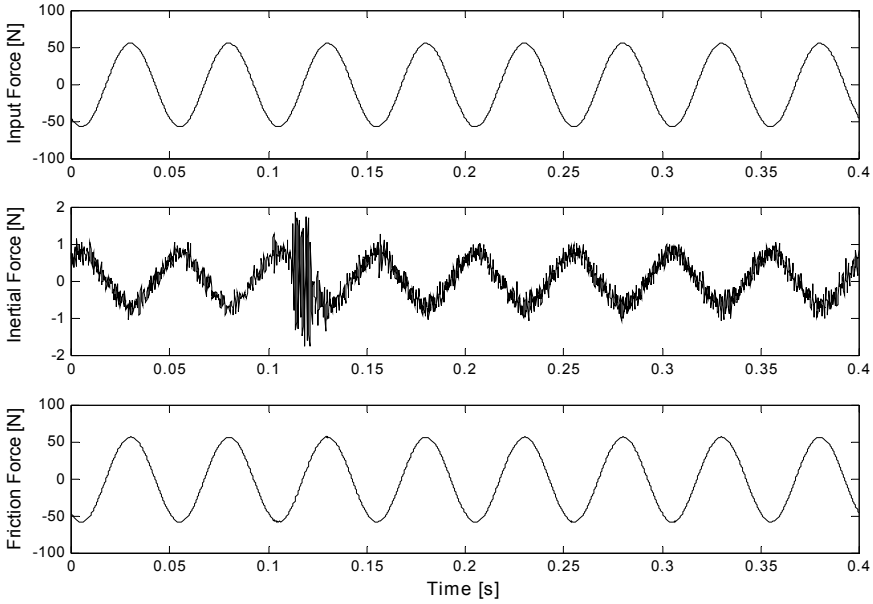

Figure A-13 Results at 120 V actuator voltage, 5 V shaker voltage and 20 Hz frequency

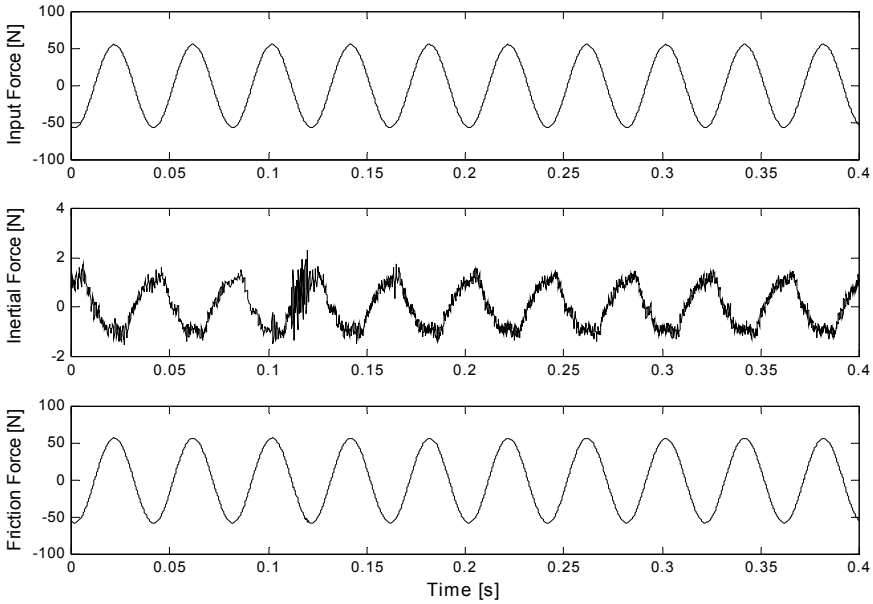

Figure A-14 Results at 120 V actuator voltage, 5 V shaker voltage and 25 Hz frequency

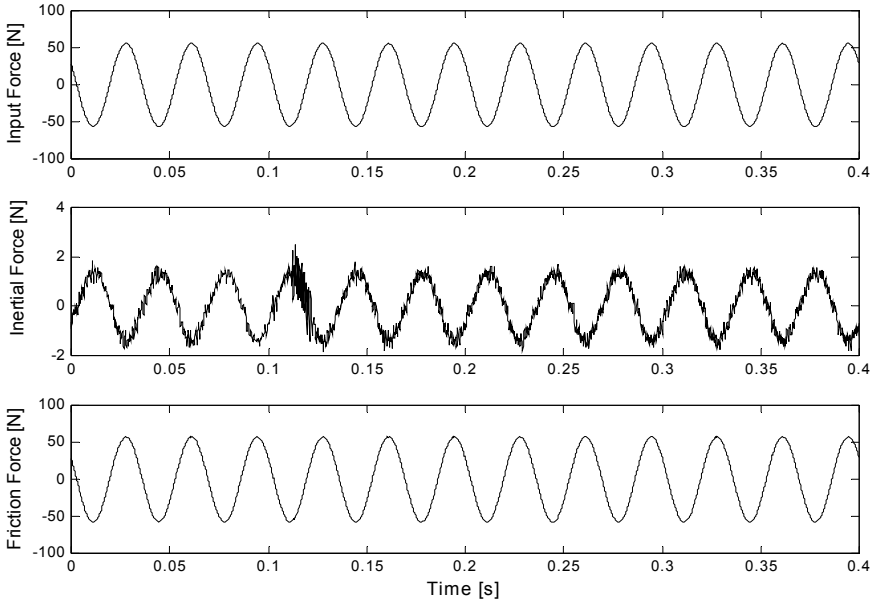

Figure A-15 Results at 120 V actuator voltage, 5 V shaker voltage and 30 Hz frequency

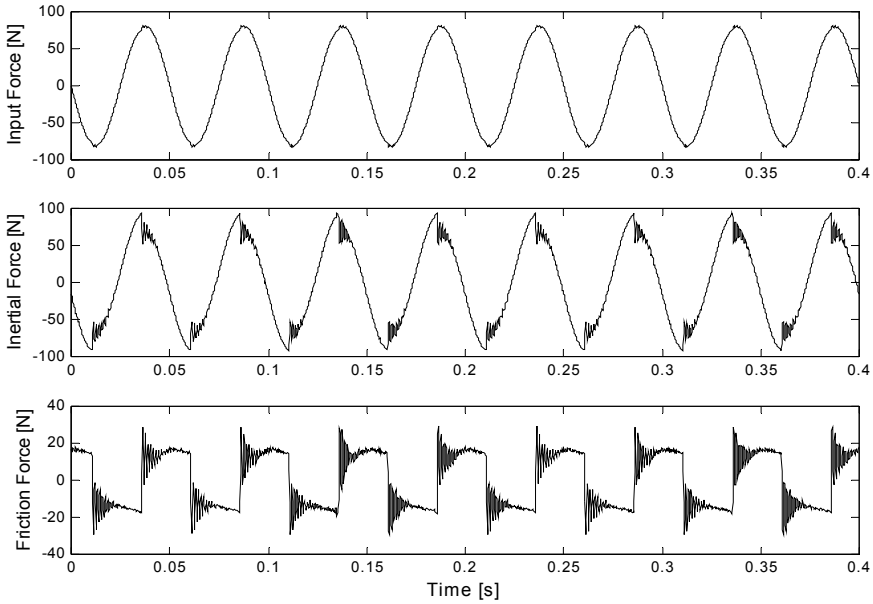

Figure A-16 Results at 0 V actuator voltage, 7 V shaker voltage and 20 Hz frequency

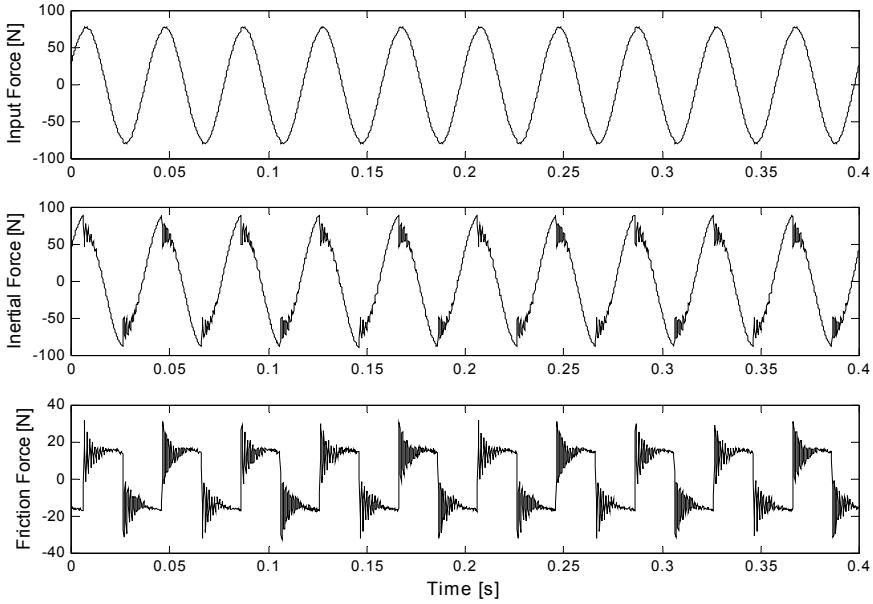

Figure A-17 Results at 0 V actuator voltage, 7 V shaker voltage and 25 Hz frequency

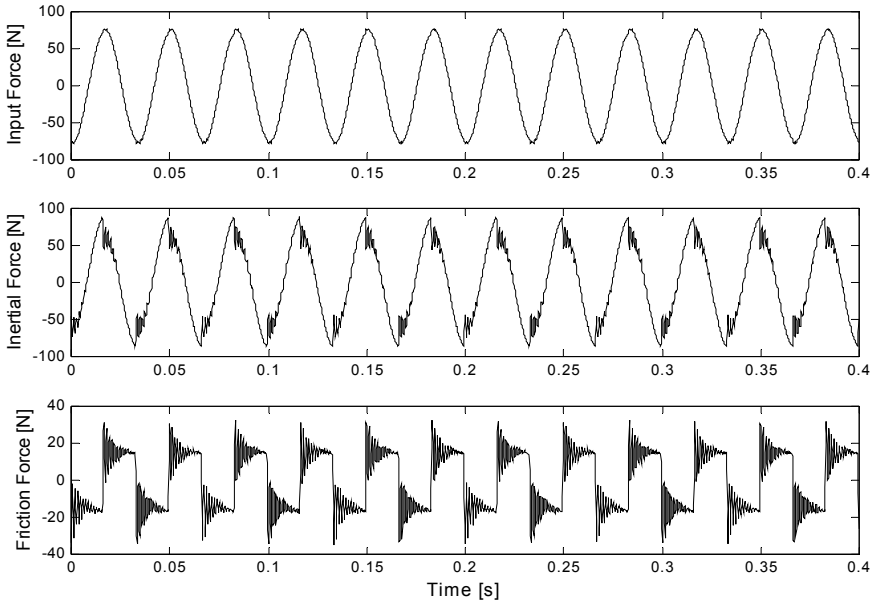

Figure A-18 Results at 0 V actuator voltage, 7 V shaker voltage and 30 Hz frequency

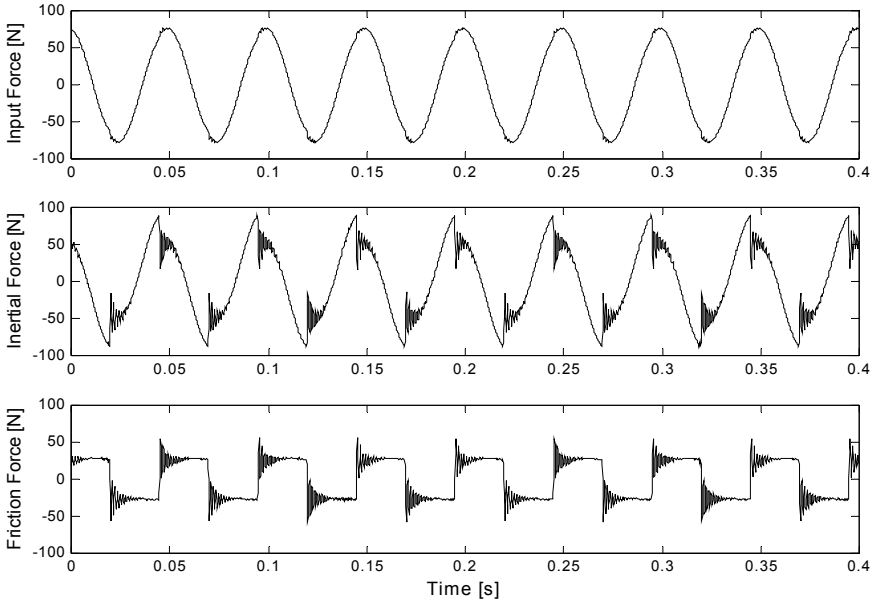

Figure A-19 Results at 30 V actuator voltage, 7 V shaker voltage and 20 Hz frequency

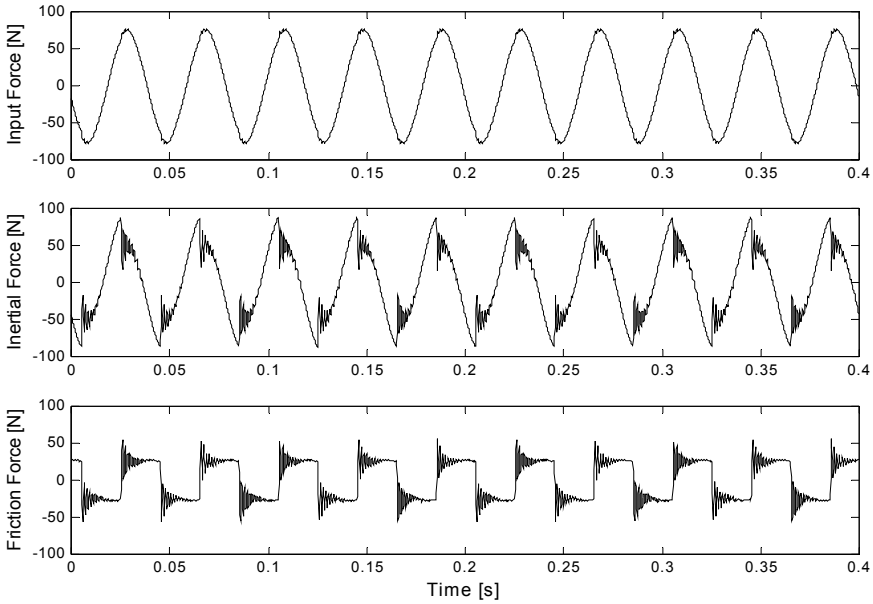

Figure A-20 Results at 30 V actuator voltage, 7 V shaker voltage and 25 Hz frequency

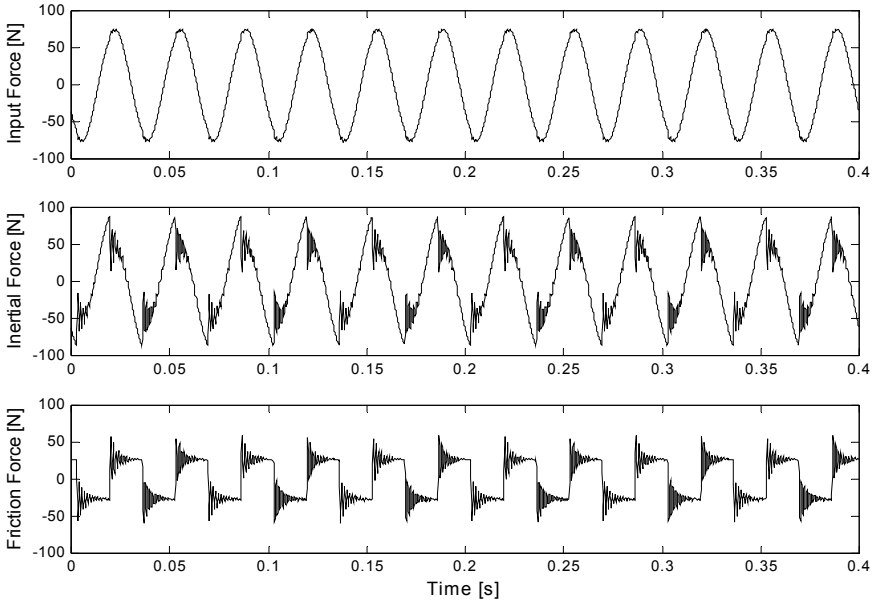

Figure A-21 Results at 30 V actuator voltage, 7 V shaker voltage and 30 Hz frequency

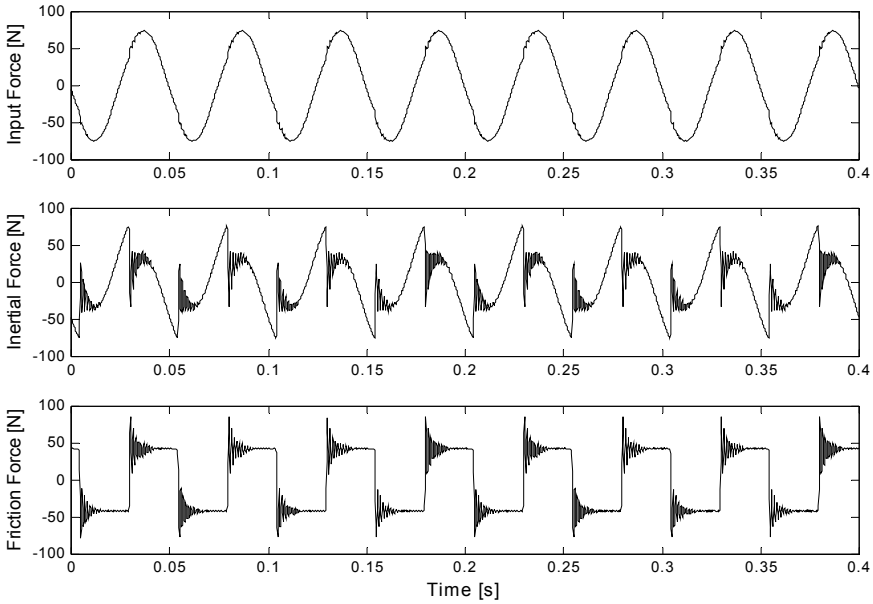

Figure A-22 Results at 60 V actuator voltage, 7 V shaker voltage and 20 Hz frequency

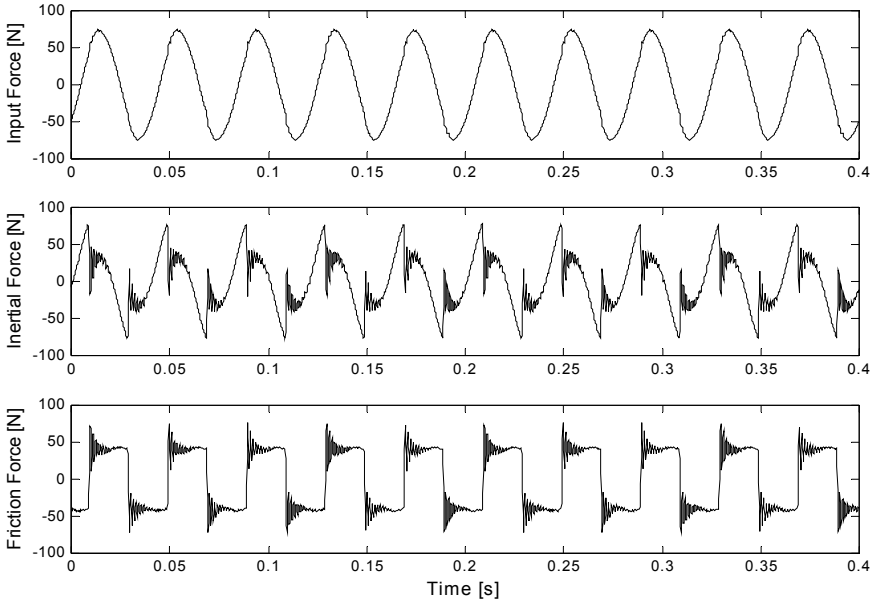

Figure A-23 Results at 60 V actuator voltage, 7 V shaker voltage and 25 Hz frequency

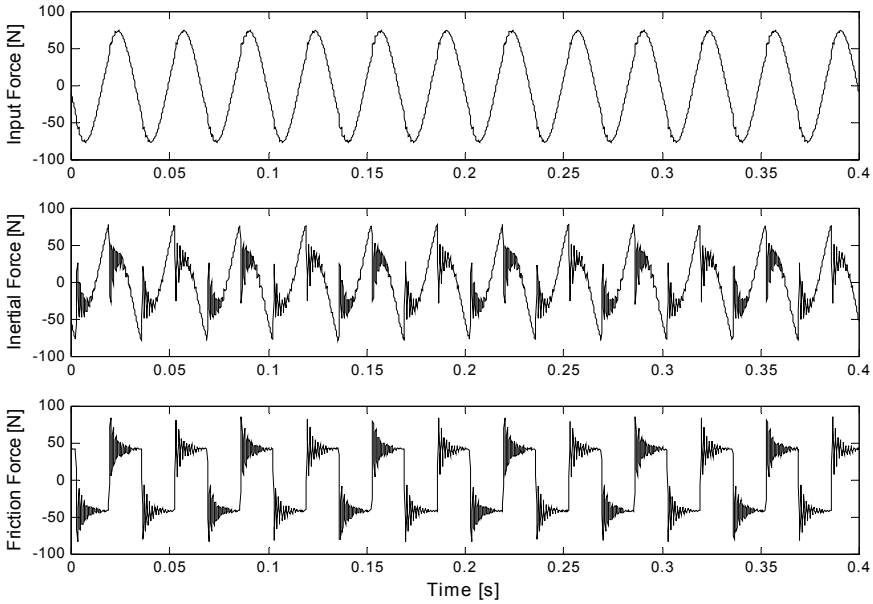

Figure A-24 Results at 60 V actuator voltage, 7 V shaker voltage and 30 Hz frequency

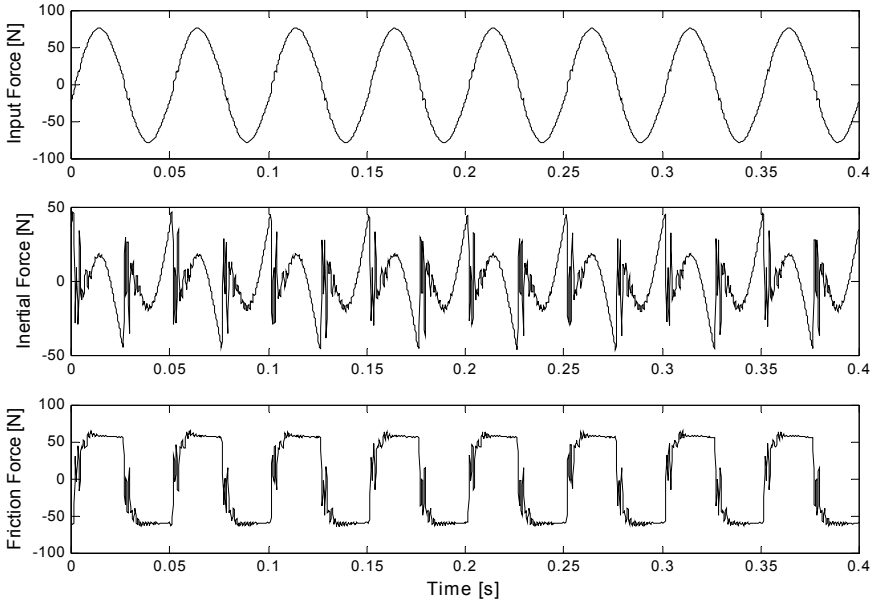

Figure A-25 Results at 90 V actuator voltage, 7 V shaker voltage and 20 Hz frequency

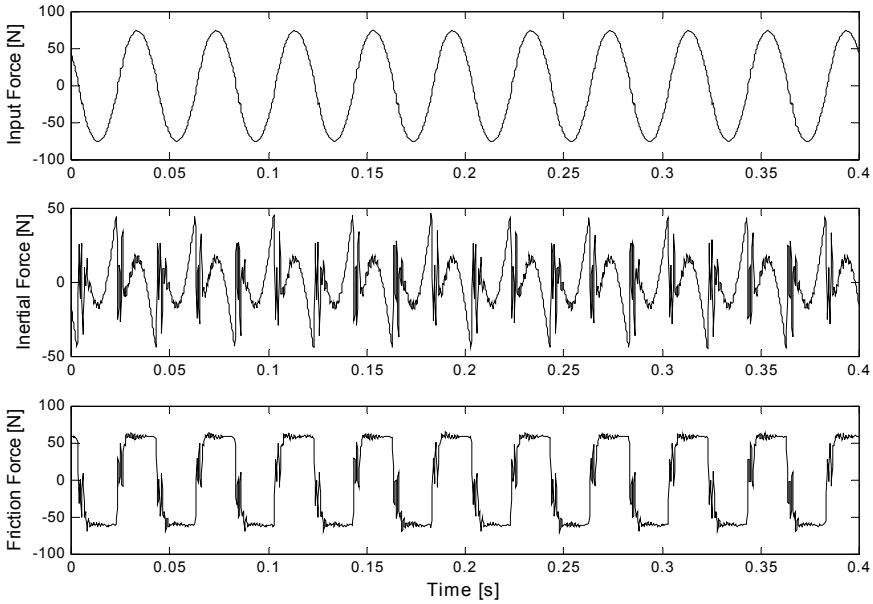

Figure A-26 Results at 90 V actuator voltage, 7 V shaker voltage and 25 Hz frequency

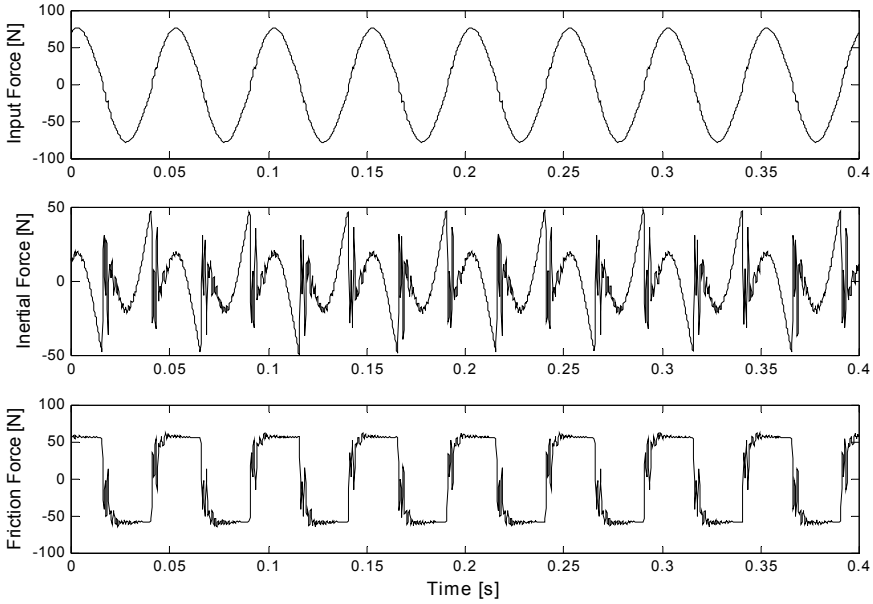

Figure A-27 Results at 90 V actuator voltage, 7 V shaker voltage and 30 Hz frequency

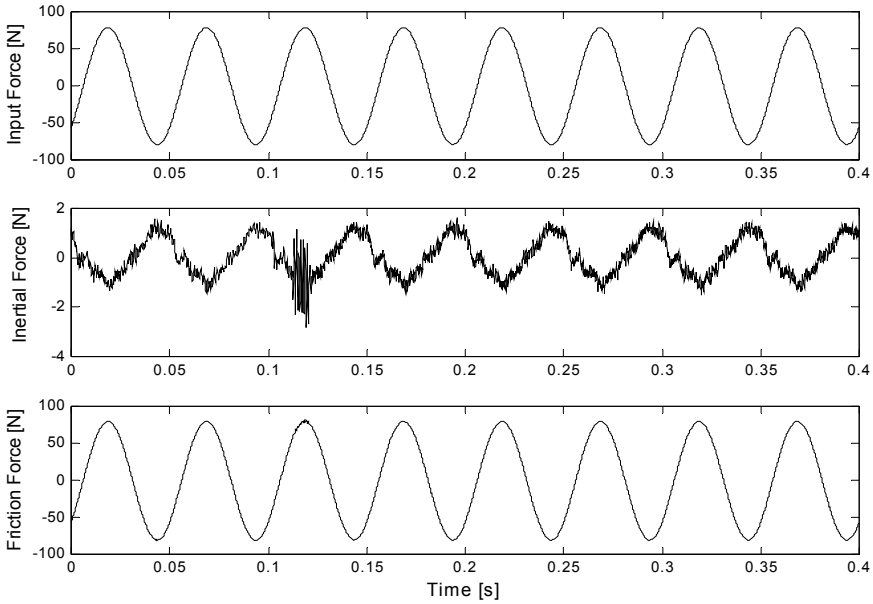

Figure A-28 Results at 120 V actuator voltage, 7 V shaker voltage and 20 Hz frequency

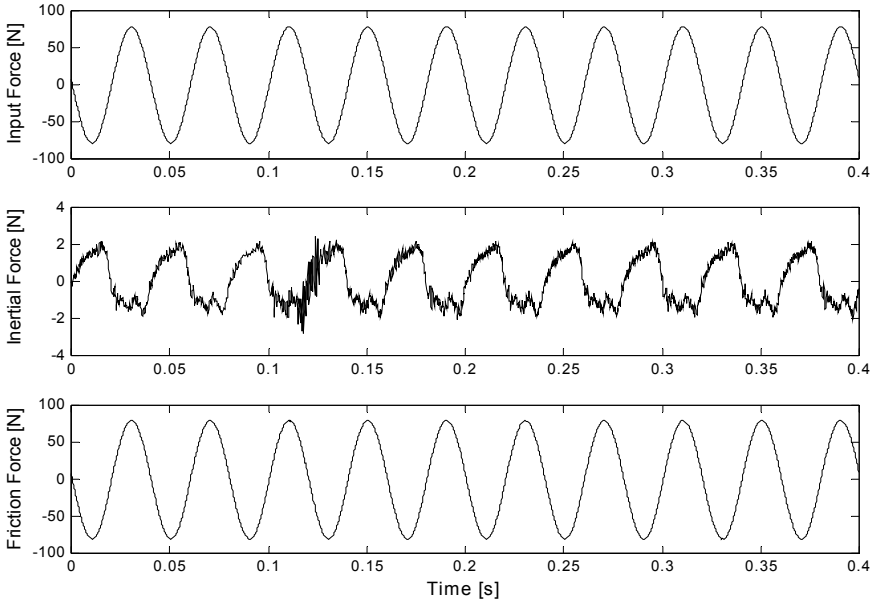

Figure A-29 Results at 120 V actuator voltage, 7 V shaker voltage and 25 Hz frequency

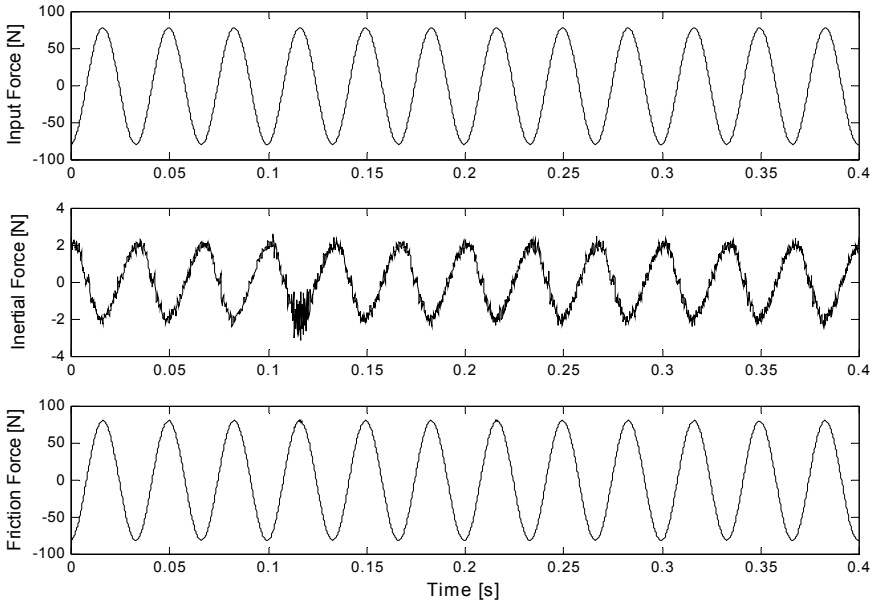

Figure A-30 Results at 120 V actuator voltage, 7 V shaker voltage and 30 Hz frequency

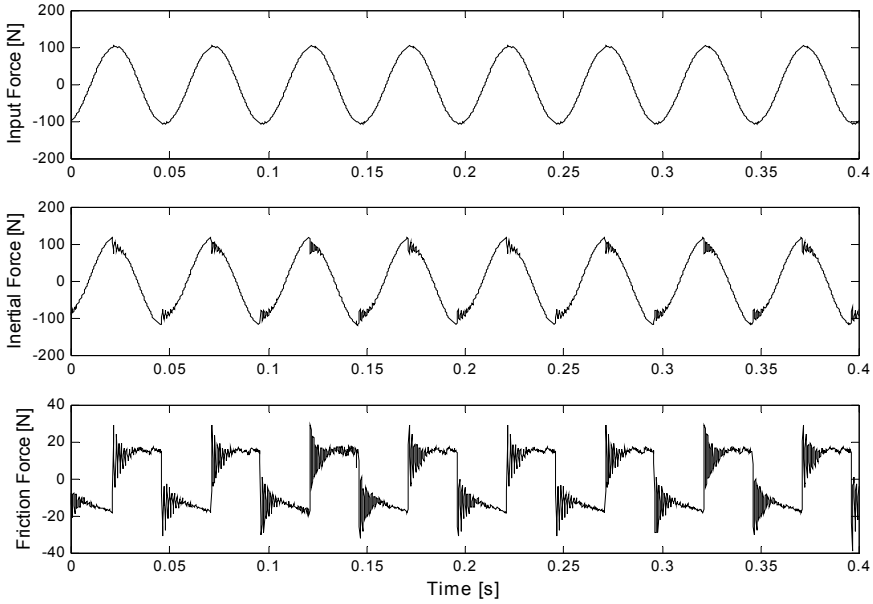

Figure A-31 Results at 0 V actuator voltage, 9 V shaker voltage and 20 Hz frequency

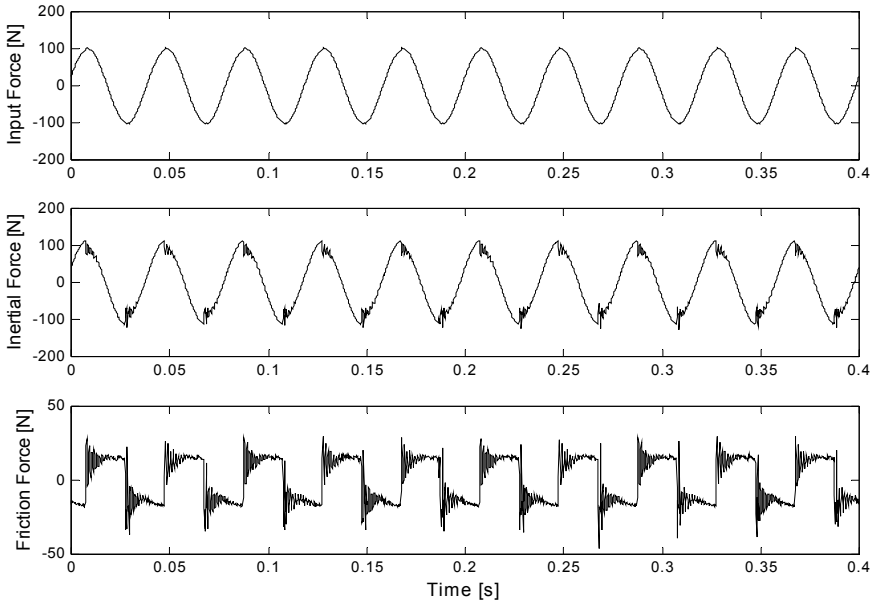

Figure A-32 Results at 0 V actuator voltage, 9 V shaker voltage and 25 Hz frequency

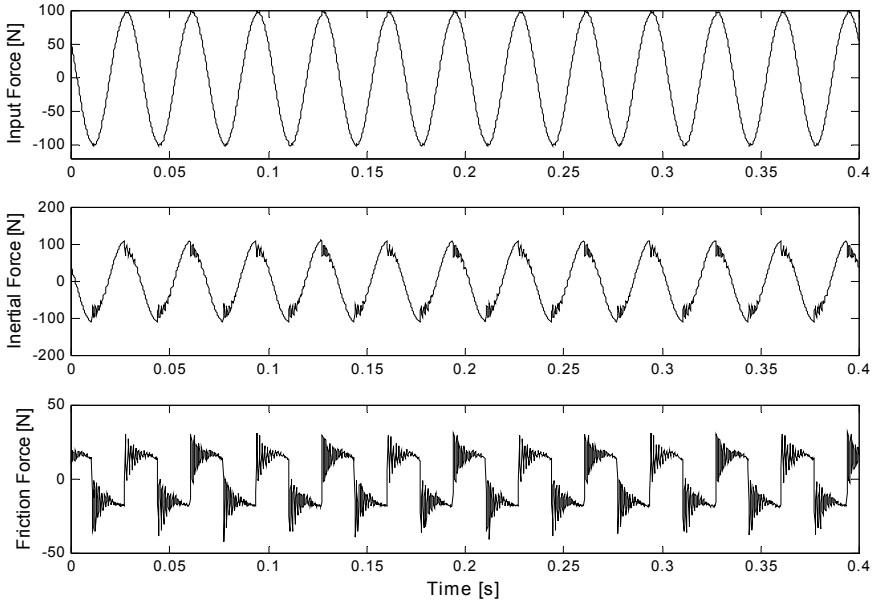

Figure A-33 Results at 0 V actuator voltage, 9 V shaker voltage and 30 Hz frequency

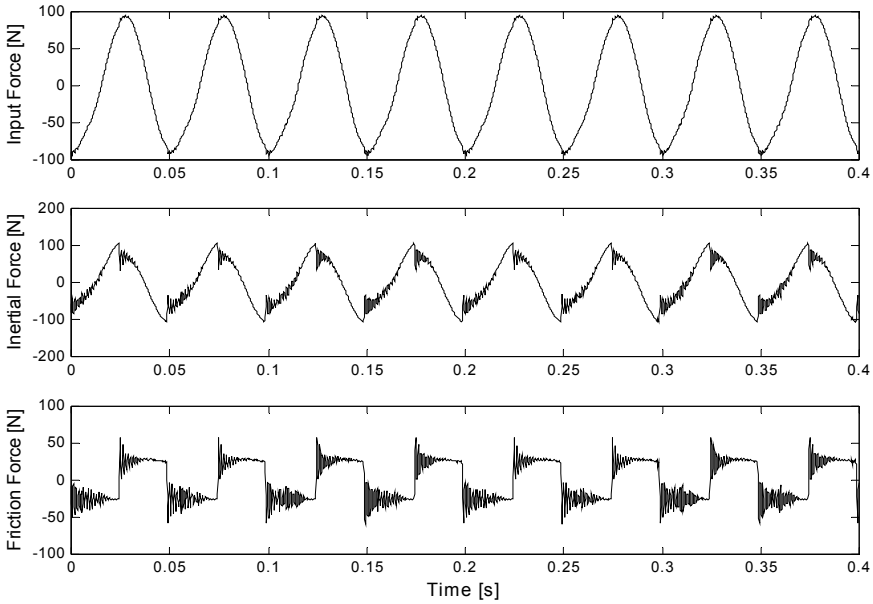

Figure A-34 Results at 30 V actuator voltage, 9 V shaker voltage and 20 Hz frequency

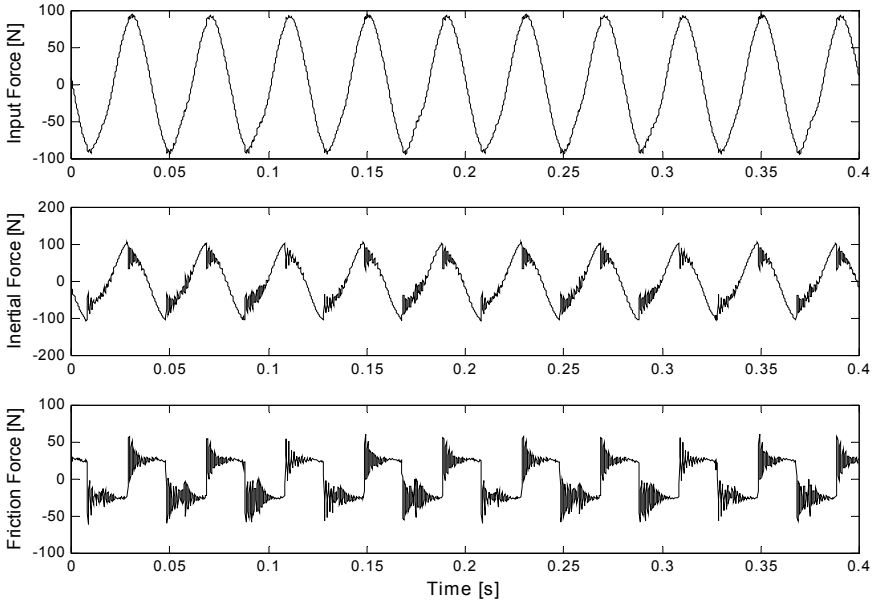

Figure A-35 Results at 30 V actuator voltage, 9 V shaker voltage and 25 Hz frequency

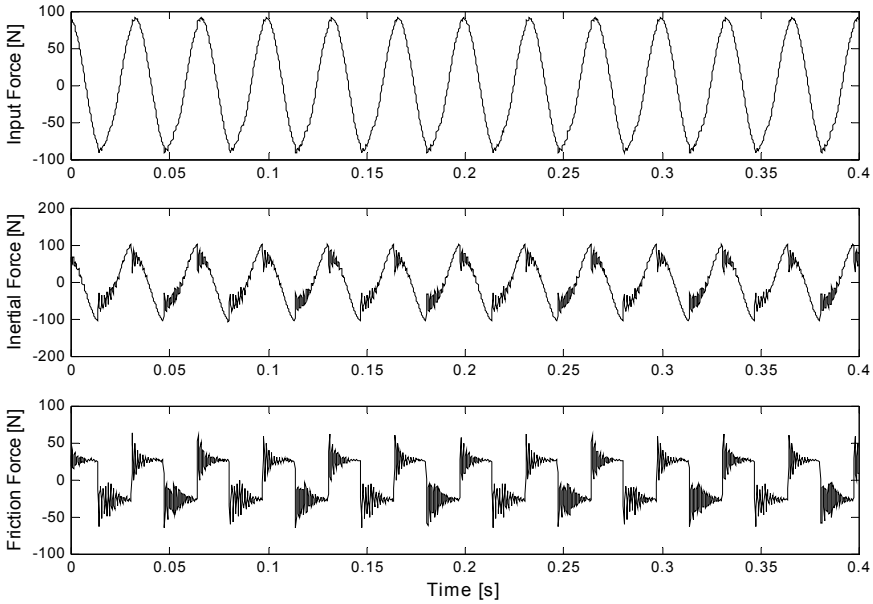

Figure A-36 Results at 30 V actuator voltage, 9 V shaker voltage and 30 Hz frequency

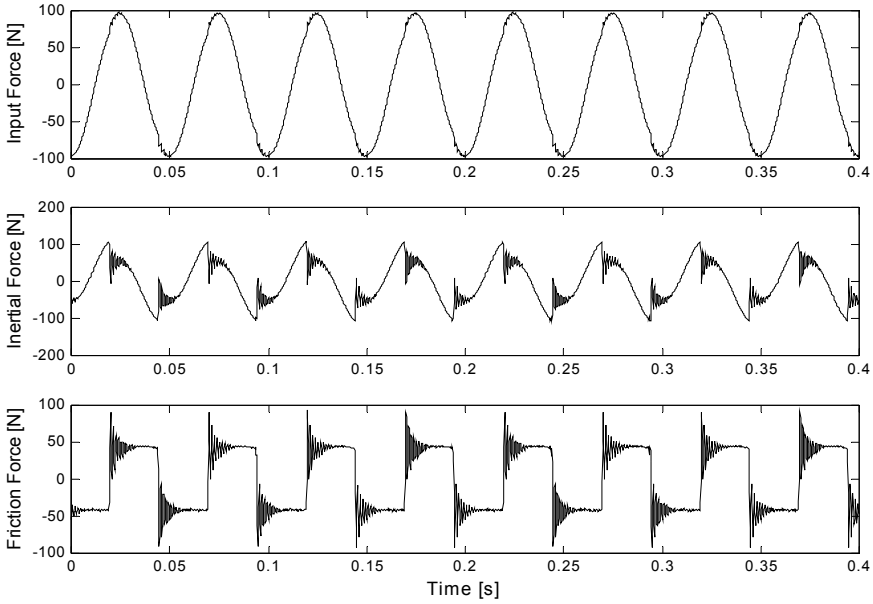

Figure A-37 Results at 60 V actuator voltage, 9 V shaker voltage and 20 Hz frequency

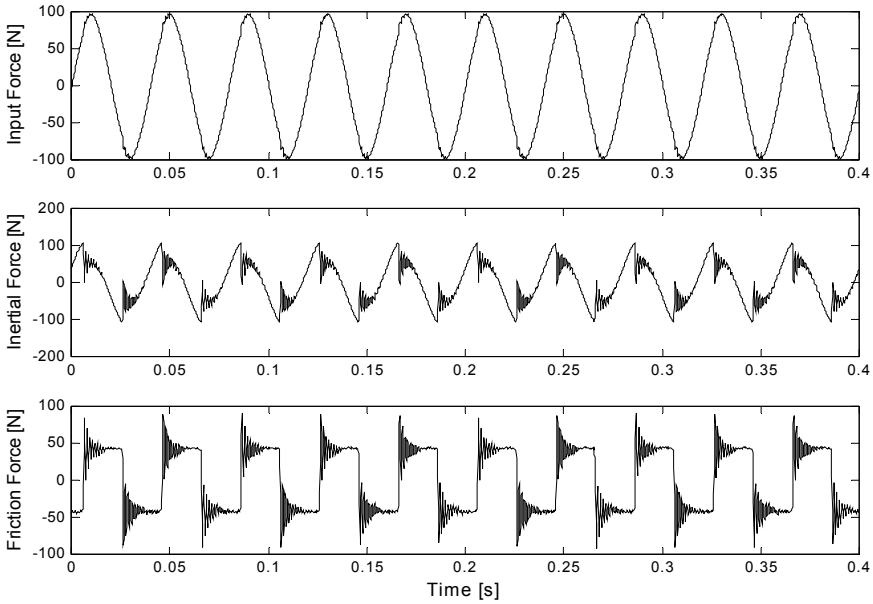

Figure A-38 Results at 60 V actuator voltage, 9 V shaker voltage and 25 Hz frequency

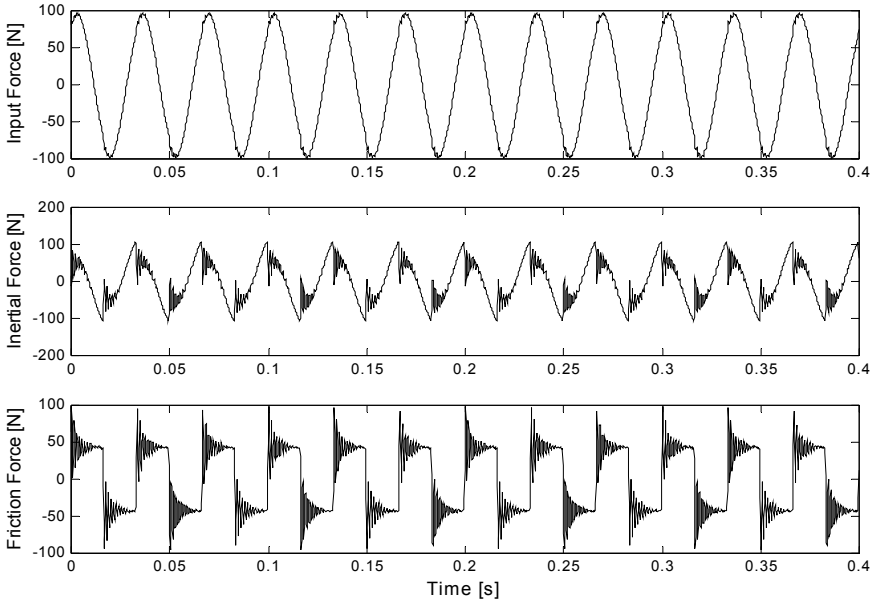

Figure A-39 Results at 60 V actuator voltage, 9 V shaker voltage and 30 Hz frequency

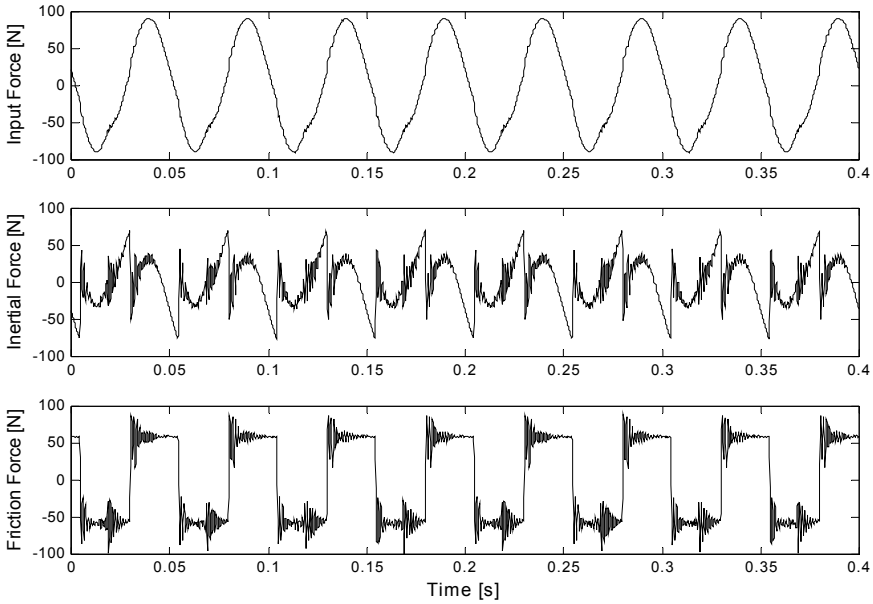

Figure A-40 Results at 90 V actuator voltage, 9 V shaker voltage and 20 Hz frequency

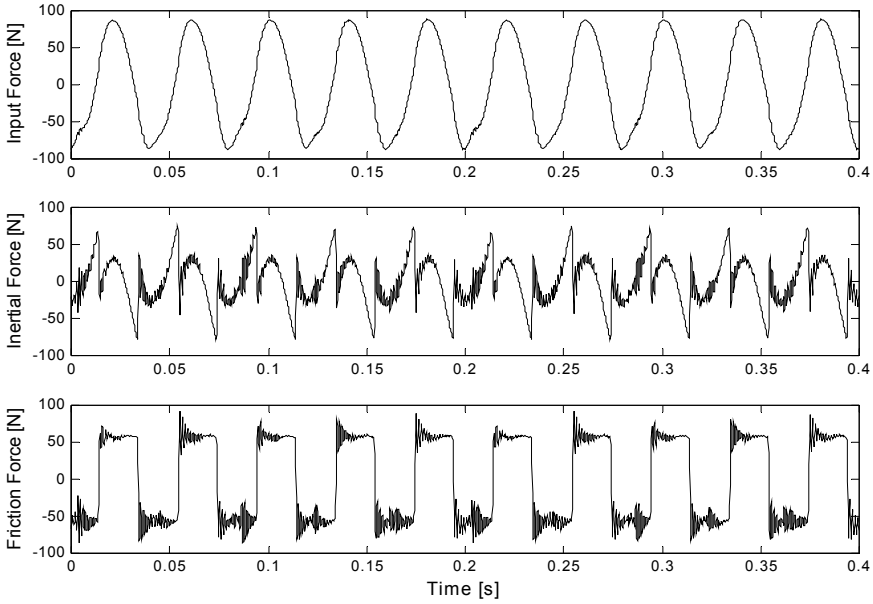

Figure A-41 Results at 90 V actuator voltage, 9 V shaker voltage and 25 Hz frequency

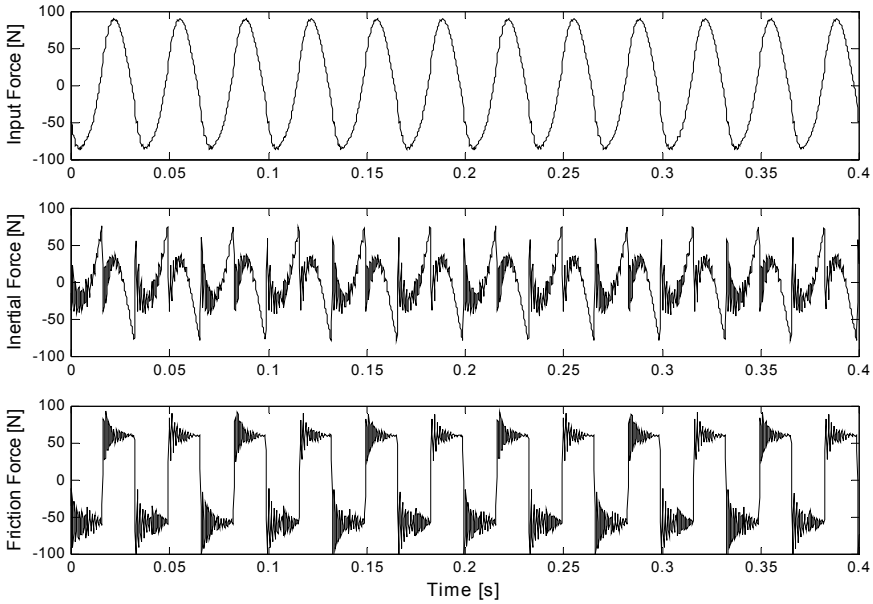

Figure A-42 Results at 90 V actuator voltage, 9 V shaker voltage and 30 Hz frequency

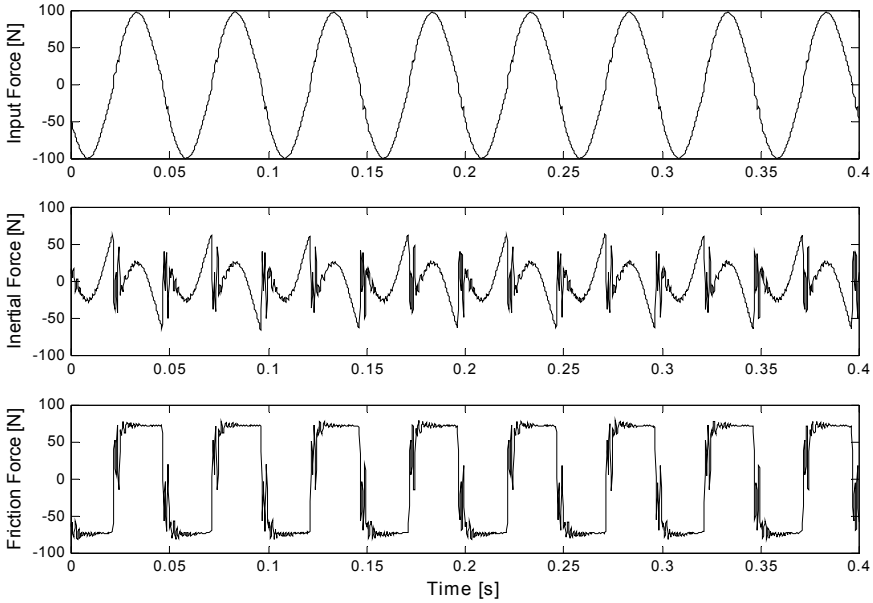

Figure A-43 Results at 120 V actuator voltage, 9 V shaker voltage and 20 Hz frequency

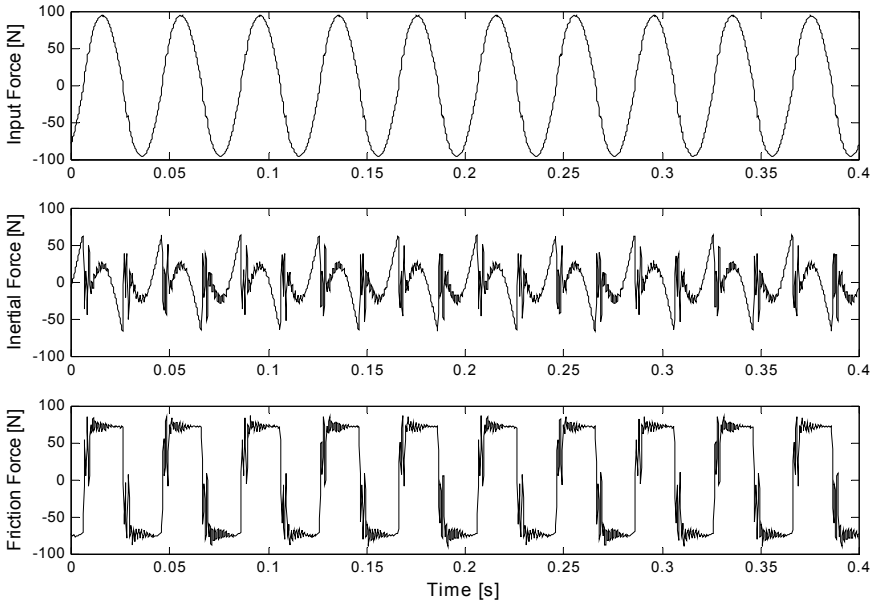

Figure A-44 Results at 120 V actuator voltage, 9 V shaker voltage and 25 Hz frequency

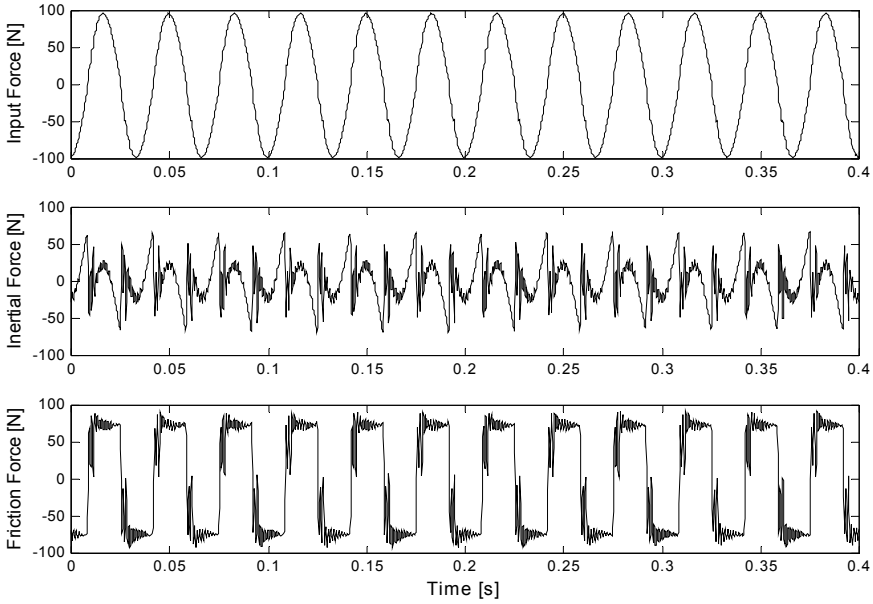

Figure A-45 Results at 120 V actuator voltage, 9 V shaker voltage and 30 Hz frequency

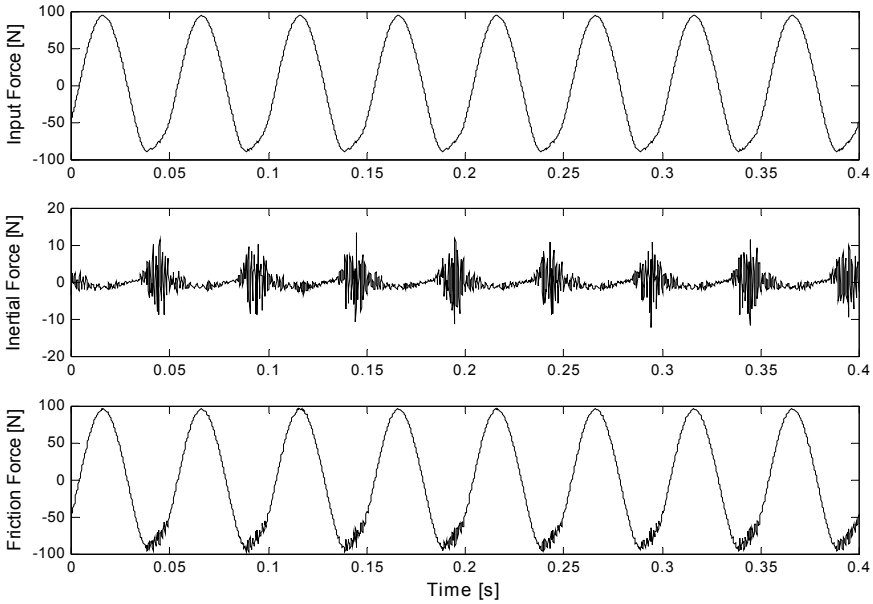

Figure A-46 Results at 150 V actuator voltage, 9 V shaker voltage and 20 Hz frequency

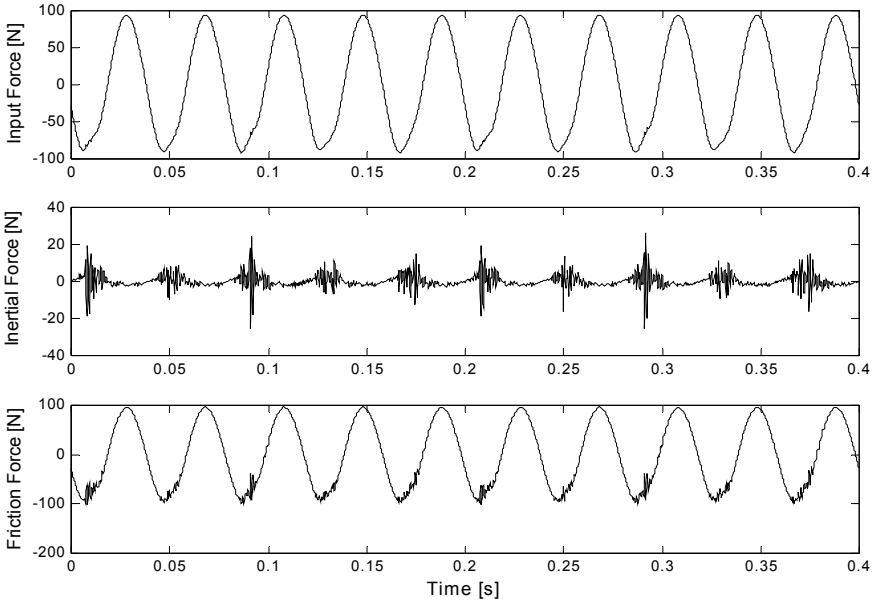

Figure A-47 Results at 150 V actuator voltage, 9 V shaker voltage and 25 Hz frequency

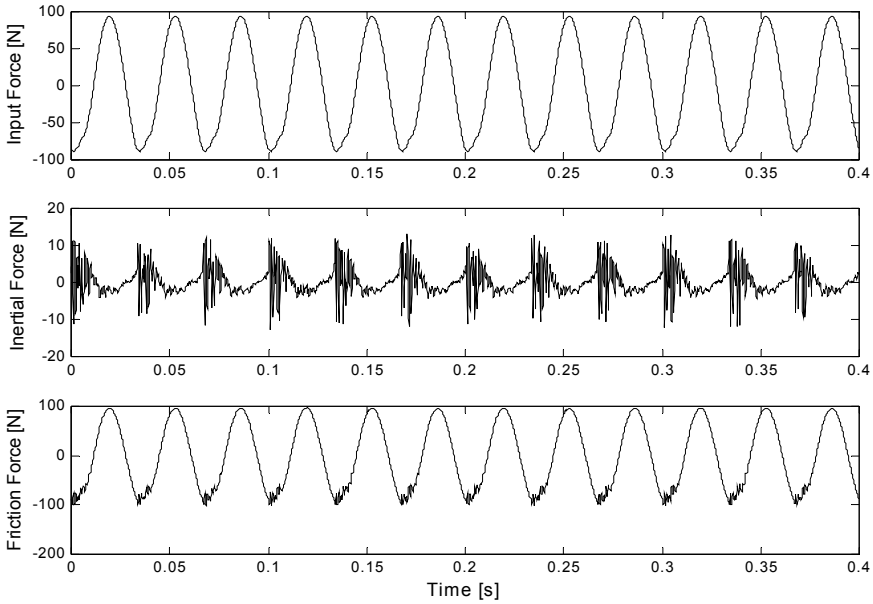

Figure A-48 Results at 150 V actuator voltage, 9 V shaker voltage and 30 Hz frequency

LIST OF REFERENCES

Akbay Z. and Aktan H.K., “Actively Regulated Friction Braces,” Proceedings of the 6th Canadian Conference on Earthquake Engineering, 1991.

Armstrong-Helouvry, B., “Control of Machines with Friction,” Kluwer Academic Press, Boston, pp. 1-125, 1991.

Armstrong-Helouvry, B., Dupont, P. and Canudas de Witt, C., “A Survey of Models, Analysis Tools and Compensation Methods for the Control of Machines with Friction,” Automatica, Vol. 30, No. 7, pp. 1083-1138, 1994.

Bamford, R., Kuo, C. P., Glaser, R. and Wada, B. K., “Long Stroke Precision PZT Actuator,” Proceedings of the 36th AIAA/ASME/ASCE/AHS/ASC Structures, Structural Dynamics, and Materials Conference and AIAA/ASME Adaptive Structures Forum, New York, NY, pp. 3278-3284, 1995.

B&K “Vibration Exciter Type 4808 Instruction Manual,” 1980.

Blau, P.J., “Friction Science and Technology,” Marcel Dekker, Inc., NY, pp. 108-148, 1996.

Bliman, P.A. and Sorine, M., “Easy-to-use Realistic Dry Friction Models for Automatic Control,” Proceedings of 3rd European Control Conference, Rome, Italy, pp. 3788-3794, 1995.

Brennan, M.J., Day, M.J. and Randall, R.J., “An Experimental Investigation into the Semi-Active Control of Longitudinal Vibrations in a Large Tie-Rod Structure,” Journal of Vibration and Acoustics, Vol. 120, pp. 1-12, 1999.

Canudas de Wit, C., Astrom, K.J. and Braun, K., " Adaptive Friction Compensation in DC-Motor Drives.” IEEE Transactions Robotics and Automation, RA-3, pp. 681-685, 1987.

Canudas de Wit, C., Olsson, H., Astrom, K.J. and Lischinsky, P., “A New Model for Control of Systems with Friction,” IEEE Transactions on Automatic Control, Vol. 40, No. 3, pp. 419-425, March 1995.

Chen, G. and Chen, C., "Behavior of Piezoelectric Friction Dampers Under Dynamic Loading, Proceedings of the SPIE – Smart Structures and Materials, New Port Beach, CA, Vol. 3988, pp. 54-63, 2000.

Dahl, P., "A Solid Friction Model," Technical Report TOR-0158(3107-18)-1, The Aerospace Corporation, El Segundo, CA, 1968.

Dowdell, D.J. and Cherry S., "Semi-Active Friction Dampers for Seismic Response Control of Structures," Proceedings of the 5th US National conference on Earthquake Engineering, Palm Springs, CA, Vol. 1, pp. 819-828, 1994.

Dupont, P. E., Prakash, S. K. and Stokes, A. W., "Experimental Evaluation of a Semi-Active Friction Damper," Elasto-Impact and Friction in Dynamic Systems, American Society of Mechanical Engineers, Design Engineering Division (Publication) DE-Vol. 90, pp. 69-74, 1996.

Dupont, P. E. and Stokes, A. W., "Semi-active Control of Friction Dampers," Proceedings of the 34th Conference on Decision and Control, New Orleans, LA, pp. 3331-3336, December 1995.

Dynamic Structures & Materials, LLC. "Piezoelectric Actuators," © 2001-2002. http://www.dynamic-structures.com/piezo.html, 05/20/2002.

Ferri, A.A., "Friction Damping and Isolation Systems," Journal of Mechanical Design, Transactions of the ASME, Vol. 117, pp. 196-206, June, 1995.

Ferri, A. A. and Heck, B. S., "Semi-Active Suspension using Dry Friction Energy Dissipation," Proceedings of the American Control Conference, Green Valley, AZ, Vol. 1, pp. 31-35, 1992.

Fujita, T., Tagawa, Y., Kajiwara, K., Yoshioka, H., Takeshita, A. and Yasuda, M., "Active 6-DOF Microvibration Control System Using Piezoelectric Actuators," Proceedings of the SPIE, Bellingham, WA, Vol. 2040, pp. 514-528, 1993.

Garrett T. G., Chen, G., Cheng,F.Y. and Huebner, W., 'Experimental Characterization of Piezoelectric Friction Dampers,' Proceedings of the SPIE, New Port Beach, CA, 2001.

Guntur, R.R. and Sankar, S., "Fail-Safe Vibration Control Using Active Force Generators," ASME Journal of Vibration, Acoustics, Stress, and Reliability in Design, Vol. 105, No. 3, pp. 361-368, 1983.

Hac, A. and Youn, I., "Optimal Semi-Active Suspension with Preview Based on a Quarter Car Model," Journal of Vibrations and Acoustics –Stress Reliability Design, Vol. 114, No. 1, pp. 84-92, 1992.

Iiyama, F., Sunakoda, K. and Suzuki, K., "Hybrid Control of Seismic Isolation System Using Mechatro Damper," Proceedings of the ASME/JSME Joint Pressure Vessels and Piping Conference, San Diego, CA, Vol. 379, pp. 157-161, 1998.

Inaudi, J.A., "Modulated Homogeneous Friction: A Semi-Active Damping Strategy," Earthquake Engineering and Structural Dynamics, Vol. 26, No. 3, pp. 361-376, March 1997.

Kagawa, K., Fujita, K., Yamasaki, Y., Yoshimura, Y. and Ayabe, S., "Semi-active and passive vibration control of structure by fluid system," *Active Passive Control of Mechanical Vibration American Society of Mechanical Engineers*, Pressure Vessels and Piping Division (Publication) PVP, Vol. 289, pp. 41-48, 1998.

Kannan. S., Uras H.M. and Aktan, H.M., "Active Control of Building Seismic Response by Energy Dissipation," Earthquake Engineering and Structural Dynamics, Vol. 24, pp. 747-759, 1995.

Lane, J.S. and Ferri, A.A., " Control of a Flexible Structure Using Combined Active and Semi-Active Elements." AIAA/ASME/ASCE/AHS Structures, Structural Dynamics & Materials Conference - Collection of Technical Papers, Vol. 2, pp. 719-728, 1995.

Lane, J. S., Ferri. A. A. and Heck, B. S., "Vibration Control Using Semi-Active Friction Damping," Proceedings of the Winter Annual Meeting of the American Society of Mechanical Engineers, New York, NY, Vol. 49, pp. 165-171, 1992.

Lee, J. K. and Clark, W. W., "Semi-Active Control of Flexural Vibrations with an MR Fluid Actuator," Proceedings of the SPIE – Smart Structures and Materials, Newport Beach, CA, Vol. 3672, pp. 167-174, 1999.

Park, S. E. and Shrout, T. R., "Ultrahigh Strain and Piezoelectric Behavior in Relaxor Based Ferroelectric Single Crystals," Journal of Applied Physics, Vol. 82, No. 4, pp. 1804-1811, 1997.

Pinkos, A., Shtarkman, E. and Fitzgerald, T., "Actively Damped Passenger Car Suspension System with Low Voltage Electro-Rheological Magnetic Fluid," Vehicle Suspension and Steering Systems SAE Special Publications, No. 952, pp. 87-93, 1993.

Rabinowicz, E., "Friction and Wear of Materials," John Wiley and Sons, NY, 1965.
Scruggs, J. and Lindner, D., "Active Energy Control in Civil Structures," Proceedings of the SPIE, Newport Beach, CA, Vol. 3671, pp. 194-205, 1999.

Scruggs, J. and Lindner, D., "Active Energy Control in Civil Structures," Proceedings of the SPIE - The International Society for Optical Engineering, Newport Beach, CA, Vol. 3671, pp. 194-205, 1999.

Sims, N. D., Stanway, R. and Johnson, A. R., "Vibration Control Using Smart Fluids: A State-of-the-Art Review," The Shock and Vibration Digest, Vol. 31, No. 2, pp. 195-203, 1999.

Symans, M.D. and M.C. Constantinou, "Experimental Testing and Analytical Modeling of Semi-Active Fluid Dampers for Seismic Protection," Journal of Intelligent Material Systems and Structures, Vol. 8, No. 8, 644-657, August 1997.

Taniwangsa, W. and Kelly, J. M. "Experimental Testing of a Semi-Active Control Scheme for Vibration Suppression," Proceedings of the SPIE – Smart Structures and Materials, Bellingham, WA, Vol. 3045, pp.130-139, 1997.

Tarics, A.G., Way, D. and Kelly, J.M., "The Implementation of Base Isolation for the Foothill Communities Law & Justice Center," Technical Report, RTA, San Francisco, 1984.

The Salt Lake City Corp., Proceedings of International Seismic Isolation/Historic Preservation Symposium, 1988.

Vaillon, L., Petitjean, B., Frapard, B. and Lebihan, D., "Active Isolation in Space Truss Structures: From Concept to Implementation," Smart Materials and Structures, Vol. 8, No. 6, pp. 781-790, 1999.

Yalla, S.K., Kareem, A. and Kantor, J.C., "Semi-Active Variable Damping Liquid Column Dampers," Proceedings of the SPIE –The International Society for Optical Engineering, Vol. 3988, pp. 75-83, 2000.

Yang, C and Lu, L.W., "Seismic Response Control of Cable Stayed Bridged by Semi-Active Friction Damping," Proceedings of the US National Conference on Earthquake Engineering, Vol. 1, pp. 911-920, 1994.

BIOGRAPHICAL SKETCH

The author was born in 1977 in Ankara, Turkey. He graduated with a Bachelor of Science in Mechanical Engineering in May 2000 from Istanbul Technical University, Istanbul, Turkey. He then obtained a Master of Science in Mechanical Engineering in August 2002 from the University of Florida, Gainesville, FL, U.S.A.